GASL TR No. 387

The Nitrous Oxide – Propane Rocket Engine

A Final Report For BAA 99-22

In support of

Small Scale Propulsion Systems

For

DARPA
Tactical Technology Office
Attention: Dr. Robert L. Rosenfeld

August 16, 2001

DISTRIBUTION STATEMENT:
APPROVED FOR PUBLIC RELEASE; DISTRIBUTION IS UNLIMITED

Jason S. Tyll, Ph.D.
Principal Investigator
Allied Aerospace Industries Inc.
GASL Division
77 Raynor Ave
Ronkonkoma NY 11779
(631)737-6100 X178
Jtyll@GASL-USA.com

Roger Herdy
Project Manager
Allied Aerospace Industries Inc.
Flight Systems Division
726 Arcadia Circle
Huntsville, AL 35801
(256)533-7929 X 20
Rherdy@MICROCRAFT.com

REPORT DOCUMENTATION PAGE

Form Approved
OMB No. 0704-0188

Public reporting burden for this collection of information is estimated to average 1 hour per response, including the time for reviewing instructions, searching existing data sources, gathering and maintaining the data needed, and completing and reviewing this collection of information. Send comments regarding this burden estimate or any other aspect of this collection of information, including suggestions for reducing this burden to Department of Defense, Washington Headquarters Services, Directorate for Information Operations and Reports (0704-0188), 1215 Jefferson Davis Highway, Suite 1204, Arlington, VA 22202-4302. Respondents should be aware that notwithstanding any other provision of law, no person shall be subject to any penalty for failing to comply with a collection of information if it does not display a currently valid OMB control number. **PLEASE DO NOT RETURN YOUR FORM TO THE ABOVE ADDRESS.**

1. REPORT DATE (DD-MM-YYYY) August 16, 2001	2. REPORT TYPE Final	3. DATES COVERED (From - To) 6/30/00 to 8/16/01

4. TITLE AND SUBTITLE
Nitrous Oxide / Propane Rocket Engine

5a. CONTRACT NUMBER
DABT63-00-C-1026

5b. GRANT NUMBER
N/A

5c. PROGRAM ELEMENT NUMBER
N/A

6. AUTHOR(S)
Jason S. Tyll, Ph.D. (Principal Investigator) and Roger Herdy (Program Manager)

5d. PROJECT NUMBER
N/A

5e. TASK NUMBER
N/A

5f. WORK UNIT NUMBER
N/A

7. PERFORMING ORGANIZATION NAME(S) AND ADDRESS(ES)

Allied Aerospace Industries
Flight Systems Division
Micro Craft Incorporated
726 Arcadia Circle
Huntsville, AL 35801

Allied Aerospace Industries
GASL Division
77 Raynor Ave.
Ronkonkoma NY 11779

8. PERFORMING ORGANIZATION REPORT NUMBER
GASL TR No. 387

9. SPONSORING / MONITORING AGENCY NAME(S) AND ADDRESS(ES)

Bob Rosenfeld (TTO)
DARPA
3701 N. Fairfax Drive
Arlington, VA 22203-1714

Vicky Warford
Directorate of Contracting
Attn: ATZS-DKO-I
P.O. Box 12745
Fort Huachuca, AZ 85760-2745

10. SPONSOR/MONITOR'S ACRONYM(S)
TTO:
Tactical Technology Office

11. SPONSOR/MONITOR'S REPORT NUMBER(S)
N/A, done per CDRL A001

12. DISTRIBUTION / AVAILABILITY STATEMENT
Approved for Public Release; Distribution is Unlimited

13. SUPPLEMENTARY NOTES
Also documented in paper AIAA 2001-3258

14. ABSTRACT
This work, in response to DARPA BAA 99-22, topic title "Small Scale Propulsion Systems," focused on the development of a nitrous oxide (N_2O) / propane (C_3H_8) rocket engine (NOP), that utilizes catalytic decomposition of N_2O as an ignition system for propane. This propellant combination is proposed as an alternative to the present space propulsion systems that use hypergolic or cryogenic liquids, or solid propellants. Phase I work has resulted in a successful demonstration of the key technologies associated with the development of such a propulsion system. In particular, rocket performance for the NOP propellants and catalytic decomposition of nitrous oxide were demonstrated. The work began with two parallel efforts: the experimental evaluation of rocket performance using nitrous oxide and propane as propellants, and an experimental evaluation of various catalysts for the decomposition of nitrous oxide. The development of a catalytic reactor to efficiently decompose N_2O for propane autoignition was central to this research effort.

15. SUBJECT TERMS
nitrous oxide / propane rocket engine; catalytic decomposition of nitrous oxide; catalytic autoignition; benign propellants; microthruster

16. SECURITY CLASSIFICATION OF:			17. LIMITATION OF ABSTRACT	18. NUMBER OF PAGES	19a. NAME OF RESPONSIBLE PERSON Roger Herdy
a. REPORT Unclassified	**b. ABSTRACT** Unclassified	**c. THIS PAGE** Unclassified	UL	156	19b. TELEPHONE NUMBER (include area code) 256-533-7929 x 20

Standard Form 298 (Rev. 8-98)
Prescribed by ANSI Std. Z39.18

1   Executive Summary

This work, in response to DARPA BAA 99-22, topic title "Small Scale Propulsion Systems," focused on the development of a nitrous oxide (N_2O) / propane (C_3H_8) rocket engine (NOP), that utilizes catalytic decomposition of N_2O as an ignition system for propane. This propellant combination is proposed as an alternative to the present space propulsion systems that use hypergolic or cryogenic liquids, or solid propellants. Phase I work has resulted in a successful demonstration of the key technologies associated with the development of such a propulsion system. In particular, rocket performance for the NOP propellants and catalytic decomposition of nitrous oxide were demonstrated. The work began with two parallel efforts: the experimental evaluation of rocket performance using nitrous oxide and propane as propellants, and an experimental evaluation of various catalysts for the decomposition of nitrous oxide. The development of a catalytic reactor to efficiently decompose N_2O for propane autoignition was central to this research effort. Experiments to demonstrate rocket ignition using the catalytically decomposed nitrous oxide began in late January 2001. These rocket tests were performed using improved rocket hardware (NOP Rocket 2), an improved thrust stand and a new atmospheric pressure test stand, (Test Stand 2) constructed at the Johnson Research Center on the campus of UAH in Huntsville, Alabama. Pitot pressure surveys and radiometric measurements were conducted by AEDC. A pitot pressure system was designed, fabricated, and deployed for the UAH test series on 15 March 2001. The pitot pressure measurements were used to determine the thrust of the rocket engine. This was intended as a technology demonstration and as a back-up to the UAH thrust stand. This final report summarizes the design, development and testing of a NOP rocket system and outlines work required to further develop this concept to the point that a flight weight prototype can be fabricated.

2 Table of Contents

3 List of Authors

4	Introduction	J.S. Tyll, Ph.D.	AAII
		R. Herdy	AAII

5 Discussion of Environmental, Safety, and Health Issues   Associated with Rocket
Propellants   J.K. Woosley, Ph.D.   3DR

6 Discussion of Potential Missions For a Nitrous Oxide / Propane Rocket

		Jason Tyll, Ph.D.	AAII
		N. Tiliakos, Ph.D.	AAII

7	Design and Development Approach and Overview	N. Tiliakos, Ph.D.	AAII
		R. Chue, Ph.D.	AAII

8	Catalyst Reactor Design, Testing and Results	J. Smith, Ph.D.	UAH
		P.Addepalli	UAH
		B.S.Madhanbharatha	UAH

9	NOP Rocket Experimental Results	N. Tiliakos, Ph.D.	AAII
		M. Moser, Ph.D.	AAII
		R.S. Hiers III, Ph.D.	AEDC
		Danny Brown	AEDC

11	Conclusions	J.S. Tyll, Ph.D.	AAII
		N. Tiliakos, Ph.D.	AAII

10	Alternative Applications	J.S. Tyll, Ph.D.	AAII

4 Introduction

This work, in response to DARPA BAA 99-22, topic title "Small Scale Propulsion Systems," focused on the development of a nitrous oxide (N_2O) / propane (C_3H_8) rocket engine (NOP). This propellant combination is proposed as an alternative to the present space propulsion systems that use hypergolic or cryogenic liquids, or solid propellants. Phase I work has resulted in a successful demonstration of the key technologies associated with the development of such a propulsion system. In particular, rocket performance for the NOP propellants and catalytic decomposition of nitrous oxide were demonstrated. This final report summarizes the design, development and testing of a NOP rocket system and outlines work required to further develop this concept to the point that a flight weight prototype can be fabricated.

Also included in the report are generalized mission analyses to help determine future uses for such a propulsion system. Details associated with the individual propellants, their properties, and handling qualities are discussed. Nitrous oxide is considered here as a cold gas propellant, monopropellant, and oxidizer for a bipropellant.

4.1 Problem Identification

A serious limitation on the ability of the commercial aerospace industry to place into and keep satellites in Low-Earth-Orbit at economical prices is the choice of propellants and propulsion technologies used for rocket boost, attitude control systems (ACS), reaction control systems (RCS), orbital maneuvering systems (OMS), and auxiliary power units (APU). Present systems are either liquid propellants that are hypergolic or cryogenic, or solid propellants that are single use only, are unthrottleable, and are explosive in nature. A proposed solution to the problem is to select propellants for a chemical propulsion system that are readily available, are easier to handle, non-toxic, produce high performance, and provide significant reduction in cost of operations.

High operating costs are a result of occupational safety requirements associated with the handling of toxic, hypergolic propellants and of added complication of operating a cryogenic propellant system. This cryogenic system also adds considerable dry weight, further reducing the payload weight fraction.

By using nontoxic, benign propellants that are relatively safe to handle, low cost can be realized through simplified ground operations. Such a propellant combination could also benefit other systems for which safe and simple ground operations are a requirement. Rocket assisted takeoff systems (RATO) for unmanned aerial vehicles (UAV) could definitely benefit from a system that would provide simplified ground operations since these systems may be deployed in future battlefield scenarios. Military personnel would benefit from the safe handling characteristics of benign propellants, and superior performance to other propellant combinations allowing the UAV to perform its mission with lower risk of neutralization by the enemy. For similar

reasoning, potential applications for a ballistic missile defense systems (BMD) can be envisioned.

4.2 Identification and Significance of the Innovation

The technological innovation proposed is to exploit several unique properties of the propellants, propane and nitrous oxide, for a chemical rocket propulsion system. These self-pressurizing propellants have a distinct advantage over current systems that use hydrazine as a monopropellant and monomethylhydrazine and nitrogen tetroxide (MMH/NTO) as bipropellants. They are standard liquefied industrial gases and are classified by the U.S. Department of Transportation as simple asphyxiates, with propane as a flammable gas and nitrous oxide as a mild oxidizer. They are neither highly explosive nor hazardous to work with or handle. The proposed chemical liquid propulsion system, using these environmentally benign propellants, is economically advantageous to current hypergolic or cryogenic systems. They possess commercial availability at low prices and are easy to handle, thereby producing a significant reduction in operating costs.

4.2.1 Unique Features of NOP Propellants

A unique feature of nitrous oxide facilitates autoignition of the propane without the use of hypergolics. Nitrous oxide can be catalytically decomposed using a wide variety of catalysts, including platinum, iridium, rhodium, tungsten carbide, copper, cobalt, and gold. The decomposition process is exothermic resulting in nitrogen and oxygen at 2988 °F, for complete decomposition. This hot oxidizer will ignite propane (and most hydrocarbon fuels) on contact and will facilitate sustained combustion in a rocket combustion chamber. Using this technique, autoignition and rigorous and complete combustion can be accomplished using stable, non-toxic, storable propellants. Along the same lines nitrous oxide could be decomposed and used as a monopropellant similar to hydrazine and hydrogen peroxide.

In addition to these qualities, nitrous oxide and propane both store as high-pressure liquids. This facilitates self-pressurization, which eliminates the need for a pressurant system. Although high-pressure storage (750 psia for nitrous oxide, 125 psia for propane) increases tank weight, this can be mitigated with the use of a variety of low-weight, high-strength composite materials. Although the vapor pressure for propane is quite low, it can be pressurized with nitrous oxide utilizing a single tank with a diaphragm. Ethylene is being considered as a replacement fuel for propane since its vapor curve and critical conditions are similar to that of nitrous oxide. Ethylene would improve the specific impulse over propane by several seconds, and has been listed as a candidate replacement for ethane in an OF_2/C_2H_6 thruster.[1]

Nitrous oxide and propane also have relatively low freezing temperatures as compared to hydrazine and MMH. This eases problems associated with line freezing in orbit. Freezing point temperatures as well as a host of other properties for nitrous oxide and propane are shown, compared to those of hydrazine, MMH, and NTO, in Table 1. Although the storage density for the NOP propellants is lower than that of the hypergolic propellants, the benefit comes from the stability of the liquids, the lower freezing point conditions, and self-pressurization.

7

	N_2O	C_3H_8	C_2H_4	N_2H_4	MMH	N_2O_4	H_2O_2
Critical Temp (F)	97.2	114.5	49.3	716.4	561.0	316.0	
Critical Pressure (psia)	1048.2	983.2	729.7	2128.3	1195.0	1465.0	
Freezing Point (F)	-130.9	-305.0	-271.8	36.0	-61.2	15.7	12.6
Boiling Point (F)	-126.9	-43.2		237.6	189.9	70.2	286.2
Storage density (lb_m/ft^3)	47.9	44.2	35.3	62.9	54.8	90.3	86.0
Stability	Stable	Stable	Stable	Hypergolic	Hypergolic	Hypergolic	Unstable[2]
Toxicity	-	-	-	Toxic	Toxic	Toxic	-
Decomposition	Exothermic	-	-	Exothermic	Exothermic	-	Exothermic
Catalyst	Shell 405			Shell 405			Silver

Table 1: Properties of liquid rocket propellants

Table 2 shows a comparison of performance for candidate propellant combinations, including both bipropellant and monopropellant systems with nozzle expansion to vacuum conditions. It is evident from Table 1 and Table 2 that the NOP propellant combination has comparable rocket performance and more benign qualities than MMH/NTO, although it is at the price of a slightly lower storage density.

	NOP	MMH/NTO[3]	H_2O_2/Kerosene	N_2O	Hydrazine[4]	Peroxide
I_{sp} (s)	300	292	273	187	-	182
I_{sp} (s) Vac	312	339	319	192	230	187
C* (ft/s)	5234	5874	5494	3496	3073	3344
T_c (R)	5699	5850	5247	3195	1010	2207

Table 2: Rocket Performance Comparison

Although the NOP rocket concept deals specifically with nitrous oxide and propane as propellants, the greater theme is one of using nitrous oxide as an oxidizer and ignition source for use alone as a monopropellant or with a fuel as a bipropellant. The concept is based on the ability to catalytically decompose nitrous oxide into a hot nitrogen/oxygen mixture, and use this mixture to ignite and burn a fuel. This catalytic decomposition has been demonstrated in this
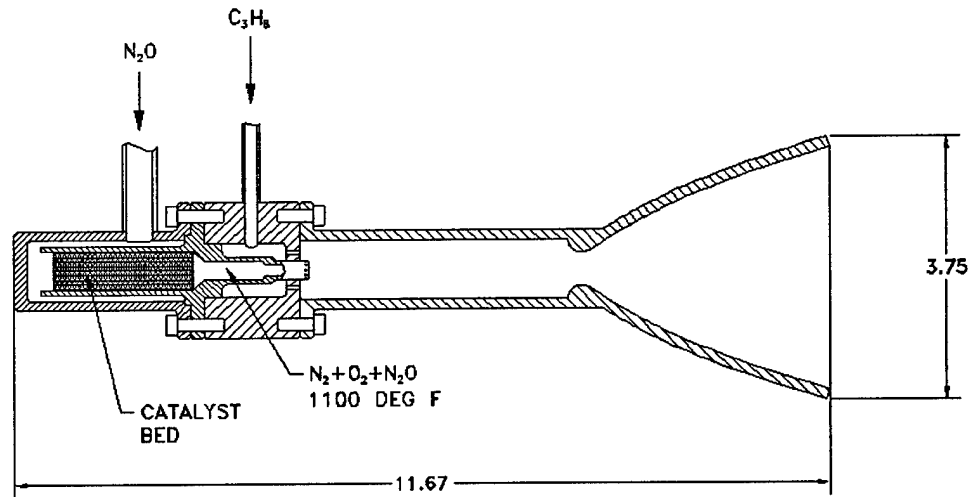
Figure 1: Conceptual Drawing of NOP Rocket Flight Hardware

Phase I effort under a DARPA/TTO BAA 99-22 (Section 8), using a number of catalysts including the iridium based Shell 405, which has a rich space flight heritage as a hydrazine catalyst. A schematic diagram of such a proposed system is shown in

Figure 1. The nitrous oxide passes over the catalyst reactor before entering the combustion chamber. Fuel is injected into the combustion chamber and thermally autoignites.

We propose a nitrous oxide / hydrocarbon propellant combination as an alternative to the MMH/NTO bipropellant, which is the mainstay for current systems. Nitrous oxide has already been used as an oxidizer for bipropellants in hybrid rockets and has extensive use as a performance enhancer in auto racing.

4.2.2 Nitrous Oxide Monopropellant

Since nitrous oxide decomposes exothermically it can also be used as a monopropellant. This monopropellant could serve as a replacement for hydrazine monopropellant rockets, or as an alternative to cold gas thrusters. Nitrous oxide is listed as a candidate propellant for cold gas thrusters[5] and has already been used as a propellant for a resistojet on the UoSat-12 (designed and built by Surrey Satellite Technology Limited[6] (SSTL) and Polyflex, Inc.[7]). With the minimal added catalyst weight, a nitrous oxide cold jet thruster can nearly triple its specific impulse as a warm jet thruster. Such a system would be of tremendous use for microsatellites / minisatellites or minor orbit adjustments since chemical rockets suffer reduced thrust-to-weight ratio at small scales (Figure 2).
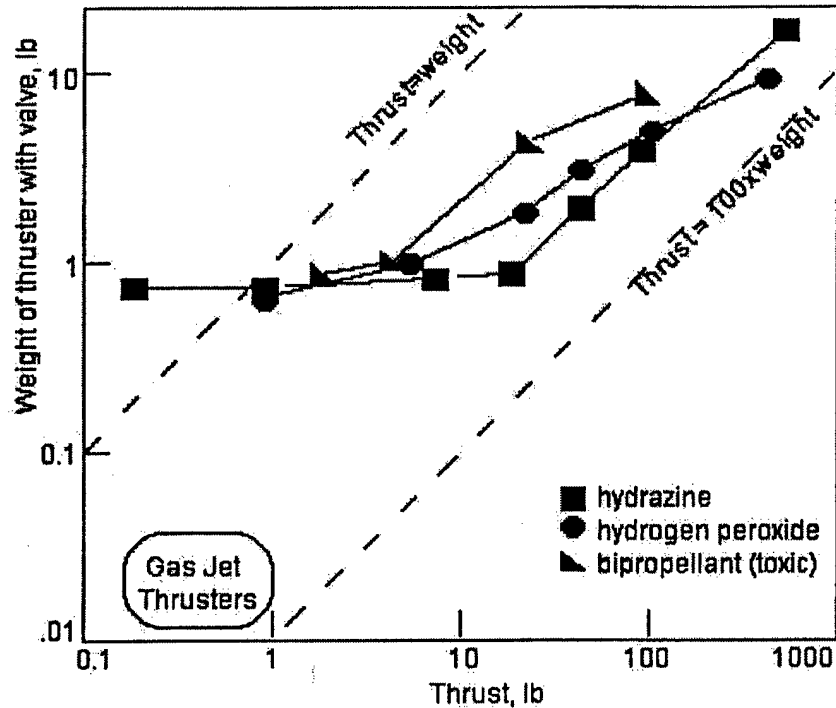
Figure 2: Thrust-to-Weight Ratio as a function of rocket scale.[8]

The SSTL resistojet is a 125mN sized thruster that has flown on the UoSat-12 satellite. The resistive element has a 100W power requirement and produces 127s of specific impulse. Nearly complete nitrous oxide decomposition is possible using a 600W heater. This would result in higher thrust and a 182 s specific impulse[9]. This level of nitrous oxide decomposition is possible by catalytic reaction without the expense of high power requirements.

Surrey Satellite Technology Limited has also been exploring the idea of using catalytically decomposed nitrous oxide for a monopropellant rocket[10] and as an igniter/oxidizer for a kerosene bipropellant rocket[11]. Although they have not yet performed rocket tests using catalytically decomposed nitrous oxide, they have tested over 50 different catalysts. Tests showed nitrous decomposition using a variety of catalysts (including Shell 405) with light-off temperatures as low as 392°F. They made no attempt to develop low light-off temperature catalysts and instead have focused on catalyst stability issues at excessively high temperatures. SSTL's previous resistojet work and future research and development plans indicate their recognition of the potential benefit of nitrous oxide as a rocket propellant and of catalytic decomposition as a low-power alternative to resistive heating and ignition. Additional trade studies by Zakirov[12,13] indicate tremendous benefit for nitrous oxide use as a monopropellant and cold gas thruster and underscores the added benefits of developing a multi-modal propellant system where nitrous oxide is used for all small satellite propellant needs.

Nitrous oxide has added benefit as a space propellant in that it stores as a liquid and injects as a gas. This is important for attitude control (AC), since liquid injection rockets cannot provide the

10

shorter pulse times required for an ACS mission. Liquid storage gives tremendous weight benefit since a liquid tank can hold multiple times its own weight in propellant, whereas the same is not true for gas storage systems.

4.2.3 Nitrous Oxide as an Alternative to Hydrogen Peroxide

With similar goals in mind, hydrogen peroxide is being considered more and more as both a monopropellant and oxidizer for a bipropellant, for space applications and upper-stage booster rockets[14]. We propose the NOP rocket concept as a viable alternative or even a complementary technology as it has some advantages over peroxide as well as some disadvantages (Table 1 and Table 2). Concurrent development of the two technologies is ideal in that many of the challenges are the same and the expanding knowledge base can mutually support both.

The resurgence of hydrogen peroxide as a potential rocket propellant is based partially on the promise of new technologies that can solve the long-standing technical issues associated with its use[15]. In particular, improvements to the silver catalyst beds are required for high temperature operation. The silver catalyst used for peroxide is also prone to "poisoning" by contaminants and stabilizers in the peroxide. Stabilizers are required to avoid inadvertent decomposition, which occurs during long periods of storage. Although "poisoning" can affect most catalysts, this is less likely to occur with nitrous oxide since it does not require stabilizers for long-term storage. Peroxide vapors can be explosive and shock sensitive in the presence of contaminants. Highly concentrated hydrogen peroxide, such as is required for efficient propellant use, is almost as toxic as hydrazine based on IDLH, and the OSHA PEL and ACGIH TLV values governing occupational exposure are actually much lower than those of NTO (see Section 5).

Other work seeks out non-toxic, storable fuels that become hypergolic in the presence of peroxide. Ignition for our proposed propellant combination is provided by the high-temperature products of the nitrous oxide decomposition and not by the hypergolic nature of propellants. A similar approach to ours was also in development for hydrogen peroxide rockets by Beal Aerospace Technologies Inc.[16] before they shut down in October, 2000.

4.2.4 Multi-modal Space Propulsion System

Due to the versatility of nitrous oxide as both a monopropellant and oxidizer for a bipropellant system, the potential exists to set up a multi-mode propulsion system, which will improve space mission capability by reducing the dry weight overhead. A single propellant system serving all space propulsion missions from attitude control to orbital maneuvering would reduce the component count, system weight, and cost. Lower dry weight can be converted into higher payload weight fraction or DV.[12]

4.2.5 Propellant System for Self Pressurizing Liquids

Most propellants commonly used today have relatively low vapor pressure (lower than the rocket chamber pressure) and consequently have to be pressurized. This is accomplished in one of several ways. Turbo pumps are used for launch vehicle applications. The pumps are driven using onboard propellant and form part of the thermodynamic cycle for the system. For space applications, expulsion systems are used to pressurize the propellant and drive it out of the propellant system. Expulsion systems are either blowdown or regulated. Both versions use high pressure gas (either helium or nitrogen) to pressurize the liquid propellant.

For blowdown systems the pressurant gas is stored in the same tanks with the propellant. As the propellant is consumed tank pressure decays, as does thrust. Regulated systems keep a very high pressure source of pressurant gas, which is regulated down to the required tank pressure. As the propellant is consumed, the regulator maintains a constant tank pressure, and correspondingly constant thrust. Blowdown systems are used mainly for monopropellant thrusters, while regulated systems are used for bipropellant thrusters. Expulsion systems lower the useful tank volume, and, in the case of regulated systems, add considerable dry weight. Blowdown systems can occupy over 20% of the tank volume. Regulated systems require a lower ullage volume (~3%), although a separate high-pressure tank is required to store the pressurant gas.

In contrast to these systems the NOP propellants are self-pressurizing due to their relatively high vapor pressures (higher than the rocket chamber pressure). Consequently, they do not require separate expulsion systems and the entire tank volume can be used to store propellant. The vapor pressure of nitrous oxide is approximately 750 psi and that of propane is 125 psia at ambient temperature.

For a self-pressurizing system the vapor pressure is maintained in the tanks until all of the liquid propellant is consumed. By taking a ratio of the vapor to liquid densities of nitrous oxide, we could see that constant pressure and thrust conditions can be supplied using 83.1% of the propellant. The remaining 16.9% remains as a high-pressure gas and can be used with decaying conditions as a blowdown system. The metering orifices would now operate in a choked fashion and could therefore still be used to meter flow rate. With 7.1% mass still remaining in the tanks, there would be insufficient pressure remaining to meter the flow using the choked orifice. The system would continue to work until approximately 3.5% mass is left remaining in the tanks, although with increasingly decaying performance.

The self pressurizing system has both advantages and disadvantages as compared to the other systems mentioned. Although regulated systems can provide constant tank pressure for the entire propellant mass, such systems add considerable dry weight and complications. Blowdown systems suffer pressure decay over the spacecraft's entire operational lifetime and could occupy over 20% of the tank volume. In comparison, the NOP self-pressurized propellants utilize the entire tank volume, allowing for up to 20% more propellant mass. The self-pressurized system provides constant tank pressure for over 80% of its operational life, and then transitions to a blowdown system with as little as 3.5% unusable propellant. A self-pressurizing system would incur higher tank weight, although this could be mitigated by material choices.

The vapor pressure of propane is slightly low inorder to be used as a true self-pressurizing propellant. For the case of a NOP system, high-pressure nitrous oxide vapor would be used as a

pressurant gas for the propane. Issues associated with maintaining mixture ratio for the bipropellant case will require some research. Ethylene is also being considered as a propane replacement due to its higher vapor pressure.

4.3   Identification of Operational System Payoffs

The NOP rocket offers a non-toxic, environmentally benign propellant combination that is storable in space over long periods of time and offers comparable specific impulse to current systems. Table 2 compares the performance of nitrous oxide / propane with MMH/NTO and hydrogen peroxide / kerosene. Nitrous oxide monopropellant is also compared with hydrazine.

The non-toxic nature of the NOP propellants will serve to reduce operating costs due to the handling issues associated with the hypergolic propellants currently in use for space applications. The NOP propellants are benign and not highly reactive. They remain so until the nitrous oxide is catalytically decomposed and combined with the fuel. Exhaust products consist mainly of nitrogen, water, and carbon dioxide.

The NOP propellants are storable over long periods of time without degradation. Inadvertent decomposition is one of the main technical obstacles for hydrogen peroxide use in space propulsion systems.

4.4   Potential Customers for the Technology

The proposed rocket propellants could be used for satellite applications with the intended objective of providing economical service in a LEO (Low Earth Orbit) environment. Space applications will include auxiliary power units, attitude control systems, reaction control systems, and orbital maneuvering systems. These applications appear feasible using the proposed propellants and ignition scheme. Potential weight savings exist by using the same propellant combination for all satellite rocket systems (i.e. multi-modal propulsion system). Any larger derivatives would target requirements for the upper stage of launch vehicles for routine placement of satellites in LEO.

This work suggests future concentration on the satellite propulsion market for both technical and marketing reasons. Technically, this rocket combination is well suited for use as a space propellant and upper stage booster, although it is probably not dense enough to be advantageous as a first stage booster over solids and cryogenic propellants. The satellite market is also rapidly growing. Competition will create a need for better and cheaper propulsion solutions.

Other potential customers exist in the areas of upper stage launch vehicles, low and medium altitude BMD interceptors, and RATO systems for the UAV market. A potential application as a pilot and torch igniter for hypersonic airbreathing propulsion systems opens up another potentially large future market. Operational ramjets and scramjets are expected on hypersonic weapon systems within the next ten years. Operational vehicles using airbreathing propulsion systems are in the works, with the eventual goal of low-cost access to LEO. Application of

13

catalytically decomposed nitrous oxide to high altitude re-light of gas turbine engines is also being considered.

5 Discussion of Environmental, Safety, and Health Issues Associated with Rocket Propellants

5.1 ESH Overview

Environmental, Safety, and Health (ESH) analyses and comparisons hinge on the following properties of materials:

- Health effects, which includes the risks of chemical burning due to the action of the chemical, severe burns or frostbite due to the temperature at which the material is stored, used, or reacts, and toxicity and delayed toxic effects (including carcinogenic and teratogenic effects) on persons exposed to the chemical, the latter often in quite small but chronic concentrations.
- Flammability, which includes the risk of fire if the chemical is directly exposed or mixed with air or other oxidizers.
- Reactivity, which includes the risk that the chemical, if released, can react spontaneously with air or with other common materials in the vicinity of the release site. To some extent, this factor also deals with storability, as most chemicals will react at some level with the materials of the tank or drum in which they are stored.

The greater the hazard associated with a chemical, the greater the cost of handling it due to the level of protection mandated by law and safety practice, and correspondingly the greater the cost of the material to the end user.[17]

Propellant aging is also concerned primarily with the overall reactivity of a propellant, in this case as a measure of performance degradation over time due to various reactions of the propellant *in situ* in it's storage system.

This section provides a comparison of these different factors for several common propellant chemicals, and concludes on the basis of this comparison that nitrous oxide and propane is a better propellant combination than other propellants studied.

5.2 Propellant Background

For the sake of this study, the following propellants have been considered:

    Monopropellants:
        hydrazine
        hydrogen peroxide
        catalyzed nitrous oxide

    Bipropellant combinations
        nitrous oxide – propane
        nitrogen tetroxide – hydrazine
        nitrogen tetroxide – monomethylhydrazine
        nitrogen tetroxide – unsymmetrical dimethylhydrazine
        hydrogen peroxide – propane
        hydrogen peroxide – hydrazine
        hydrogen peroxide – unsymmetrical dimethylhydrazine

The classical propellants for steering rocket motor applications are nitrogen tetroxide (NTO) and the hydrazine family of compounds. This combination was selected because the reactions are hypergolic and because the compounds do not require pressurized storage (although the range of storage materials is sometimes limited due to the high reactivity/corrosivity of the compounds. However, the high toxicity of these compounds places a strong premium on protection of ground crews, requiring considerable special equipment to mitigate hazard limits at or below the 1 ppm limit.

Hydrogen peroxide has been widely described as an alternative to hydrazine as a monopropellant and as alternative to NTO as the oxidizer for bipropellant applications. However, highly concentrated hydrogen peroxide, such as is required for efficient propellant use, is almost as toxic as hydrazine based on IDLH, and the OSHA PEL and ACGIH TLV values governing occupational exposure are actually much lower than those of NTO.

Conversely, nitrous oxide is a comparatively benign oxidizer. It has a lower reactivity rating than hydrogen peroxide, and an equivalent health rating based primarily on the risk of exposure of the liquefied gas. Short term health effects are limited ; nitrous oxide is routinely used at high concentrations as an anesthetic, and the only IDLH requirement is to assure that any nitrous oxide vapor does not dilute ambient oxygen below the 19.5% limit required by safety regulation. The NIOSH Recommended Exposure Limit (REL) for nitrous is 25 ppm continuous exposure because of suspected teratogenic effects (impacting women in their childbearing years, particularly if pregnant), not because of prompt toxicity as is the case for the competing fuels. This figure is roughly the level of nitrous oxide established in a typical dental examination room if the patient receiving nitrous is permitted to vent a few breaths of anesthetic nitrous into the

room at large. It is reasonably managed with normal ventilation controls and periodic testing to verify the effectiveness of ventilation.

Similarly, propane is an extremely benign fuel. While more flammable than the hydrazine family, the reactivity, toxicity, and potential for health effects are substantially lessened. Propane is routinely used in liquefied gas canisters in the home, both for home heating systems and for cooking grills. Despite the hazards associated with vaporization, liquefied propane is also becoming increasingly common as a substitute for room-temperature liquid fuels such as gasoline on the highway.

5.3 Parameters Evaluated

A number of specific parameters for the materials in these monopropellants and bipropellant combinations are specified in the accompanying Appendix I. They include:

- NFPA ratings for flammability, reactivity, and health effects.
- Exposure limits published by NIOSH, ACGIH, and OSHA, including the IDLH values. Note that the IDLH values are the most recently published by NIOSH (available at http://www.cdc.gov/niosh/idlh/intridl4.html) and may have changed from classical/conventional values published in the older literature.
- Specific physical properties flammability and pressurization properties, including flash point, and autoignition/autodecomposition temperatures. Information in the above is obtained from published MSDS and values available in on-line reference libraries at the EPA, NIOSH, and OSHA.
- Ionization energy and appearance energy. Ionization energy is the energy at which individual electrons are removed from the molecule; appearance energy is the lowest energy at which individual ions are formed during radiolysis or thermal excitation of the molecule. The values shown are obtained from http://webbook.nist.gov and are shown when available. For the first ionization energy, the quoted ionization energy is supplied where available, or the lowest value quoted in the table of ionization energy measurements if no first ionization is quoted. Multiple values of ionization energy occur either because of mechanistic differences in different modes of ionization (electron impact or EI being the most common but not the only one used in determination) or because of the removal of different electrons from the molecule, differentiated by methods of polarization or X-ray spectroscopy. Appearance energy is determined by the same method and by detection of the specific species measured (usually differentiated by mass spectroscopy). The species with the lowest quoted appearance energy is shown. In cases where appearance energies are shown to be associated with excited "rebound" states, only ground states are shown in the accompanying Appendix, since more detailed information is not available in the Webbook. These values are obtained and placed in the Appendix because they related to radiation stability and to overall reactivity of the molecules for aging analysis.
- Specific toxic effects, protection requirements, and material incompatibilities. Data is available from published MSDS (on-line) and from either specific chemistry or chemical

class material compatibility properties in Perry's Chemical Engineer's Handbook, 5th Edition.

5.4 Environmental, Safety, and Health Protection Impacts on Different Common Propellants

The simplest health comparison method is the comparison of National Fire Protection Association (NFPA) Flammability, Reactivity, and Health ratings, which is shown in Table 3.

Rating	N_2O	NTO	H_2O_2	C_3H_8	N_2H_4	MMH	UDMH
Flammability	0	0	0	4	3	4	3
Reactivity	0	0	3	0	3	0	1
Health	2	3	2	1	4	3	4

Table 3: Comparison of NFPA Ratings for Oxidizers and Fuels

For nitrous oxide, the health rating is alternatively given a 0 for gas and 3 for liquid due to the pressurization of the propellant and the risks of frostbite in the event of a liquid splash. For hydrogen peroxide, the numbers are obtained from data for typically 50 – 70% peroxide solutions and conditions may be worse for the 90 – 98% solutions desired for space travel.

In comparison of oxidizers, it is immediately seen that concentrated peroxide is the most reactive of the oxidizers, and hence the greatest hazard for fire ignition in the event of a spill. Because of the notes above, the health ratings are more difficult to compare; however, in consideration of the possibility of liquid splash only, 50 –70% peroxide is considered less hazardous than nitrous oxide due to the freezing effect of an nitrous oxide (or NTO) splash. In comparison of fuels, propane is clearly superior; since flammability is a desirable and inescapable consequence of fuel efficiency, the reactivity and health factors dominate the comparison.

The next simplest is the comparison of the occupational exposure limits as determined by the National Institute of Occupational Safety and Health (NIOSH), the American Conference of Government Industrial Hygienists (ACGIH), and the Occupational Safety and Health Administration (OSHA), which publish the Recommended Exposure Limit (REL) and Immediately Dangerous to Life and Health (IDLH) values, the Threshold Limit Value (TLV), and the Personnel Exposure Limit (PEL), respectively. These values are all based on airborne concentration of vapors or aerosols and are expressed as ppm by volume (or equivalent for air, mole fraction as a ppm). These values are reproduced in Table 4.

Rating	N_2O	NTO	H_2O_2	C_3H_8	N_2H_4	MMH	UDMH
NIOSH REL	25	1	NS	1000	0.03	NS	NS
ACGIH TLV	50	3	1	ASP	0.01	0.01	0.01
OSHA PEL	NS	20	1	1000	1	0.2	0.5
IDLH	ASP	20	75	2100	50	20	15

Table 4: Occupational Exposure Limits of Oxidizers and Propellants (ppmv)

In this table, NS means "Not Specified," e.g. that the standards body in question has not determined an appropriate value for the chemical in question. ASP means that the limit is reached when the chemical reaches asphyxiating concentrations, defined to mean that the concentration is sufficiently high as to reduce available oxygen to below 19.5%. This corresponds to about 5% concentrations of nitrous oxide and propane. The IDLH for propane is set at 10% of the lower explosive limit, as is the practice with any nontoxic flammable gas.

In this comparison, it must be remembered that nitrous oxide and propane are liquefied gases stored at pressure. During any spill or release in confined spaces under comparable circumstances, the concentration which enters the vapor phase quickly will be greater than that of the other fuels. Safe management of liquefied gases does require experience and controls; however, because of the higher toxicity of the competing compounds, the risks associated with loss of propane and nitrous oxide are substantially less. Indeed, these compounds are typically stored and used in liquefied or gaseous form outside of industrial controls – e.g. the home propane heating and cooking tank; the smaller tank for the gas grill; the tank of nitrous anesthetic in the dentist office; the nitrous oxide used as a propellant in refrigerated whipped cream and other pressurized food products.

It is true that this anesthetic effect of nitrous oxide can result in impairment of workers at very high concentrations (much higher than the asphyxiant concentration), creating hazards beyond the simple exposure hazard, and those must be guarded against in an industrial setting.

The most direct comparison of the costs associated with safe management of fuels comes from consideration of the per-unit-weight cost of the chemical, and to a lesser extent to the cost of any specialty materials required to safely store and handle the chemical. It is very difficult to obtain a direct quantitative cost comparison of the safety demands of handling a material, due to all of the factors which contribute to pricing (including cost of precursors, cost of process, depreciated cost of equipment, and other direct operating factors; quantity purchased and cost/nature of packaging and handling, etc) as well as to the fact that fuel grades of hydrazine family propellants represent a captive market with the U.S. Air Force and NASA. However, qualitative comparisons show the likely advantages of NOP as shown in Table 5; see other notes in the Appendix.

	N_2O	NTO	H_2O_2	C_3H_8	N_2H_4	MMH	UDMH
Price, $.kg	$2.76	$6.00	$2.00	$0.41	$17	`$17	$24
Comments	Per Cylinder; bulk quantity will be less	Bulk Quantities (Propellant)	Bulk Quantities (industrial)	Bulk Quantities (Spot Mkt)	Captive to AF	Captive to AF	Captive to AF

Table 5: Cost Comparisons of Oxidizers and Propellants (Qualitative, $/kg)

In summary, most ESH parametrics favor the nitrous oxide-propane system over other propellant combinations. This applies most directly to toxicity, hazards of handling, and unit cost associated with handling. The most significant risk associated with the nitrous oxide – propane system is the fact that the fuels are liquefied gases with the associated risks of handling materials

under pressure. However, in industrial settings, this risk is minor compared to the handling costs associated with the more toxic NTO and hydrazine family propellants. The advantages compared to hydrogen peroxide are minor based on available data, but a lack of experience at the concentrations of peroxide required for propulsion systems increases the risk of using peroxide relative to nitrous oxide.

5.5 Comparison of Aging of Different Common Propellants

Materials age and lose potency through a variety of different reactive mechanisms, depending upon the environment in which they are stored. For materials stored in a space environment, the following mechanisms are the most prevalent:

1. Decomposition (e.g. hydrogen peroxide to oxygen and water, or nitrous oxide to nitrogen and oxygen, or hydrazine to ammonia, nitrogen, and hydrogen), spontaneous at low rates due to ambient conditions, catalyzed by impurities of material or container, or self-catalyzed as either the spontaneous or catalyzed reaction products (and heat) build up.
2. Degradation by buildup of dissolved and suspended corrosion products from reaction with the storage container. Degradation may also be self-catalyzed, or may slow down or stop if the corrosion products reach their solubility limits in the material.
3. Radiolysis by ambient radiation; ions and free radicals formed by radiolysis may contribute to self-decomposition or to degradation by similar mechanisms as those summarized above.

In all cases, the reactivity is directly related to the activation energy of reaction, which in turn is related to the ionization energy of the species under consideration, and the appearance energy of it's decomposition products. This information also relates to such data as the self-decomposition temperature, the autoignition temperature, and other thermochemical and kinetic data. This information is documented in the Appendix, obtained from the MSDS, the molecular energetics data obtained from webbook.nist.gov, and other sources.

The propellants studied are ranked by these properties in the order 1 (most stable) to 7 (least stable) in Table 6.

Property	N_2O	NTO	H_2O_2	C_3H_8	N_2H_4	MMH	UDMH
Autoignition Temperature	-	-	-	1	2	4	3
Autodecomposition Temperature	1	2	3	1	3	2	NS
Ionization Energy	1	2	3	1	2	3	4
Lowest Appearance Energy	1	NS	2	1	2	3	4

Table 6: Ranking of propellant candidates by properties which contribute to aging, from most stable to least stable (highest to lowest; oxidizers first)

As can be seen immediately by comparison of the available data, nitrous oxide is the most stable of the oxidizers against aging, and propane is the most stable of the fuels against aging.

The case against peroxide is worth noting. Peroxide spontaneously decomposes into oxygen and water at all temperatures, although the rate of decomposition is quite small unless catalyzed by light or certain reactive chemicals. With optimal materials under conditions associated with space missions, this rate of decomposition is projected to be about 1% per year.[18]

In conclusion, while all of the fuels and propellants appear to meet typical aging requirements, the NOP system appears to possess the greatest stability against aging, and thus the lowest risk from propellant aging of any system in development.

Now that the operational and handling benefits of the NOP rocket system, as well as its unique features, have been assessed, the next section focuses on potential missions for this innovative technology.

6 Discussion of Potential Missions For a Nitrous Oxide / Propane Rocket

Mission trade studies are performed here and are based solely on the rocket equation and mass breakdowns. The rocket equation describes the relationship between wet mass (M_o), burnout mass (M_b), specific impulse (I_{SP}), and the potential change in velocity (DV). Change in velocity can be converted into a total impulse for a given system with a specified wet mass. The rocket equation and breakdown of system mass are shown below.

$$\frac{\Delta V}{g_c I_{sp}} = \ln\left(\frac{M_o}{M_b}\right) \tag{6-1}$$

$$M_o = M_P + M_b \tag{6-2}$$

$$M_b = M_{PL} + M_{Dry} \tag{6-3}$$

$$M_{Dry} = M_{Fixed} + TF * M_P \tag{6-4}$$

The wet mass is simply the sum of the burnout mass and propellant mass. The burnout mass is the sum of the payload mass (M_{PL}) and the dry mass (M_{Dry}). The dry mass is broken into two groups. The fixed mass (M_{Fixed}) is the portion of the dry mass that does not scale with the mass of propellant (M_P). The portion of the dry mass that scales with propellant mass is represented as the product of the propellant mass and a constant tankage factor (TF). The tankage factor is calculated as the ratio of the mass of all scalable components (fuel tanks, diaphragms, expulsion system, pressurant gas, etc.) to the propellant mass and is assumed to remain constant for a given system.

These equations can be reduced to describe the rocket performance as a function of ratios of component mass to the wet mass, called mass fractions. By comparing plots of mass fractions versus DV for different systems and propellant combinations, the usefulness of these propellants for particular missions can be evaluated.

According to the rocket equation, two factors contribute to produce DV: specific impulse and propellant mass. The greater the propellant mass, the greater the ratio of M_o to M_b in the rocket equation. Therefore, propellant combinations should be judged not only on their ability to produce high specific impulse, but also on their storage density. Propellant combinations can be judged based on a single figure-of-merit that combines both: density specific impulse is the product of specific impulse and specific gravity.

$$I_d = SG * I_{SP} \tag{6-5}$$

Therefore maximum DV is sometimes accomplished with high specific impulse, sometimes with high propellant density, and sometimes a combination of both.

For example, for cold gas thrusters, both nitrogen and nitrous oxide provide better performance (based on DV) than does helium, even though helium gives the highest specific impulse of the three (Table 7). This is reflected in the superior values of density specific impulse for nitrous oxide and nitrogen over helium.

	I_{sp} (sec)	I_d (sec)
Helium	158.0	5.4
Nitrogen	68.0	16.2
Nitrous Oxide	60.0	47.0

Table 7: Cold Gas Thruster Propellants

Figure 3 shows a plot of density specific impulse for a number of propellant combinations including those with nitrous oxide. This plot illustrates the balance between specific impulse and propellant density required for superior performance. The argument made for cold gas thrusters in Table 7 is obvious here, showing the superior specific impulse of helium and the performance issue associated with the low storage density. Nitrous oxide is shown to be an excellent propellant choice for cold gas thrusters.

Through catalytic decomposition, nitrous oxide can also be used as a monopropellant. Figure 3 shows nitrous oxide compared to hydrazine and hydrogen peroxide. The benefits of hydrogen peroxide as a monopropellant are evident here. Its high storage density results in a density specific impulse that is significantly higher than the current workhorse of monopropellants, specifically hydrazine. Nitrous oxide shows the lowest performance of the three for monopropellant operation, although overall system performance improvement would be achieved if nitrous were used for both the monopropellant and cold gas thruster missions. Using a common propellant would reduce dry mass overhead as compared to vehicles with multiple propellant systems.

NOP rocket is also shown compared to NTO/MMH in Figure 3. The later is definitely superior to NOP for both specific impulse and density specific impulse. The benefit of NOP comes from its nontoxic classification, benign nature, and storability, discussed in Section 5. Figure 3 also illustrates the benefit associated with solid propellants. Despite the lower specific impulse as compared to most bipropellants, the high storage density provides for performance comparable to the bipropellant systems. This is furthered by the low dry weight fraction associated with solid rockets.
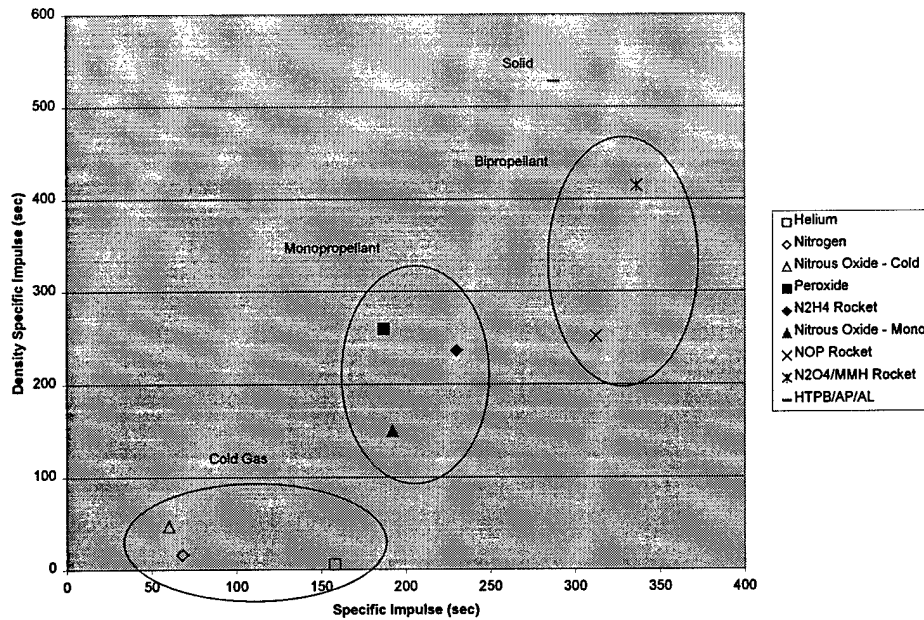
Figure 3: Density specific impulse for various propellant combinations.

The propellant of choice for a given mission depends not only on the specific impulse and propellant density, but also on its effect on system dry weight. Since the mission goal can usually be reduced to imparting a DV to a payload of given mass, minimizing the dry weight fraction also serves to improve overall performance. This is why the propellant with the highest specific impulse is not always used. As an example, we could look at general mission descriptions and common propellants currently in use. This is accomplished in the following subsections, along with performance comparisons of corresponding nitrous oxide based propellants.

6.1 Launch Vehicle Propulsion

Booster rockets used to bring a payload to low-earth-orbit (LEO) must deliver extremely high DV (~23760 ft/s) as specified by orbital mechanics. As a result, payload weight fractions are very low and rocket staging is required to eliminate dry weight en route. For these missions, which are generally not volume constrained, high specific impulse bipropellants are commonly used (NTO/MMH, H_2/O_2). These bipropellants are highly toxic, or, in the case of H_2/O_2 stored as cryogenic liquids. With NTO/MMH, the issues and added cost associated with toxicity and hypergolic behavior are dealt with in exchange for the specific impulse and storage density it affords the rocket. Liquid hydrogen / liquid oxygen are used for their extremely high specific impulse which outweighs the increase in dry mass associated with the cryogenic propellant storage. Solid propellants are also used for first stage boost and are sometimes strapped on in addition to a liquid bipropellant system (ex. Space shuttle, Delta). The high storage density, high propellant weight fraction and low dry weight fraction make solids an attractive choice for first stage boost. Their main drawbacks are the explosive nature of the solid propellants and the inability to throttle or turn off solid boosters in the event of an aborted launch.

For upper stage booster rockets the mission requirements are slightly different than that of the first stage. Since these rockets are used following a stage separation, the payload weight fraction is higher than that of the first stage and the DV requirement is usually smaller. Second stage boosters are usually propelled using hypergolic bipropellants.

Boost from LEO to GEO is usually accomplished by a final stage on the launch vehicle. Due to this fact this particular orbital maneuvering mission is dealt with here and not in the subsection on space propulsion. Such an orbital maneuver requires a maximum of 7920 ft/s in DV although can require less depending on the initial state of the vehicle. At this point in a boost most of the booster rocket has separated and all that remains is the payload and final boost stage. Consequently, payload weight fraction is high and overall system weight must be minimized since this final stage acts as dry weight for the previous rocket stages. Solid propellant rockets are generally used for such a mission due to its high storage density and high density specific impulse. Orbital maneuvering of this sort is also accomplished with a single burn so solid propellants can be used to provide an accurate impulse bit for the transfer orbit. Other longer duration missions with more complicated burns, such as interplanetary missions, might be more inclined to use highly dense liquid bipropellants.

Trade study results for booster rockets are shown in Figure 4 and Figure 5 with supporting information provided in Table 8 and Table 9. The mission is broken up into first stage and upper stage missions with specific impulse adjusted according to the back pressure. Table 8 shows trade study information for the NOP rocket and a solid propellant. Numbers for tankage factor and fixed mass fraction were calculated based on a system mass breakdown for a hypergolic propellant outlined in Reference 5. The

25

tankage factor was adjusted to account for the effect of the higher storage pressure on tank weight and the difference in propellant storage densities between the NOP propellants and propellants used in the example case. This results in a higher tankage factor than corresponding hypergolic propellant combinations (0.047). Fixed mass fraction is also determined from component weights in this example case[5]. One column is devoted to a low tankage factor case for the NOP rocket propellants to show the effect of lowering this parameter on the overall rocket performance. Since a tankage factor of 0.153 was determined based on scaling an existing system, this number does not reflect factors that might mitigate the tankage weight such as the use of low-weight composite tanks and the reduction of NOP storage pressure by a corresponding reduction in storage temperature. This can be accomplished through the onboard thermal management system. The vapor pressure of nitrous oxide can be reduced considerably with small reductions in temperature from the nominal case of room temperature storage. This would directly effect the tankage factor since storage pressure directly scales with tank thickness, which corresponds to tank weight. It is the belief of the authors that the tankage factor could be reduced to a value closer to that of solid rocket systems.

Since solid propellant rockets do not require components usually included in the fixed mass (valves, lines, etc.), the fixed mass ratio is zero. Tankage factor is also low due to the high storage density and low storage pressure of the solid propellants.

	NOP Rocket	NOP Rocket	NOP Rocket	HTPB/AP/ AL	HTPB/AP/ AL
Stage	1st	Upper	Upper (Low TF)	1st	Upper
Specific Impulse, I_{sp} (sec)	250	312	312	210	287.3
Tankage Factor, TF	0.153	0.153	0.075	0.07	0.07
M_{Fixed}/M_o	0.049	0.049	0.049	0	0

Table 8: Booster rocket trade study information

Figure 4 shows a plot of DV versus payload weight fraction for booster rockets. Curves represent performance for the cases described in Table 8. It is interesting to note the effects of varying specific impulse and tankage factor. Both serve to increase the DV for a given payload weight fraction. The affect of fixed mass can be seen partially as a shift of the curve to the left. Note how the solid propellant curves are able to reach a payload mass fraction of one, whereas the maximum payload mass fraction for NOP is reduced by the amount of the fixed mass fraction.

Table 9 describes two examples of launch vehicles and their mission descriptions. These can be used to compare performance of NOP propellants for similar missions. The Delta II launch vehicle, developed originally by McDonnell Douglas (now Boeing), has the capability of delivering a 4120 lb_m payload to geosynchronous transfer orbit. The vehicle consists of three stages, each with different propellants as outlined in Table 9. Stage 1 consists of a liquid bipropellant rocket and nine strap-on solid boosters for thrust augmentation. The liquid bipropellant is liquid oxygen and RP-1, requiring a cryogenic

storage system. Stage 2 consists of a liquid bipropellant rocket using toxic, hypergolic propellants. Stage 3, which provides the DV required for geosynchronous transfer, is a solid rocket. The propellant specific impulses, stage DV, and mass fractions are all shown in Table 9.

This Delta II information is also plotted in Figure 4. As previously mentioned, as compared to lower stages, upper stages are characterized by higher payload mass fraction and lower DV requirement. By comparison with the NOP curves, NOP cannot accomplish the first stage mission of the Delta II, which is performed using a mixture of solid and liquid propulsion systems. The curve for HTPB solid propellant comes very close to the Delta II first stage data point indicating its capability, as is demonstrated by the actual rocket. The second stage Delta II mission can be accomplished by NOP, as indicated by the NOP rocket upper stage curve. The Delta II third stage orbital transfer mission shows a good match to the predictive curve for the solid rocket, as it should. The NOP rocket upper stage curve cannot provide the same DV at the given payload weight fraction (0.46). It can provide the required DV for a payload weight fraction of 0.37, which would correspond to a payload weight of 3333 lb_m. For a NOP rocket with the low tankage fraction the payload weight fraction could be increased to 0.40, corresponding to a payload weight of 3603 lb_m.

Table 9 also describes the Russian Proton launch vehicle. The vehicle was used to launch planetary probes and high altitude satellites[19]. This four stage booster has three NTO/UDMH propellant stages and a fourth liquid oxygen / kerosene stage. This launch system relies entirely on toxic, hypergolic, and cryogenic propellants. Unlike the Delta II, there are no solid rockets involved.

Vehicle	Stage	Propellant	I_{sp} (sec)	ΔV (ft/s)	M_P/M_o	M_{PL}/M_o	M_{Dry}/M_o
Delta II	9 SOS	Solid	259.5				
	1	LO$_2$/RP-1	278.0	18069.4	0.88	0.01	0.12
	2	N$_2$O$_4$/A-50	319.2	8067.5	0.54	0.17	0.29
	3	Solid	292.2	6369.4	0.49	0.46	0.05
Proton	1	N$_2$O$_4$/UDMH	291.5	8836.4	0.61	0.01	0.38
	2	N$_2$O$_4$/UDMH	327.0	11293.9	0.66	0.02	0.32
	3	N$_2$O$_4$/UDMH	325.0	11610.8	0.67	0.07	0.26
	4	LOx/Kerosene	352.0	11902.6	0.65	0.25	0.10

Table 9: Examples of operational booster rocket systems.

Figure 4 shows the Proton performance for each of the four stages. Due to a larger number of stages, the lower DV requirements for each, and the lower payload mass fractions, NOP rocket appears to be able to accomplish the mission of each of the first three stages. NOP cannot produce the required DV for the fourth stage with the given payload mass fraction of 0.25. NOP can, however, produce this DV for a payload mass fraction of 0.17, corresponding to payload weight of 7001 lb_m, as compared to the Proton's current maximum payload of 10384 lb_m.

27

Figure 5 shows a plot of the mass fractions for all of the cases considered for is launch vehicle trade study. It is seen that systems with greater mission capabilities correspond to lower dry weight fraction and higher propellant weight fraction.

In conclusion, the analysis for launch vehicle missions shows that the NOP propellants can be used for this application. Use as a first stage propellant can be realized for larger boosters with four or more stages, where the DV for the first stage is not excessively high. Use for upper stage applications and transfer orbits to GEO or planetary missions are also possible. Increased use for first stage applications can be accomplished by combining NOP with strapped on solid rockets, such as is done on the Delta II. Increased payload weight fraction for upper stage applications can be accomplished through design adjustments to lower the tankage factor for the NOP rocket.
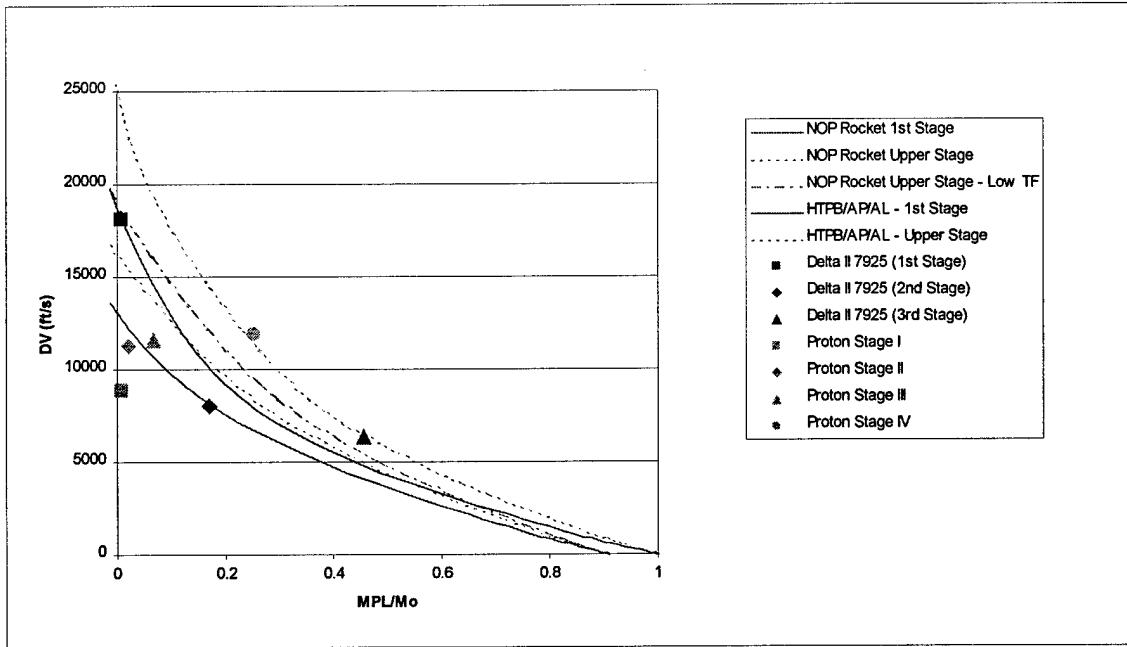
Figure 4: Performance trades for booster rockets
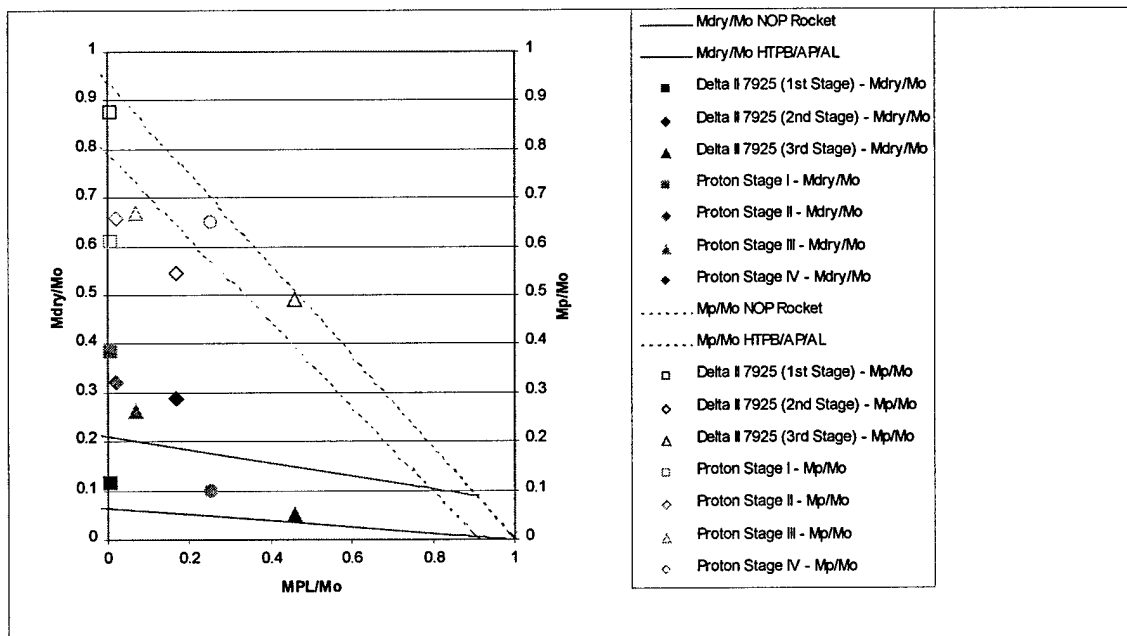
Figure 5: Mass breakdown for booster rockets

6.2 Space Propulsion

Space propulsion missions fall into one of several categories including orbital maneuvering, reaction control, and attitude control. These missions can be described in terms of DV and mass fractions. The DV requirements are determined by orbital mechanics for each particular maneuver and are multiplied by the quantity of each maneuver to determine the overall DV requirements. Space propulsion systems are generally volume constrained and operate with high payload and dry mass fractions.

Orbital maneuvering missions include all those in which the shape of the orbit is changed by the addition of an impulse from an orbital maneuvering system (OMS). These missions range from large orbit changes required for transition from LEO to GEO or from LEO to interplanetary transition orbits, to small changes in orbit shape at LEO. Transition to geosynchronous orbit was already covered under Section 6.1 and will only be discussed here in general terms. DV requirements for transition from LEO to GEO can be as high as 14250 ft/s. Transition from LEO to a Mars flyby can be as high as 10770 ft/s. Large transitions such as these are generally performed only once. It is therefore common to use solid propellants since these would give the lowest dry weight and are the simplest systems for single use applications.

Smaller orbital maneuvers can range between 2218 ft/s and 7920 ft/s, and might be performed multiple times in the life of a satellite. For these systems, bipropellants might be used if multiple applications are required and solids if single applications are required. Mission requirements for specific orbital maneuvering missions are presented in Table 10.

The reaction control mission involves small orbital corrections that are required over the multi-year life of an orbiting satellite. Estimates of total DV requirements for a seven year mission are shown in Table 10. Since the individual impulse bits are small and the total DV requirements are low, reaction control missions are usually accomplished with a monopropellant rocket. Monopropellant and cold gas systems are advantageous over bipropellant systems due to their impulse precision and lower dry mass for small systems.

Attitude control also requires highly precise impulse bits and may require even lower total DV than reaction control. The impulse bit precision mandates the use of cold gas thrusters. Missions such as this, with low propellant mass requirements, favor systems with low fixed mass such as the cold gas thruster.

		ΔV (ft/s)	ΔV (km/s)
OMS	LEO to GEO	14256	4.5
	LEO to Mars flyby	10771	3.4
	20 deg. orbital shift	2218	0.7
	20 deg orbital shift	7920	2.5
RCS (7 years)	N/S variations ±0.1 deg	1109	0.35
	E/W variations ±0.1 deg	95	0.03

Table 10: Typical DV requirements for space applications

Table 10 shows information used to construct a trade study for a variety of space propellant candidates. It should be noted that fixed mass fraction for the cold gas thrusters is lower than that for monopropellants and is nearly a third of that for bipropellants. Figure 6 and Figure 7 show predictive curves for performance of these propellants in space. The order of performance naturally ranges from cold gas thrusters on the low end to bipropellants and solid propellants on the high end.

Performance predictions for the orbital maneuvering mission are shown in Figure 6. The horizontal bar representing orbital maneuvering from LEO to GEO is crossed by all of the bipropellant and solid propellant rockets and by two of the monopropellant rockets. The same is the case for the interplanetary maneuvers represented by a LEO to Mars burn. These missions can be satisfied with adequate payload mass fractions only by the bipropellants and solids. Small orbital shifts in the range represented by two horizontal bars in Figure 6 labeled 20° orbital shift, can be accomplished satisfactorily by all of the monopropellants as well as the bipropellants and solids. Such missions might be best suited for the monopropellants since those systems take up less room than bipropellants, an important consideration for the volume constrained spacecraft.

The reaction control mission is also represented by a horizontal bar in Figure 6. This mission can best be met by the monopropellants when considering payload weight fraction, impulse precision, and system weight. With somewhat lower payload weight fraction, the nitrous oxide cold gas thruster can also be used for reaction control. This is not the case for the nitrogen and helium cold gas thrusters due to their lower density specific impulse.

The cold gas thrusters are best suited for the attitude control mission, which is not shown in Figure 6. Nitrous oxide would be the best choice for cold gas thruster propellant. Added benefit could be drawn by use of nitrous oxide in a multi-modal system in which nitrous oxide would also be used as a monopropellant and oxidizer for a bipropellant.

	I_{sp} (sec)	TF	M_{Fixed}/M_o
NOP	312	0.153	0.049
NTO/MMH	336	0.047	0.049
HTPB/AP/AL	287	0.07	0
Hydrogen Peroxide	187	0.042	0.042
Hydrazine	230	0.074	0.042
Nitrous Oxide – Mono	192	0.139	0.042
Helium	158	12.8	0.017
Nitrogen	68	1.83	0.017
Nitrous Oxide - Cold	60	0.158	0.017

Table 11: Space Propulsion trade study information

Also shown in Figure 6 are data points for two actual spacecraft; the Viking I orbiter and the Integrated Apogee Boost Subsystem (IABS).

The Viking project consisted of two separate spacecraft launched to explore Mars. Viking 1, launched on August 20, 1975 and Viking 2 launched on September 9, 1975. Each spacecraft contained an orbiter and a lander. The Viking Orbiter used a N_2O_4/MMH bipropellant liquid fueled rocket engine, providing 297 lb_f of vacuum thrust, for a ΔV=4854 ft/sec, and a vacuum I_{sp} of 291 sec. System mass information is given in Table 12. It is clear from Figure 6 that such a mission could also be accomplished using NOP propellants, as well as some monopropellants.

The other mission scenario used in the NOP Rocket Propulsion Trade Study was an Integrated Apogee Boost Subsystem (IABS). This subsystem uses a R-4D rocket engine, with two N_2O_4/MMH bipropellant liquid fueled rocket engines, providing 220 lb_f of vacuum thrust, for a ΔV=17,568 ft/sec, and a vacuum I_{sp} of 312 sec. System mass information is given in Table 12. Figure 6 indicates that this mission is only achievable using the N_2O_4/MMH bipropellant and a solid propellant. The ΔV requirement and payload weight fraction are too high for the NOP rocket.

Figure 7 shows the mass fractions for NOP, the solid propellant, and the Viking and IABS systems.

Mission	M_o (lb_m)	M_b (lb_m)	M_{DRY}(lb_m)	M_p (lb_m)	M_{PL}(lb_m)	M_{FIXED}(lb_m)
Viking I	5084	493.4	443	3137	1504	N/A
IABS	3479	606	365	2873	241	230

Table 12: Component weights for given spacecraft

6.2.1 Multi-modal Operation

Additional overall performance benefits can be achieved with the use of a multi-modal propellant system. Use of the same propellants for all missions would eliminate the dry weight overhead of multiple propellant systems. This is indeed achievable using NOP. A NOP multi-modal system would consist of a nitrous oxide – propane bipropellant rocket for orbital maneuvering, a nitrous oxide monopropellant rocket for reaction control, and a nitrous oxide cold gas thruster for attitude control. A quantitative analysis of the benefits of a multi-modal propellant system are not shown here. This topic is discussed in more detail by Zakirov[12,13].
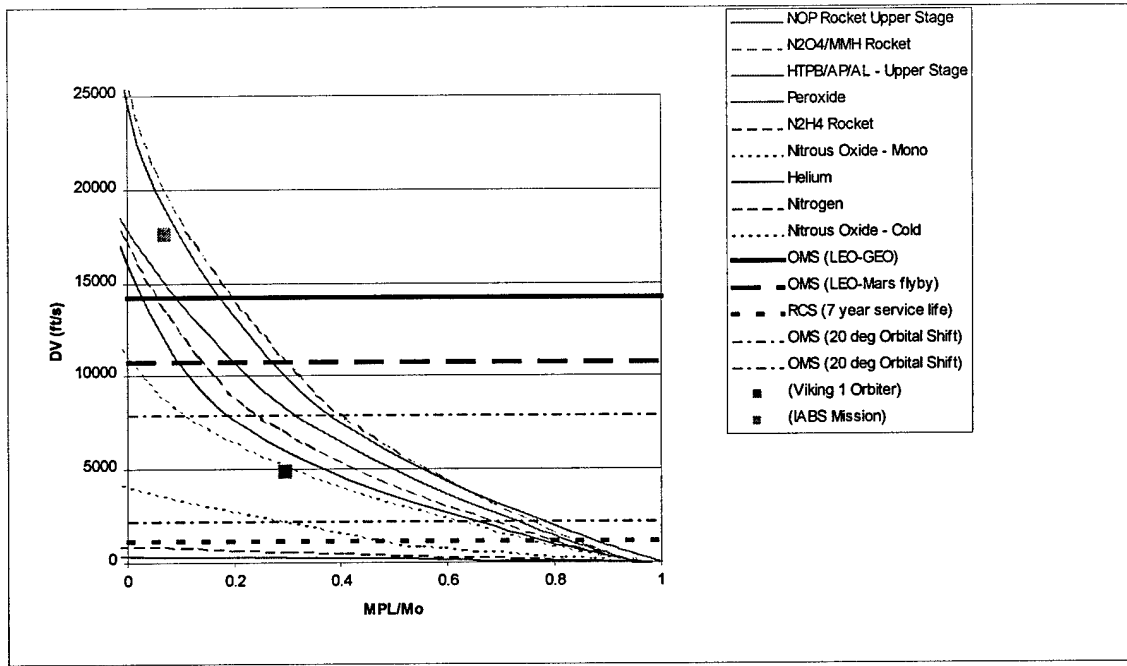
Figure 6: Performance trade for space propulsion
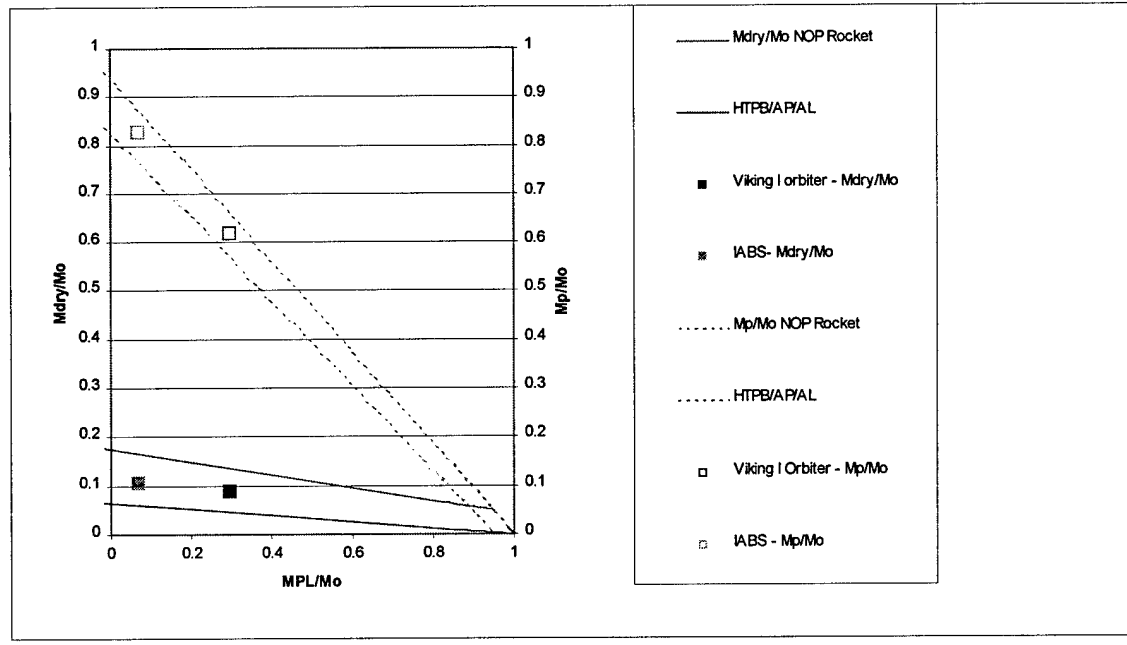
Figure 7: Mass breakdown for space propulsion

6.3 BMD

The BMD and NMD programs are currently evaluating a variety of interceptor concepts with different missions ranging from low-altitude endgame intercepts of short-range and intermediate-range ballistic missiles (SRBMs/IRBMs), to high-altitude intercepts of intercontinental ballistic missiles (ICBMs). Each of these concepts has different performance requirements depending on response time, planned engagement range and altitude, and other factors. In order to bracket the set of possible mission requirements, it has been concluded that calculations will be performed for hypothetical interceptors with DV's of 1, 2.5, and 6 km/s, depending on available response time and required range gate.

The 1.0 km/s mission corresponds approximately to the edge-of-envelope for a low altitude intercept (e.g. 25 - 40 km) with a battle timeline of 40 - 75 seconds against a ballistic threat (5.5 km/s incoming). The 2.5 km/sec mission corresponds approximately to the edge-of-envelope for a medium altitude intercept (e.g. 75 - 125 km altitude and 150 - 250 km downrange) with a battle timeline of 100 - 150 seconds against a ballistic threat. The 6.0 km/sec mission corresponds approximately to the edge-of-envelope for a high altitude intercept (e.g. 300 + km altitude and 1000 + km downrange) with a battle timeline of 300 - 500 sec against a ballistic threat with launch at apogee.

Figure 8 shows performance predictions for NOP and solid propellants, as well as the DV requirements described above. NOP appears to be an option of low to medium altitude interceptors. Hypergolic bipropellants and solid propellants might be better suited for high altitude interceptors. For Naval BMD and NMD systems based on board ships, the comparative ease of handling the effectively non-toxic propellants may offset the disadvantage of any weight penalty.
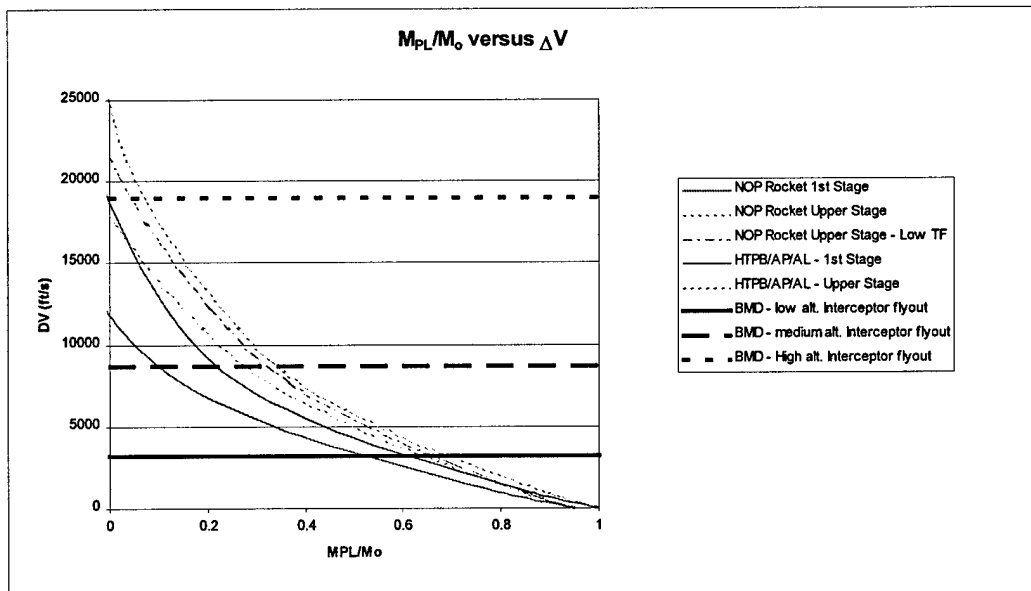
Figure 8: Performance trade for BMD propulsion systems

35

6.4 UAV

Unmanned aerial vehicles (UAV) generally use airbreathing propulsion systems for normal operations. Takeoff and landing are performed in a number of different ways including hand-launch, catapult, VTOL (for rotorcraft), standard runway TOL, and rocket assisted takeoff (RATO). The longest serving UAV in the U.S. military, the RQ-2A/Pioneer takes off from Navy ships using a RATO system. Although most RATO systems utilize solid propellants, it is also possible to use nitrous oxide, either as a monopropellant or bipropellant system for such a mission. Nitrous oxide could also be used with solid propellant as a hybrid propulsion system.
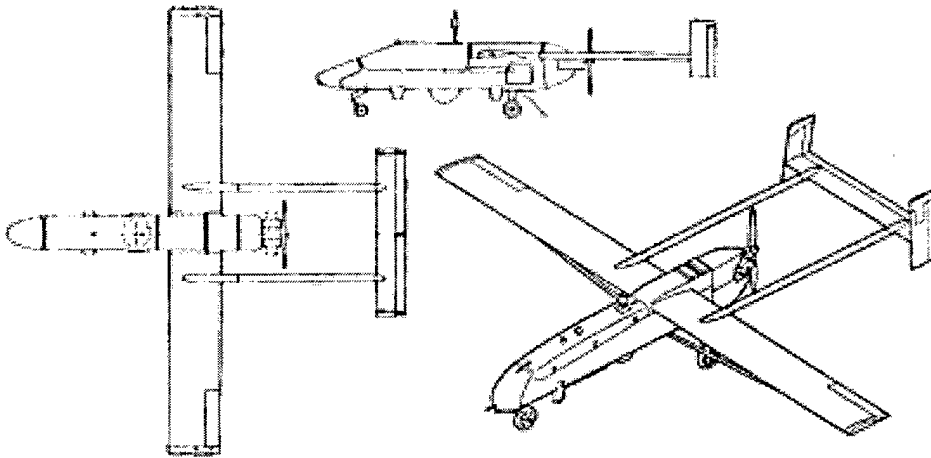
Figure 9: Pioneer UAV Inc., RQ-2A/Pioneer

6.5 Catalytically Decomposed N_2O as a Torch Igniter

Due to its exothermic decomposition characteristics, N_2O can be used as a torch igniter for various applications, such as an igniter and pilot for hypersonic air-breathing engines or a high altitude relight igniter for an aeropropulsion gas turbine.

Figure 10 shows a schematic of typical flame stabilization characteristics as a function of equivalence ratio and Ozawa's stability correlation parameter[20] that depends on static pressure P, atmospheric pressure P_o=1 atm, flow velocity at the flameholder V, an effective dimension ratio d_e/d, and the mixture total temperature, T_{to}. Using the relation between equivalence ratio and the stability correlation parameter (as defined in Figure 10), we notice that an increase in the mixture total temperature and static pressure results in stable high-speed combustor conditions over a wider range of equivalence ratios. Catalytically decomposed N_2O can improve this stability parameter in many cases since it introduces a hot gas plume (up to 2988 °F) at relatively high pressures, thus decreasing the stability correlation factor for a given equivalence ratio. These characteristics may find utility as a torch igniter or pilot for a hypersonic air-breathing propulsion system or high altitude relight capabilities for gas turbine engines.

Stability Correlation Parameter $\dfrac{V}{d}\dfrac{d}{d_e}\dfrac{P_o}{P}\left(\dfrac{1000}{T_{to}}\right)^{1.5}$
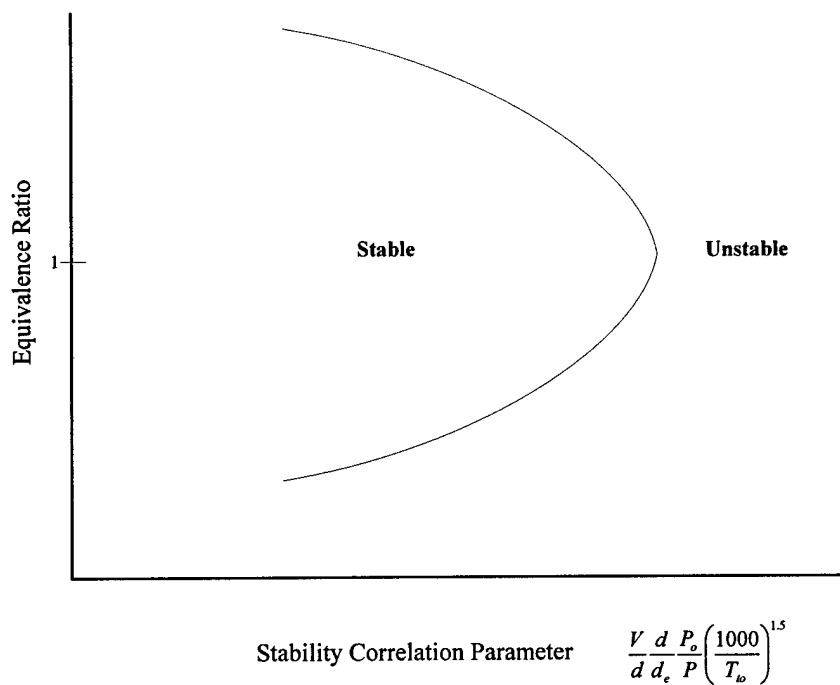
Figure 10: Schematic showing the equivalence ratio as a function of the stability correlation factor [Reference 2].

6.5.1 Hypersonic Air-Breathing Propulsion

The use of catalytically decomposed nitrous oxide may have a promising application as a torch igniter for hypersonic air-breathing propulsion systems. These propulsion systems operate in a number of different modes over the full range of flight Mach numbers from low supersonic Mach numbers to orbital insertion conditions. At low supersonic Mach numbers, ramjets provide highly efficient propulsive thrust with specific impulse 10 times that of a rocket engine. At Mach numbers above approximately 6, the ramjet is transitioned to a scramjet in order to avoid excessive inlet losses. Specific impulse decreases with increasing flight Mach number, although always remains significantly higher than that of rocket propulsion.

A major technology driver for these air-breathing engines is the ability to achieve complete and stable combustion over the wide range of flight conditions experienced by the engine. Figure 11 shows combustor entrance pressures and temperatures over a range of flight Mach numbers for a typical hypersonic air-breathing trajectory[21]. Air velocity through the combustor ranges from 2000 to 8000 ft/s over this Mach number range, with corresponding residence times on the order of approximately 1 to 0.1 millisecond. The combination of temperature, pressure, and short residence time serves to make combustion difficult at several points through the trajectory.

Methods of flame stabilization include providing adequate flameholder geometry, the use of chemical enhancement, catalytic combustion, and the use of pilots. Flameholder geometry must provide adequate residence time for a given quantity of fuel/air mixture to mix and burn in a recirculation region to provide a high temperature source and radical pool required for flame propagation. Designing flameholders for the tough spots in the flight trajectory results in excessively large obstructions which will result in high total pressure losses and corresponding performance decrements over all other flight conditions.

The use of chemical enhancements such as pyrophoric fuels is a possible solution although it introduces safety issues due to volatility and toxicity. Catalytic combustion is a current area of research which could prove promising in the near future.

Piloting flameholder regions is a workable solution, and one which need only be used for specific points in the trajectory and turned off for all others. The pilot could consist of localized injection of a monopropellant or the localized addition of energy through plasma or laser igniters.

In the low Mach number range, the low combustor makes combustion difficult for ramjet operation. Figure 11 does not show any trajectory information below Mach 3 since this is a common ramjet takeover condition. Low static pressure and low static temperature combine to prevent ignition and sustained combustion for most fuels at these conditions,

thus increasing the stability correlation parameter and promoting unstable combustion for a given equivalence ratio, Figure 10. The great loss here is that, thermodynamically, ramjet engines can operate at peak performance down to approximately Mach 2, a flight condition that is not practical for reasons discussed.
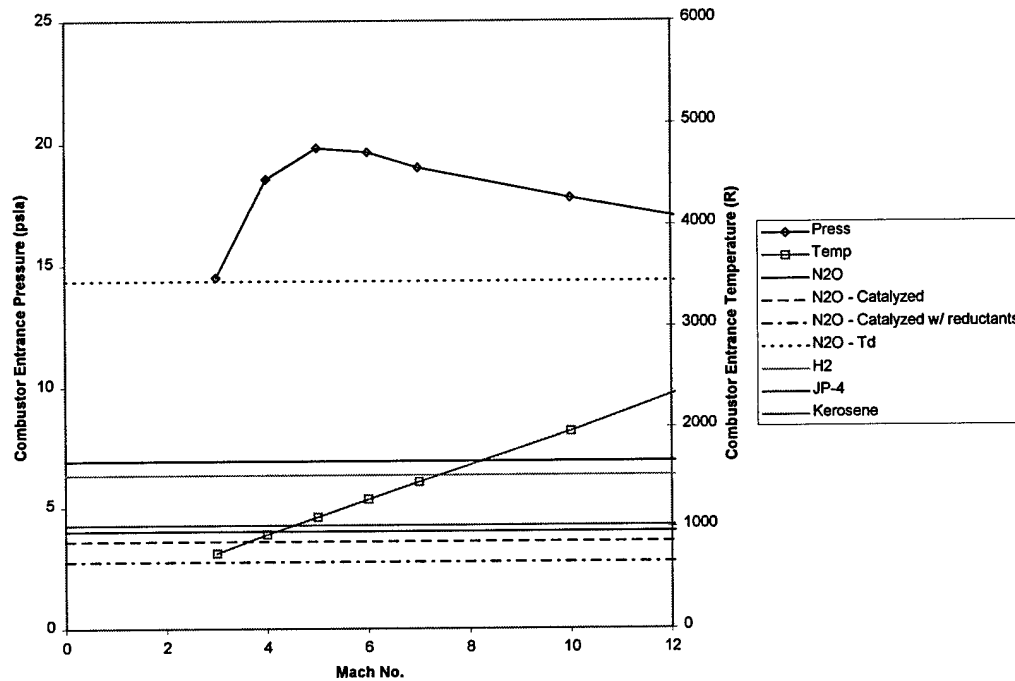

Figure 11: Typical air-breathing propulsion trajectory[21]

We propose here to use catalytically decomposed nitrous oxide as a pilot for ramjet combustion. Nitrous oxide, as previously mentioned, thermally decomposes at 1200°F, and can be catalytically decomposed using the Shell 405 catalyst at much lower temperatures. In particular, we have shown in the laboratory, catalytic decomposition at 400°F for pure nitrous oxide over Shell 405, and decomposition at approximately 200°F with the use of a reductant. These temperatures, as well as the maximum resulting decomposition temperature of 2988°F are also indicated in Figure 11.

Other horizontal bars in Figure 11 indicate autoignition temperatures for a few common ramjet fuels at ambient pressure. These temperatures range from approximately 500°F for jet fuels to over 1000°F for hydrogen, well within the temperature range of hot decomposed N_2O products. The required combustor inlet pressure is well within the catalyst reactor inlet pressures already tested (up to 60 psi). It is clear from this plot that catalytically decomposed nitrous oxide can be used as a torch igniter or pilot for ramjet combustion, making combustion at the low speed end more robust, and potentially

extending the operating range down towards Mach 2 where high efficiency can be realized.

As an example of such an application, consider Mach 2 flight at 40,000 ft. Free stream and typical combustor entrance conditions are shown in Table 13. Based on the range of flameholder schemes for kerosene combustion handled by Ozawa[20], a maximum stability correlation parameter of approximately 10,000 mandates a minimum characteristic flameholder width of 1.2 inches. This width requirement increases dramatically for non-stoichiometric fuel/air ratios. Flameholder widths on the order of several inches would dramatically reduce engine performance due to the associated total pressure loss.

	V (ft/s)	P (psia)	Pt (psia)	T (R)	Tt (R)
Free Stream	1936	2.7	21.4	390	702
Combustor Entrance	726	12.3	15.4	659	702

Table 13: Mach 2 Flight Conditions

To the contrary, flameholder piloting could reduce the stability parameter and therefore the required flameholder size. Since nitrous oxide piloting of the flameholder base regions would mainly affect the temperature term of the stability correlation parameter, we can simply calculate the effect on this parameter due to a range of nitrous oxide mass fractions. It can be seen by review of Figure 12 shows that a 15% nitrous oxide mass fraction would roughly halve the stability parameter. Coincidentally, this is also the mass fraction of nitrous required to achieve the autoignition temperature of kerosene.
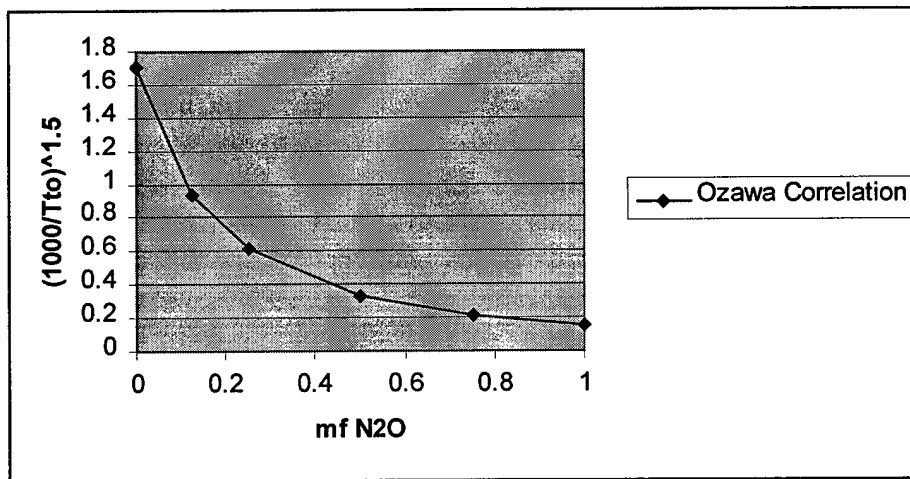
Figure 12: Effect of Nitrous Oxide Mass Fraction on Ozawa Stability Parameter for Mach 2 Flight Conditions

Piloting the recirculation regions of a flameholder would require very low flow rates of nitrous oxide. For a 25% blockage flameholder, the minimum mass exchange rate is 0.005 (or 0.5%). Of this 0.5% of the free stream flow, 15% mass fraction of nitrous would be required to halve the stability parameter. This corresponds to a minimum flowrate of 3.5x10-4 pps for a 1.2 inch wide flameholder. The chemical energy released by nitrous oxide decomposition corresponds to over 150 W of power provided to each flameholder recirculation region. Power requirements to run such a pilot system would be limited to that for the catalyst bed heater (on the order of 100 W). This compares favorably with kilowatt level power requirements for the plasma and laser igniter concepts.

In addition to extending the operating range for ramjet engines, the use of a nitrous oxide pilot can lower the minimum operating conditions for hydrogen and eliminate the need for pyrophoric additives such as silane. At slightly higher flight conditions (Mach 6-8) short combustor residence times and hydrogen ignition delay times combine to promote incomplete combustion. At these conditions, the addition of nitrous oxide and its subsequent decomposition could provide static temperatures capable of further shortening the ignition delay. Nitrous oxide pilot might also help promote stable combustion during mode transitions between ramjet and scramjet operation where the sudden loss of backpressure in the engine adversely changes the stability correlation parameter through a simultaneous increase in combustor entrance velocity and decrease in static pressure.

For takeoff and orbital insertion, rocket propulsion is required and may be integrated into a combined cycle engine. For such cases the nitrous oxide torch can be used as a rocket igniter in an identical fashion to that demonstrated in the nitrous-oxide/propane bi-propellant rocket development program. This simple igniter would replace more complicated systems such as the compression wave igniter (CWI) or hypergolic propellants.

6.5.2 High Altitude Relight

Another area of potential utility for a nitrous-oxide catalytic reactor is for a high altitude relight ignition system. At high altitudes gas turbine engines may experience flame out, i.e. extinction of the combustor flame. The in-flight flameout of a gas turbine engine is due to several factors, including the result of a reduction in air intake flow caused by certain aircraft maneuvers, or ingestion of contaminants released from self-propelled ordnance launched from the aircraft. Similarly, severe ice or large amounts of precipitation ingested into the engine could also lead to combustor flameout.

The first major effort to address gas turbine engine relight was conducted by the British in early 1956. They were successful in obtaining rapid relights, during icing conditions, by inserting a platinum glow plug into the combustor. The platinum rod is heated to incandescence during nominal engine operation, so that this heat is sufficiently maintained after flameout, thus allowing engine relight. It is also believed that the

catalytic effects of platinum upon mixtures of hydrocarbon fuels and air probably assisted in the relight process.[22]

During a study of a nitrous-oxide/propane bi-propellant rocket, funded by DARPA, a Shell-405, iridium based catalyst reactor was built and tested at an inlet pressure of 60 psia and was able to produce temperatures as high as 3000 °F at the exit. Such pressures and temperatures would be sufficient to relight jet fuel.

When flameout occurs the turbine ceases operation and the compressor also shuts down, resulting in a drop in pressure and temperature inside the combustion chamber. Initially this pressure and temperature is larger than the pressure and temperature at altitude. The maximum restart altitude[23] is 30,000 ft, where the static pressure and temperature are 4.373 psia and –47.83 °F, respectively. These pressures and temperatures allow for utilization of a nitrous oxide Shell 405 based catalyst reactor as a viable relight ignition system. The products of N_2O catalytic decomposition include hot nitrogen and oxygen. This additional oxygen into the combustor may not only serve as an igniter (due to its elevated temperature) but as an additional source of oxidizer, particularly useful at high altitudes where the air density has decreased substantially from sea level conditions.

Combustor lengths are designed for an engine "flame-out" condition, with an extra length of combustor required to increase the residence time for re-light conditions. We believe that nitrous oxide decomposition could be used to relight the gas turbine efficiently and reliably at low pressures and temperatures, resulting in shorter combustors and a weight savings for the engine. The addition of relatively high-pressure, hot, oxygen enriched air may also facilitate engine relight at higher altitude.

6.6 Mission Analysis Overview

Now that the NOP rocket system has been shown to be competitive for various mission scenarios, we proceed to discuss our design and development approach of such a rocket system.

7 Design and Development Approach and Overview

The work under this DARPA BAA 99-22 contract, dealt with a demonstration of the nitrous oxide / propane rocket to evaluate rocket performance and ignition using catalytic decomposition of nitrous oxide. The work began with two parallel efforts: the experimental evaluation of rocket performance using nitrous oxide and propane as propellants, and an experimental evaluation of various catalysts for the decomposition of nitrous oxide. Once these two efforts were completed, they were combined to demonstrate rocket ignition using the catalytically-decomposed nitrous oxide.

The initial rocket testing was performed using hardware and the rocket test stand from a previous program performed under an Alabama Space Grant, Test Stand 1, Figure 13.

Although the existing rocket hardware (NOP Rocket 1) was previously used with ablative combustor and nozzle inserts, the hardware was fitted with a non-ablative combustor liner and copper nozzle insert for testing. Modifications were also made to Test Stand 1 in order to minimize experimental uncertainty and improve operability.

The catalyst research was performed at the University of Alabama at Huntsville, (UAH), and was focused on obtaining a candidate catalyst for use in rocket tests and on finding the optimum catalyst material (or materials) for use in a future space-qualified prototype. This work showed that the Shell 405 catalyst successfully decomposes nitrous oxide with moderate light-off temperatures. Shell 405 catalyst has an extensive history of use in space as a hydrazine catalyst material.
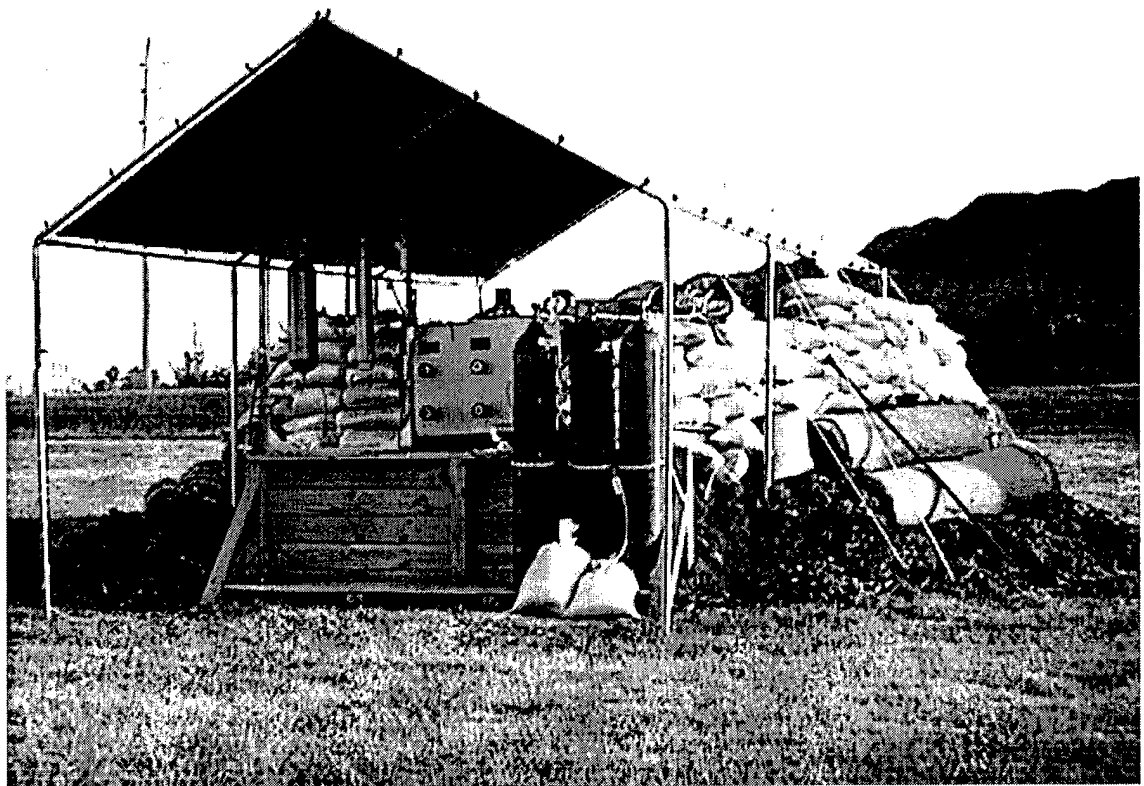
Figure 13: Photograph of Rocket Test Stand 1 at the Johnson Research Center at UAH.

Experiments to demonstrate rocket ignition using the catalytically decomposed nitrous oxide began in late January 2001. These rocket tests were performed using new rocket hardware (NOP Rocket 2) and a new atmospheric pressure test stand, (Test Stand 2). The new rocket hardware features a new fuel injection scheme, a copper heat sink design, and a nozzle design that is traceable to a full area ratio design that is verified by CFD analysis. Test Stand 2 features an improved thrust stand design and adequate room to

43

perform the planned pitot pressure surveys and radiometric measurements, conducted by AEDC.

In the following sections an overview of the design and development of the NOP Rocket 2 test article and Test Stand 2 will be the main focus. However, prior to NOP Rocket 2, a series of tests were conducted at Test Stand 1 at the Johnson Research Center at UAH, with the NOP Rocket 1 test article. Descriptions of Test Stand 1 and a brief discussion of the NOP Rocket 1 motor are also presented.

7.1 Rocket Design

The NOP rocket utilizes nitrous oxide (N_2O) as the oxidizer and propane (C_3H_8) as the fuel. The chamber pressure is 150 psia for this 50 lb_f rocket, and a fuel-rich propellant combination is used to maximize performance. According to common practice for space-based thrusters, a pressure drop between 20-30% of chamber pressure is taken across the injectors, requiring an injection pressure of approximately 180 psia. Since the vapor pressure of propane at 70 °F is only 109.6 psi the propane needs to be pressurized for this application. This is accomplished using nitrogen pressurant for the ground-based testing, and can be accomplished using the nitrous oxide as pressurant in space, via a suitable diaphragm.

To measure rocket performance using specific impulse (I_{sp}) and characteristic exhaust velocity (c^*), accurate measurements of thrust and propellant (fuel and oxidizer) flow rate are essential. Measuring the flow rate of N_2O and C_3H_8 requires using a subcritical venturi, with the fluid in the liquid state to avoid two-phase flow. In order to achieve this during the ground testing, both propane and nitrous oxide are pressurized to 1000 psia.

The nitrous oxide is injected as a two-phase fluid (-25 °F, 175 psia), while the propane is injected as a liquid (70°F, 195 psia). The rocket design involves: design of the injector for N_2O and C_3H_8, design of the combustor with an appropriate L^* (characteristic combustor length) and design of a rocket nozzle for sea level static conditions and space conditions.

Parameter	NOP Rocket 1	NOP Rocket 2
A_e/A^*	2.21	2.45
d^* (")	0.616	0.476
L^* (m)	1,2 3 (nominal L^*=3)	2, 3 (nominal L^*=3)
D_c (")	2.125	1.00

Table 14: Shown above is a comparison between NOP Rocket 1 and 2 for various selected parameters of interest.

44

The following sections briefly describe the work performed on the injector, combustor, and rocket nozzle.

7.1.1 Injector

The rocket injector design is probably the single most important component with regard to affecting engine stability and performance. The injector design for NOP Rocket 2 (NOPR2) was based on: (1) experience and knowledge gained from the initial series of rocket tests conducted in November, 1999 on the NOP Rocket 1(NOPR1) on Test Stand 1; (2) discussions with experts at GenCorp-Aerojet[24] and Sierra-Engineering[25]; and (3) ease of fabrication and cost effectiveness. This injector design was used during the Alabama Space Grant work and was carried over for this Phase I program. Plans for future development will include consideration of other injector designs, such as pintle designs.

Prior to testing the NOP Rocket 2 motor, work was already in progress on evaluating the NOP Rocket 1 test article in Test Stand 1. The injector scheme for the NOP Rocket 1 included a double coaxial swirl injector, with N_2O injected with a clockwise coaxial swirl, on the outside, while the C_3H_8 was injected with a counter-rotating swirl, on the inside. Because the injection velocity for the N_2O was approximately six times that of the C_3H_8 injection (depending on the "quality" of the propellants), the propane droplets were atomized by the swirling sheet of high angular velocity N_2O. The injector for NOPR1 is made of stainless steel.

The injector design for NOP Rocket 2, presented in Figure 14 and Figure 15, is a single element, coaxial (single) swirl injector, with liquid injection of propane and two-phase injection of nitrous oxide. Swirl tends to increase mixing and decrease the required characteristic combustor length L* and is generated by tangentially injecting the propellant off-center, with respect to the orifice through-hole. In general, swirl: (1) is better for mixing two flows and more simple than a showerhead injector design; and (2) swirl injectors operate over a wider range of conditions and are more forgiving than other types of injectors. As shown in Figure 15, the liquid fuel is injected into the inside orifice and the oxidizer is injected into the outside annulus, between the C3H8 injector tube and the sintered mesh. Initial consideration was given to a design with the fuel on the outside, coating the hot combustor walls (made of Glid-Cu, a Cu-0.15% alumina alloy) thus protecting the inner walls from any oxidation. However, injection of liquid propane in a narrow annulus is impractical, since the liquid propane surface tension leads to asymmetric injection. Although copper is not prone to oxidation, refractory metals such as columbium (commonly used for space applications) and tungsten are indeed vulnerable to oxidation.

Gaseous injection is preferred in order to operate the injectors in a choked mode, thus isolating any combustor fluctuations and "chugging" instabilities from the propellant feed systems. Gaseous injection also greatly reduces the required length for mixing and

burning since atomization and evaporation are not required. The current injectors are sized for two criteria[24]: (a) the liquid propane injector is sized for an injector pressure drop of $30\%P_c$, and (b) the two-phase nitrous-oxide injector is sized for a pressure drop of $20\%P_c$.

The liquid propane injector is designed for a nominal pressure drop of 45 psid at the orifice. For a nominal flow rate of 0.0149 lb_m/sec, at injection conditions of 70 °F and 195 psia, an orifice diameter of 0.032 in is required. A ¼" S.S. tube (0.194" I.D.) feeds into the 0.032" propane injector, which is offset 0.043" from the center of a 0.118" I.D. tube, generating a swirl component, Figure 15. The liquid propane is then injected into the combustor from the 0.118" I.D. tube at about 6 ft/sec.

The N_2O is fed through a 3/8" tube (.305" I.D.), and into a stagnation chamber, where the N_2O flow turns into a stainless steel sintered mesh material, obtained from Mott Metallurgical Corporation, Figure 14. The sintered mesh has a one micron porosity, sized to pass the required flow rate with the required pressure drop. The 0.118" I.D. propane tube is at the center of the sintered mesh disc. Approximately 75% of the N_2O flows through an annulus (with an area of ~0.039 in^2) between the mesh center hole and the liquid propane injector tube. Approximately 25% of the N_2O will flow through the porous sintered mesh, providing it with transpiration cooling. The N_2O injector is designed for a nominal pressure drop of 30 psid across the stainless steel sintered mesh material. The nominal N_2O flow rate through the annulus is 0.149 lb_m/sec, at -24°F and 175 psia.

The nitrous oxide exits the annulus at approximately 50 times the liquid propane injection velocity (286 ft/sec), thereby entraining and simultaneously atomizing the liquid propane sheet into droplets. This injector scheme has been designed to improve overall mixing and combustion efficiency.

Due to the modular design of the hardware, various injector designs can be tested with relative ease. The injector components, made of 303 stainless steel, can easily be exchanged for others that could mate with the combustion chamber using a common bolt pattern.

Figure 14 Photo of assembled N_2O and C_3H_8 modular injectors. The center orifice is the C_3H_8 injector concentric with the sintered mesh orifice. This annular region is designed to allow 75% of the total N_2O flow to pass through.
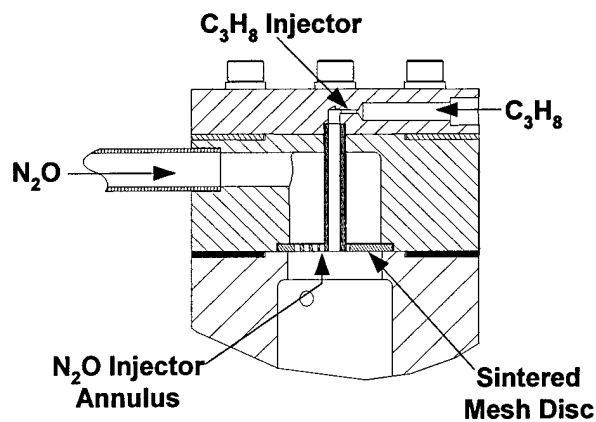
Figure 15: Injector design for N_2O and C_3H_8 used in NOP Rocket 2.

For future work, we plan to study several injector designs to optimize rocket performance and combustion efficiency, η_c. By improving mixing and burning we can also minimize

the required L*. This will minimize the combustor surface area over which viscous and heat losses act. Test results indicate nonideal performance as a result of these losses, Section 9.2. Various alternative injector geometries could also be studied in the future, such as like-unlike impingement, triplet, pintle injectors and even a premix arrangement.

7.1.2 Combustor

The NOP Rocket 1 test article has a nominal L* = 3 m, for a combustor geometry of 2.125" inner diameter and a nozzle A_e/A^* of 2.21, with a throat diameter of 0.616" and an exit diameter of 0.916". Various combustor designs with L*'s equal to 1, 2 and 3m for NOP Rocket 1, were evaluated on Test Stand 1, with the conclusion that the optimal L* was between 2m and 3m. A photograph of the NOP Rocket 1 test article is shown below in Figure 16, on Test Stand 1. The combustor overall length is 12.25".
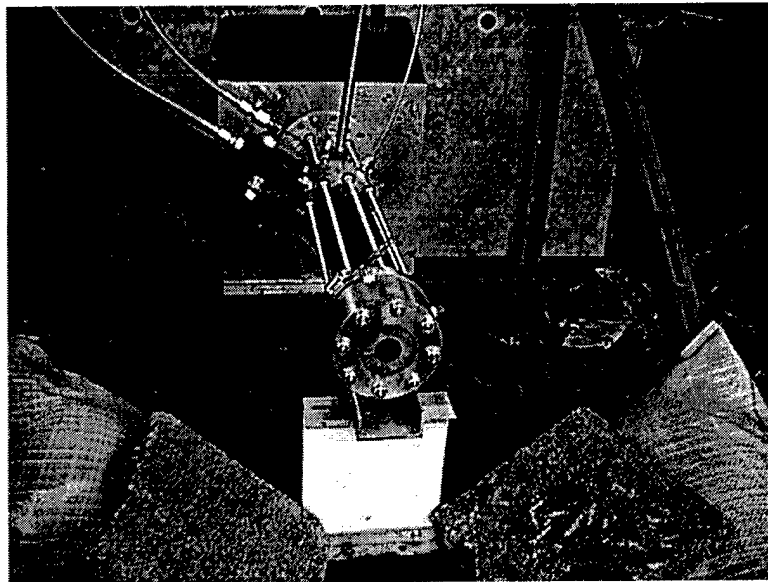
Figure 16: Photograph of NOP Rocket 1 motor shown mounted on Test Stand 1 at the Johnson Research Center at UAH.

The combustor design must provide for adequate mixing between fuel and oxidizer as well as provide sufficient residence time required to mix and burn the propellants efficiently. The area ratio on the subsonic side of the nozzle, for NOPR1 is 11.9 and for NOPR2 is 4.4, for a combustor Mach number of approximately 0.13. This area ratio was chosen as a compromise between residence time and velocity (which promotes atomization). The combustor for NOPR2 is made of Glid-Cu, a Cu-0.15% alumina matrix alloy, and carbon-steel for NOPR1.

Figure 17 shows the assembled NOP Rocket 2 motor, with the combustor, injector and nozzle sections integrated. The combustor section contains three pressure taps,

measuring injection pressure just downstream of the injector, combustor pressure and a nozzle base pressure.
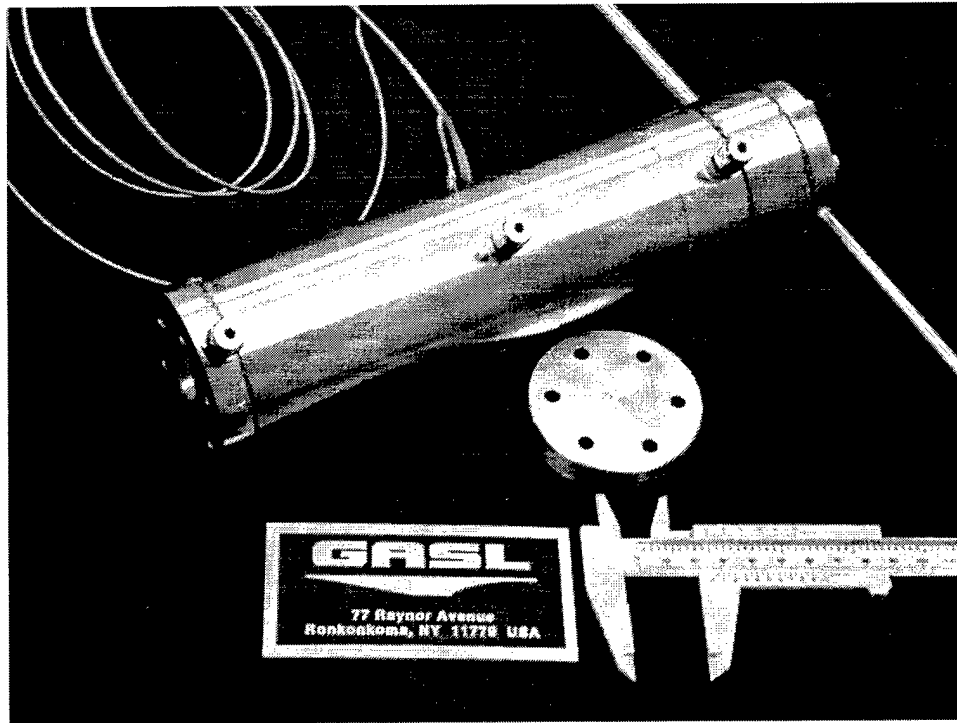
Figure 17: Photo of the assembled NOP Rocket 2 showing the injector in the upper right, the combustor with two pressure fittings and the nozzle with a base pressure fitting shown.

Selection of the appropriate combustor length L* was based on testing done at the University of Alabama at Huntsville with the NOP Rocket 1 design. The criterion for combustor length selection is maximum c* efficiency, where c* efficiency η_{c*}, is defined as:

$$\eta_{c*} \equiv \frac{P_c A^* / \dot{m}}{c^*_{theoretical}} \qquad (7\text{-}1)$$

where $c^*_{theoretical}$ is obtained from a NASA chemical equilibrium program[34] and is a function of P_c, γ, mixture ratio and reactant composition.

A characteristic combustor length L* is defined as the length that a chamber of the same volume would have if it were a straight tube with cross sectional area A* and had no converging section:[26] L* is given by:

49

$$L^* \equiv \frac{V_c}{A^*} \qquad\qquad (7\text{-}2)$$

where V_c is the combustor chamber volume ($\pi D_c^2 L_c/4$), L_c is the combustor geometric length, D_c is the combustor diameter and A^* is the nozzle throat cross-sectional area.

7.1.3 Nozzle

The nozzle design for NOP Rocket 1 utilizes a 2.21 area ratio with a 0.616" diameter throat and a 0.916" exit diameter. This nozzle is fabricated from oxygen-free copper.

The rocket nozzle design procedure for NOP Rocket 2, was based on the method described in Hill & Peterson[27]. The method starts by defining the required thrust or thrust coefficient (C_{Tv}). Then, based on the work of Ahlberg et al.[28], the optimum nozzle can be obtained by truncating the length of an ideal (uniform exit flow) nozzle. The nozzle length is truncated in order to optimize the thrust with wall friction for a given friction coefficient. For the current design, the required thrust is 50 lbs$_f$. The area ratio for the untruncated nozzle is 160. The "Noz_Code" software, developed at GASL, Inc., was used to design the nozzle wall contour using the method of characteristics. As suggested by Hill & Peterson[27], the resulting wall contour was not corrected for displacement thickness since the effect is small in the truncated nozzle. The nozzle is then truncated according to the plot by Ahlberg[28]. To verify the design, a CFD calculation using the GASP software tool[29] was carried out using both finite-rate chemistry as well as frozen chemistry. For finite-rate chemistry, the CFD solution yielded a thrust of 51.15 lbs$_f$. For frozen chemistry, the thrust was 50.84 lbs$_f$.

Figure 18 displays CFD solutions, generated using the GASP software[29], for the nozzle design for NOPR2. The nozzle throat diameter is 0.476 in. As shown in Figure 18, the profiles of velocity, Mach number and pressures show nonuniformity at the exit plane. The combustor length, L* was finalized based on experimental testing of the NOP Rocket 1 for Phase I, at Test Stand 1.

For sea level conditions, the nozzle is truncated at an area ratio, A_e/A^* of 2.45 for the supersonic region, to achieve perfect expansion to the ambient conditions. This configuration was tested at the rocket Test Stand 2. A photograph of the truncated nozzle is shown in Figure 19. The full nozzle configuration would require a vacuum chamber for testing. Table 15 summarizes the rocket design for NOP Rocket 2 for both sea level and vacuum conditions.
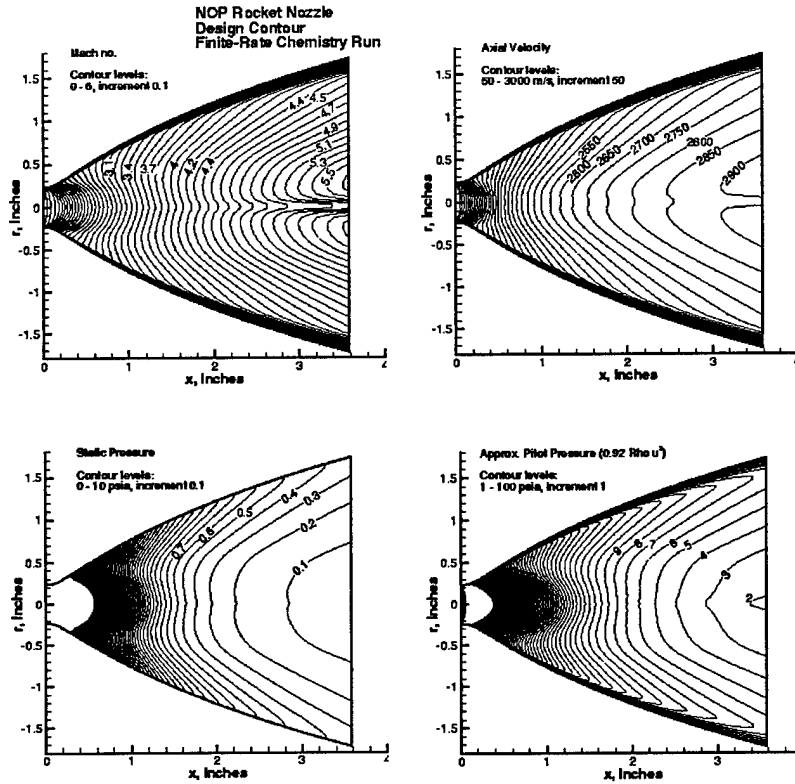
Figure 18: Contour plots of static and total pressure, Mach number and axial velocity obtained from CFD analysis using the GASP software.

	Sea Level	Vacuum
Chamber Pressure, P_c (psia)	150	150
Total Propellant $\dot{m}$ (pps)	0.164	0.164
Mixture Ratio	10.0	10.0
L_c (in)	8"	TBD
Throat Area, A* (in^2)	0.178	0.178
A/A* (subsonic)	4.4	4.4
A/A* (supersonic)	2.45	50

Table 15: NOP Rocket 2 Design Parameters

The subsonic A/A* = 4.4 refers to a typical contraction ratio for the combustor area to throat area[27]. One Dimensional Equilibrium analysis, Figure 20, shows that the vacuum specific impulse attains a maximum of 314 sec at an area ratio of A/A*=50, with a thrust coefficient of about 1.8 for a mixture ratio of 10.0, Figure 20.

51

Figure 19: Photo of the truncated rocket nozzle design (copper heat sink) for NOP Rocket 2.
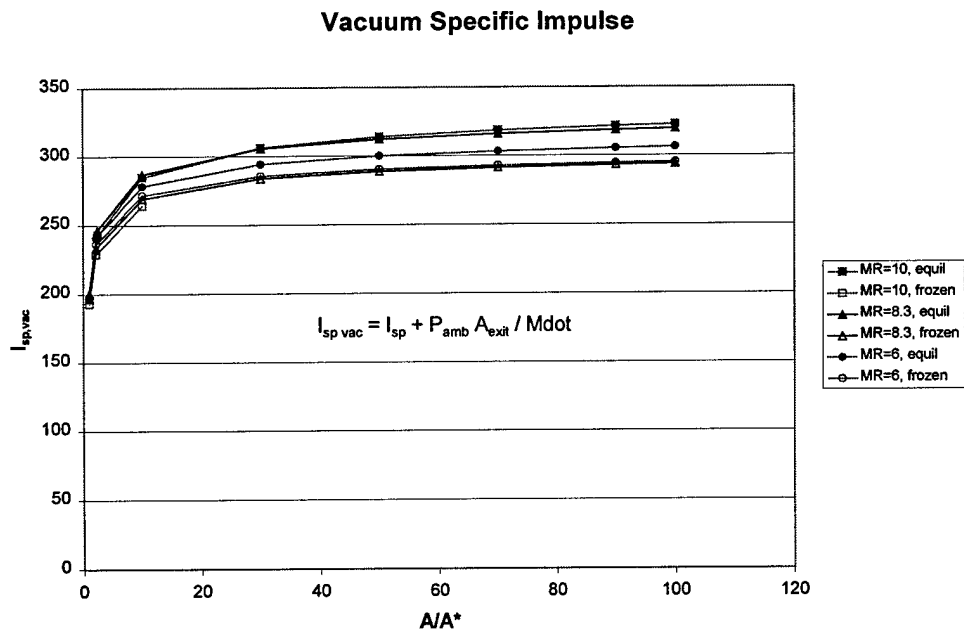
Figure 20: Vacuum specific impulse as a function of nozzle area ratio for various mixture ratios, for both equilibrium and frozen flow calculations.

52

The concept being tested utilizes decomposed N_2O (i.e., a high temperature mixture of N_2, O_2 and N_2O) as a pilot to ignite the propane fuel. Chemical kinetics calculations using LSENS and GASP[29] software, were performed to determine the rates of the combustion reactions.

Figure 21 shows the ignition delay time as a function of decomposed N_2O fraction, where the ignition delay is not a strong function of mixture ratio, but is inversely related to percentage N_2O conversion. The percentage of N_2O conversion is a function of the catalyst performance and is controlled by the catalyst length and residence time. Since the autoignition temperature of propane is only 874°F, at least 40% nitrous oxide decomposition is required to ignite the fuel (Figure 21).
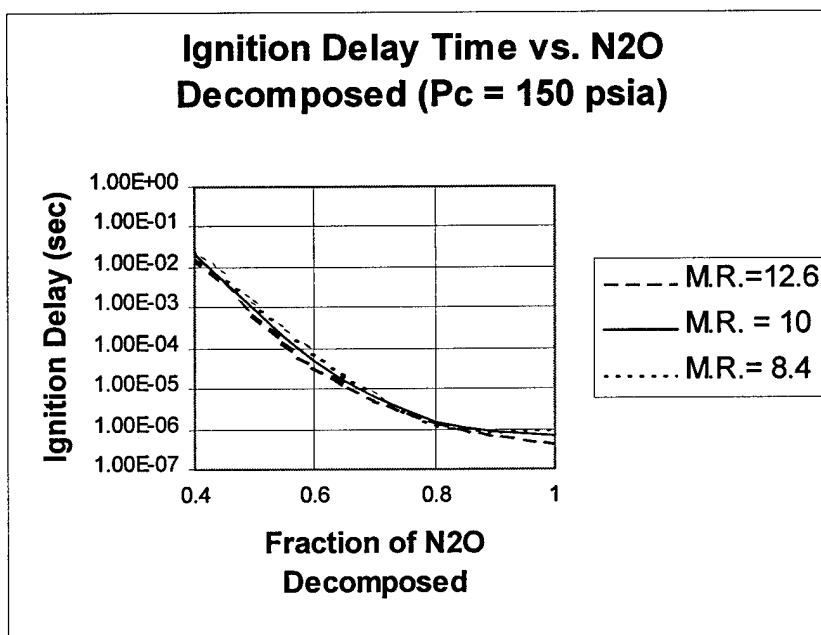
Figure 21: Ignition delay time versus fraction N_2O decomposed, for various M.R.'s.

In an effort to better understand the rocket nozzle physics for NOPR2, a CFD analysis was performed using the GASP software,[29] as discussed above, as well as a NASA chemical equilibrium code[34] analysis. Numerical results for pressure and temperature as a function of axial location in the supersonic portion of the nozzle are presented below in Figure 22-Figure 23.

Figure 22: CFD results for the axial distribution of pressure in the nozzle for NOP Rocket 2. The nozzle is truncated at x=0.317" for sea-level testing. Note that x=3.41" corresponds to A_e/A^*=50 for vacuum testing.

Figure 22-Figure 23 show that an equilibrium analysis (as provided by the NASA chemical equilibrium code[34]) matches the more realistic finite rate chemistry approach to nozzle analysis (as provided by GASP[29]) better than the frozen flow assumption. This result simplifies the rocket performance analysis, Section 9.2, since realistic nozzle physics can now be described by an equilibrium approach, using the NASA code,[34] as opposed to the more computational intensive finite rate chemistry approach using GASP.[29]

NOP Rocket Nozzle
(Pc=150 psia)
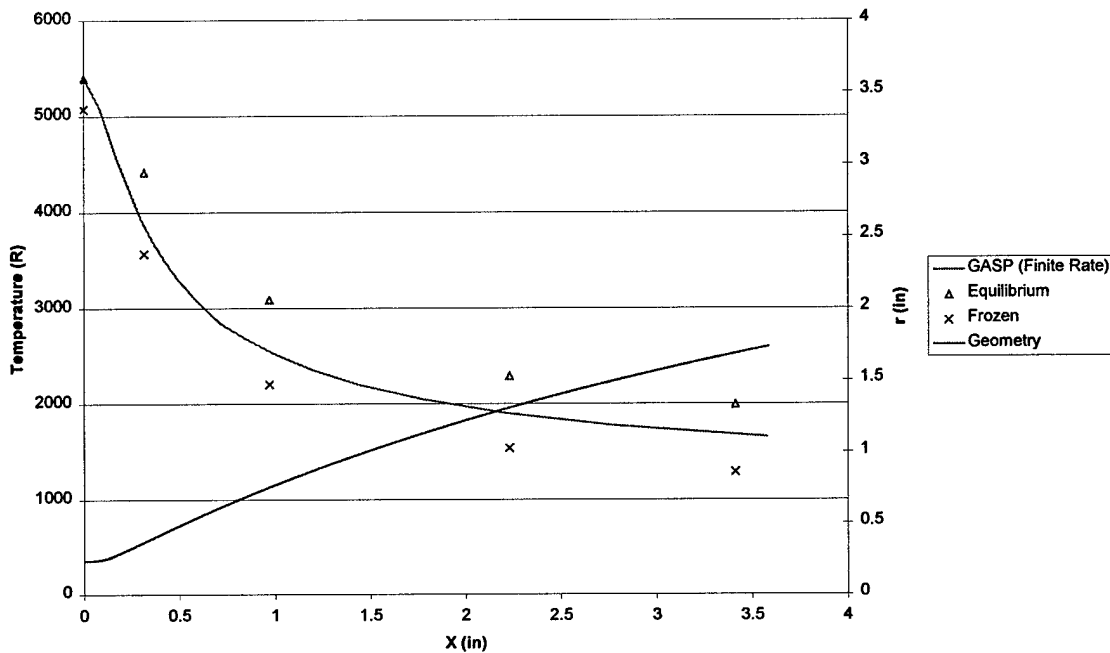
Figure 23: CFD results for the axial distribution of temperature in the nozzle for NOP Rocket 2. The nozzle is truncated at x=0.317" for sea-level testing. Note that x=3.41" corresponds to $A_e/A^*=50$ for vacuum testing.

7.2 Rocket Test Stand

Work has been performed using an existing atmospheric test stand (Test Stand 1), which was used for the Alabama Space Grant work. A new rocket test stand (Test Stand 2) was designed and constructed for rocket performance and rocket ignition testing using the catalytic N_2O decomposition reactor as an ignition source. This new rocket test stand features palletized propellant systems, improved propellant system instrumentation, an improved, more robust thrust stand, and adequate room for the rocket exhaust pitot survey equipment and radiometric measurements performed by AEDC.

The new experimental set-up for Test Stand 2 is designed to obtain more accurate measurements of thrust, propellant mass flow rates, chamber pressure, propellant system pressures and temperatures, as well as catalytic reactor pressure and exit temperature, than Test Stand 1. The following subsections describe Test Stand 2 in more detail.

7.2.1 Layout

The new rocket test stand, Test Stand 2 is situated on the UAH campus, next to the Test Stand 1, see Figure 13 and Figure 24. The rocket engine and palletized propellant systems are encased in a steel reinforced concrete bunker to provide adequate safety for operation on campus.
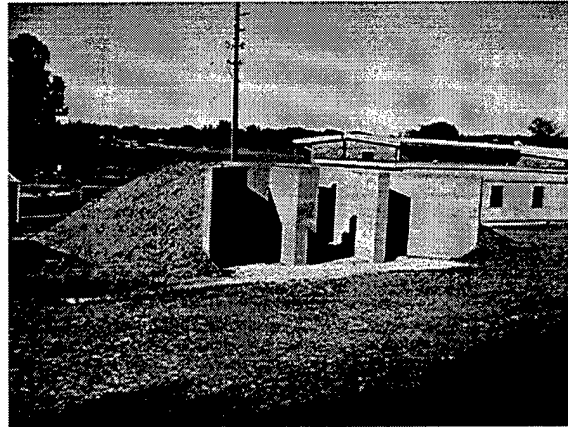
(a)
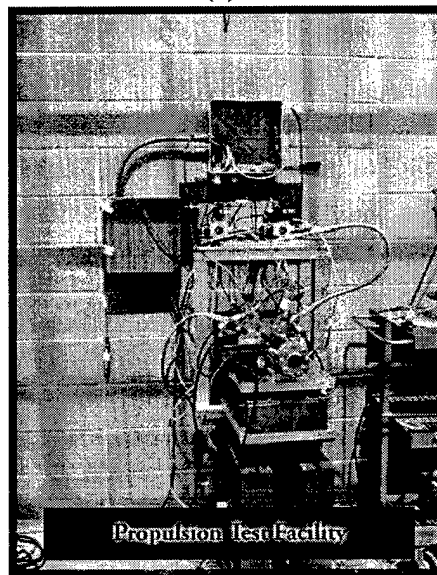
(b)

Figure 24: (a) Test Stand 2 during initial construction at the Johnson Research Center at UAH, and (b) newly operational thrust stand.

Schematics and photographs of the palletized propellant system are shown below in Figure 25 (a)-(d). Note that both the nitrous oxide and propane systems are similar in layout, except for minor differences in venturi size, metering valve size, and storage tank

volume. The idea behind using the palletized approach is to add some modularity to the facility in the event of future work.

The basic idea behind the propellant system layout is to provide the user with a safe and self-contained methodology for loading and pressurizing N₂O and C₃H₈ for use in the ignition circuit (spark ignition or catalyst reactor) and rocket engine feed-systems. The propane and nitrous oxide are first loaded into their respective run tanks, (labeled 'T-2' in Figure 25). Tank T-1 is a nitrogen pressurization tank, that is used to further pressurize the N₂O and C₃H₈ run tanks (T-2), to ensure that both propellants are in the liquid state at least through the venturi, thus assuring accurate mass flow rate measurements, Section 7.2.2. The propellants experience a large pressure drop through the metering valve, ($\Delta p \sim 400$-700 psi), which adjusts the flow to provide the required ΔP across the injector, Section 7.1.1. There are various type 'K' thermocouples and pressure transducers located throughout the system. A nitrogen purge circuit is also used to purge the lines before and after the rocket firing sequence is engaged.

(a)

(b)

(c)

(d)

Figure 25: Shown above: (a) is a schematic of the N₂O oxidizer system, (b) and (c) are photographs of the N₂O pallets, and (d) the NOP Rocket 1 on the thrust stand.

The fuel and oxidizer systems are separated by two cinderblock walls and are both separated from the rocket compartment. Fuel and oxidizer are brought together in the rocket compartment where the catalytic reactor will be mounted. The rocket is mounted on a thrust stand, and is connected to the propellant system by flex lines only, Figure 25 (d).

7.2.2 Measurements

Measurements are made of rocket thrust, propellant mass flow rates, chamber pressure, and a variety of system pressures and temperatures.

To measure rocket engine thrust, a new thrust stand was designed and fabricated at GASL, Inc. The thrust stand is shown schematically in Figure 26 and in a photograph in Figure 25(d) and Figure 27. The engine is mounted on a pendulum-type stand, supported by flexures. The thrust stand is designed to isolate any induced vibrations in the system and transmit only the engine thrust through the load cell. We are using a SENSOTEC Model 43 compression-only load cell, which is a "pancake" type load cell and has a 0-100 lb$_f$ range with a 4-20 mA output to increase S/N ratio. A dead weight calibration system is integrated into the stand. Traceable weights are used for calibration, providing a preload on the load cell. There are no hard pipe connections to the stand; all

59

connections are made with flex-hoses perpendicular to the thrust direction, to minimize any nonlinear resistive forces that may affect thrust measurements.

The N_2O and C_3H_8 flow rates are measured in the liquid state using an unchoked venturi. The following equation is used:

$$\dot{m}(pps) = \left(\frac{C_d A_{geom}(in^2)}{12}\right)\sqrt{2g_c \Delta P(psia)\rho(lb_m/ft^3)} \qquad (7\text{-}3)$$

Based on Equation (7-3), to measure flow rate a differential pressure transducer is required for each venturi, as well as a static temperature and a total pressure measurement upstream of the venturi throat. Since the state of the propellant is liquid, curves showing density as a function of upstream venturi temperature for various upstream venturi pressures were generated. Thus, to obtain mass flow rate, three measurements are required: upstream static temperature, upstream static pressure and pressure differential, Δp, across the venturi. A discharge coefficient of $C_d = 0.995$ is used, in accordance with ASME MFC-3M-1989[30]; however, the discharge coefficient can also be measured through calibration. The venturi diameters for measuring N_2O and C_3H_8 flow rates are d=0.115" and d=0.054", respectively. The venturis were sized to provide a pressure differential of about 25 psid for a nominal N_2O flow rate of 0.233 lb_m/sec and nominal C_3H_8 flow rate of 0.043 lb_m/sec.

All system pressures are measured with SENSOTEC transducers and all temperatures are measured with OMEGA thermocouples (type K).

Measurements of thrust, flow rates, system pressures and temperatures allow rocket performance parameters, such as specific impulse I_{sp}, and characteristic exhaust velocity, c^* to be calculated. In addition to these measurements, AEDC will perform an independent determination of thrust using a rocket exhaust pitot survey. Also, AEDC will conduct radiometric measurements that involve UV-VIS-IR spectral coverage using several spectrometers and infrared images. These measurements are used to determine rocket exhaust temperature and plume composition. Integration and testing of the N_2O catalyst reactor is now required to complete the NOP rocket system. The following section covers this part of the investigation in detail.
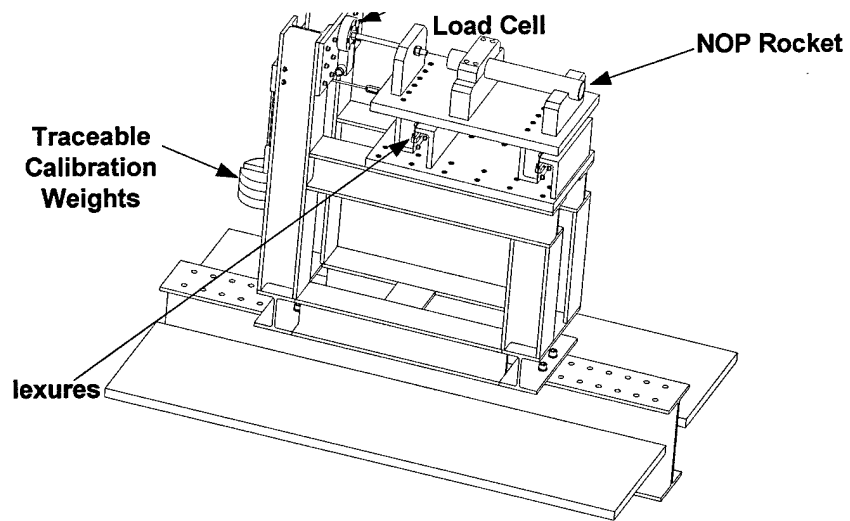
Figure 26: NOP rocket thrust stand design.
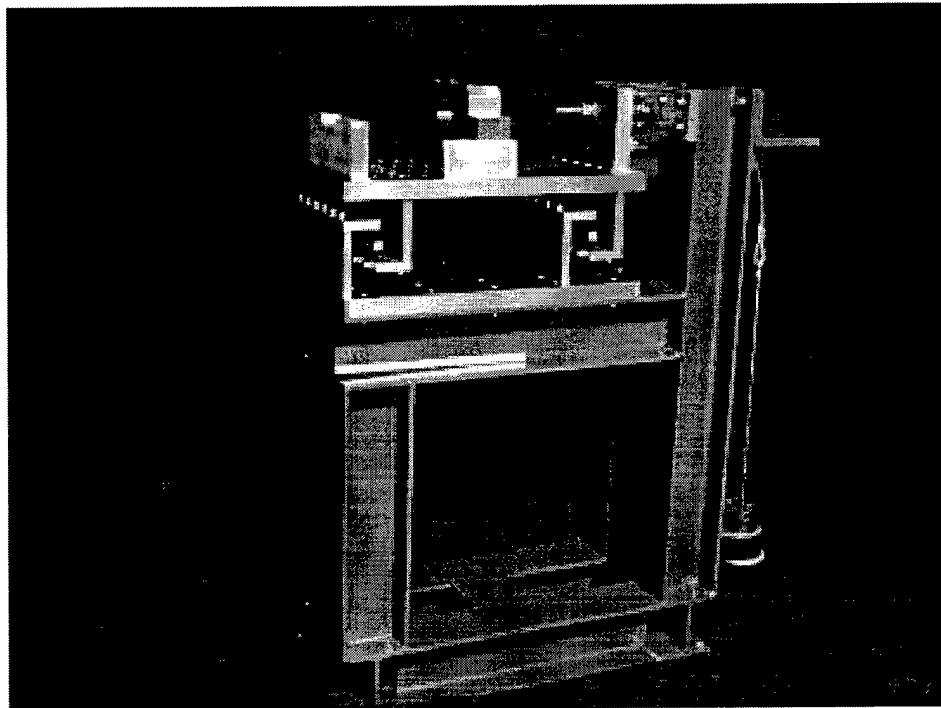
Figure 27: NOP rocket thrust stand assembly.

8   Catalyst Reactor Design, Testing and Results

In the following sections the catalyst development, material selection process and catalyst preparation are discussed. A description is also given of the various experimental set-ups and testing that were required to evaluate a suitable catalyst candidate for ignition of the NOP rocket.

8.1   Catalyst Development

The development of a catalytic reactor to efficiently decompose N_2O for propane autoignition is central to this research effort. The effort has two goals: to develop a catalytic reactor for the NOP rocket ignition testing and to research all candidate catalyst materials to search for an optimum material (or combination of materials) for a space prototype rocket engine.

Nitrous oxide decomposes exothermically with adiabatic decomposition temperature reaching $\approx 1640°C$, (2984°F).[31] This decomposition is accelerated by a catalyst. Free oxygen available by nitrous oxide decomposition can then be combusted with a wide variety of fuels. Studies have been conducted to develop catalysts that accelerate its decomposition. The ideal chemical reaction for the decomposition of nitrous oxide results in the formation of nitrogen and oxygen according to the following reaction equation.

$$N_2O(g) \rightarrow N_2(g) + \tfrac{1}{2} O_2(g) + Heat. \qquad (8-1)$$

However, heat input is required to initiate the decomposition reaction. In the case of thermal decomposition, the activation energy barrier for nitrous oxide is about 250 kJ/mole. There are other intermediate chemical reactions that can lead to oxides of nitrogen, such as NO and NO_2, that are undesirable if complete decomposition is to be achieved.

In order to attain homogenous reaction rates, the gas must be heated above its auto-decomposition temperature, unless a heterogeneous surface such as a catalyst is incorporated. Catalysts are designed to lower the activation energy barrier, thus allowing the decomposition to occur at much lower temperatures. The principal catalytic action can originate from charge donation into the antibonding orbitals, weakening the N-O bond and thereby lowering the activation energy and thus the reaction temperature.

In the following sections the catalyst material selection process, the various catalyst experimental set-ups, and the procedures for the catalyst preparation are discussed.

8.1.1 Catalyst Material Selection Process

The search for a catalyst material followed a logical path through the periodic table, considering the commonly known catalytic elements, including platinum (Pt), palladium (Pd), rhodium (Rh), and iridium (Ir). Various catalyst combinations were tested, over a range of initial pressures and reactor lengths. These catalysts include a platinum monolith, granular tungsten carbide, rhodium (0.17% granular), gold, platinum/palladium monolith, iridium (granular) and a Shell 405-Ir based catalyst bed. Each of these catalysts was preheated to various temperatures (122°F, 303°F, 398°F, 401°F and 662°F) using a linear temperature controller to determine the minimum light-off temperature. Catalyst activation requires a minimum initial temperature, with activation increasing as temperature increases. Instabilities occur at temperatures above a given value, which is material dependent.

The crystalline solids of primary catalytic interest, called aluminosilicates, incorporate Al, Si, and O. Naturally occurring minerals and many solids prepared in the laboratory exemplify this class. Zeolites are microporous inorganic compounds, mainly aluminosilicates, which exhibit crystal structures containing pores and voids large enough to permit the diffusion of organic molecules. Because of such unusual crystal structure, zeolites were widely employed as molecular sieves and for ion exchange as they commonly contain relatively loosely bound cations (i.e. positive ions) in their pores, which can be readily exchanged with other cations from solution. As polymers become more highly cross-linked and rigid, they lose this solution-like character, and their physical properties approach those of inorganic solids. However, it is in the field of heterogeneous catalysis that the most important applications of these materials can be found. Certain positions on the inner walls of the zeolite micropores can behave as active sites where catalytic conversions can take place. Moreover, since the micropores are very uniform and in the same size range as small molecules, zeolites can exhibit specificity and selectivity in adsorbing or rejecting molecules based upon differences in molecular shape, size and polarity. The diffusion and adsorption steps precede the chemical reactions at the active sites. Because the zeolites have well-defined crystalline structures, the catalytic groups in them are relatively well understood.

ZSM-5 zeolite is a medium-pore zeolite with ellipsoidal tubular pores with maximum aperture of 0.56 nm. This zeolite has received great interest because of its optimum performances as a solid acid catalyst in various industrial processes. The active sites are located both at the external surface of the crystallites and in the micropores. Often the internal surface developed by the porous channels is much larger than the external surface. The internal to external surface area ratio affects both the activity and the selectivity of the zeolite when it is used as a catalyst. The presence of molecules in the pore channels may drastically reduce the activity of zeolites and modify the selectivity in limiting the accessibility of the internal active sites to the reactants. Metal cation loaded zeolites have recently received great attention due to their activity in the decomposition and reduction of nitrogen oxides. These solids are very complex due to the presence of two distinct phases, the one crystalline (zeolite) and the other that can be amorphous or

crystalline (metal oxide), having different chemical compositions and physio-chemical properties among others, is the microstructure.

Metals loaded zeolites have been used as catalysts for a wide range of chemical reactions, such as hydrogenation, oxidation, isomerization and cracking of various feedstocks. For the selective catalytic reduction of nitrous oxide with hydrocarbons, transition metal ion exchanged zeolites are generally more active than the relevant supported catalysts since zeolites can disperse the metal at the atomic level. Recently, many studies have focused on the direct decomposition of nitrous oxide. Sivaraj *et al.*, 1988, Egerton *et al.*, 1974 and Swamy *et al.*, 1992 had reported that several metal oxides, mixed metal oxides and perovskites showed some activity for nitrous oxide decomposition, but the reaction rates were too low to have any significance. Sobolev *et al.*, 1993 has reported on studies conducted on several metal zeolites towards nitrous oxide decomposition. In 1992, Li and Armor reported that selected metal exchanged zeolites, principally copper, cobalt, rhodium or palladium on ZSM-5 were very active for N_2O decomposition. In 1998, Kannan and Swamy reported that calcined copper, cobalt or nickel hydrotalcites were effective catalysts, the activity of the catalyst being strongly affected by the temperature at which the hydrotalcite is activated. It has been reported that the catalytic activity of copper and cobalt based catalysts were higher than noble metal-exchanged catalysts such as rhodium and ruthenium. However, most of these studies have been carried out in the absence of hydrocarbons.

This research focused on the catalytic activity of copper and cobalt based catalysts for the direct decomposition of nitrous oxide, but mainly on the activity for the selective reduction of nitrous oxide in the presence of propane. Vannice,[32] 1999, showed that low temperature catalytic decomposition of ppm levels of nitrous oxide in the presence of hydrocarbons is possible. At high concentrations of nitrous oxide, previous researchers have found that the high adiabatic flame temperature of 1640°C caused the catalytic metal to literally vaporize from the support, reactively combine with the ceramic support (sinter), or even melt the ceramic support leading to eventual failure or deactivation. These types of phenomena have also been observed during this research. In 1990, Iwamoto *et al.* and Held *et al.* have shown that the most effective catalyst for this reaction is Cu-ZSM-5. However, this catalytic system suffers from several disadvantages. It appears that the Cu-ZSM-5 catalyst does not show high temperature stability for practical use. In comparison, a catalytic system of Co-ZSM-5 is proposed to be much more attractive. Armor and Farris demonstrated its higher hydrothermal stability, and stated that the loss of catalytic activity due to water vapor is completely reversible. In this research endeavor, tests were carried out on copper and cobalt based zeolite catalysts. However based on this brief overview it is important to note that other researchers in the field do not incorporate promoters. The purpose of the promoter is to alter the chemical behavior of the catalytic metal (cobalt, cobalt-copper and copper) to control their absorptive chemistry towards one of the two reactants (nitrous oxide and propane or propylene). Promoters are often added in an attempt to reduce the auto-ignition temperatures of the reactants, i.e. light-off temperatures.

Iridium, platinum, rhodium, ruthenium, copper and cobalt based catalysts have shown promising activity for the stoichiometric catalytic decomposition of nitrous oxide at low temperatures (<250°C). Based on both a review of the literature and experimentation, it was found that cobalt deposited on ZSM-5 exhibits activity in the thermal decomposition of nitrous oxide. Since zeolites have both acidic and basic sites in their structures, addition of alkali promoters like lithium, sodium, potassium, cesium and rubidium alters their basicity bringing about changes in the adsorption properties of the base metal, cobalt in this case. For a catalyst to effectively lower the activation energy of a chemical reaction, at least one of the reactive species must be chemically adsorbed onto its surface, termed chemisorption. This adsorption dissociates or significantly alters the chemical bonds, generating reactive species that can be stabilized at the catalytic surface. These chemical species are in many cases similar to those that would be generated during the auto-decomposition of nitrous oxide, but at much lower operating temperatures.

The initial focus of this research was to determine the adsorption behavior, Section 8.2.1, and catalytic activity of different catalysts towards nitrous oxide decomposition. Based on the data obtained from these experiments a pre-screening process was adopted with the objective of focusing on catalysts that would show high levels of activity towards the selective catalytic reduction of nitrous oxide with minimum preconditioning requirements. Catalysts with a base metal such as platinum, palladium, iridium, gold, rhodium, copper and cobalt were selected and tests conducted to determine their relative activities, Section 8.2.2.

During the latter part of our research into catalyst materials, work focused on the development of lower temperature and reduced cost catalytic nitrous oxide reduction approaches. The cobalt, cobalt-copper and copper catalysts listed in Table 16, Section 8.2.2 were prepared and tested in laboratories at UAH by incipient wetness techniques, while others were available commercially. The incipient wetness, or capillary impregnation technique[33] utilizes the process whereby a precursor salt is dissolved in an amount of water equal to the water pore volume, determined by slowly adding water to a carrier until it is saturated. Once dried, the carrier pore structure is assured to contain the required amount of catalytic species.[33] Those catalysts with a 1-1 notation contained an equal volume fraction of the catalytic metal(s) and sodium promoter deposited on the specified substrate. The catalysts were then reduced at 275°C (oxidation temperature) under flowing compressed air in an oxidation reactor to oxidize the metal nitrate and sodium carbonate promoter. Most catalysts include a promoter to from a co-precipitate phase.

Currently, the research effort headed by UAH concerns examining the light-off temperature of the catalysts shown in Table 16, Section 8.2.2. Catalysts prepared using cobalt appear to have greater activity than copper based catalysts. ZSM5 based catalysts appear to have greater activity than Y-Sodium zeolite. Results from the various catalyst materials used in the prototype reactor design are presented in Section 8.2.1-8.2.6.

8.1.2 *Catalyst Preparation*

The reactor research efforts focused on cobalt and copper catalysts on supported metals on a host of ceramic substrates.

During this research effort, the catalysts tested were prepared using the incipient wetness technique. This technique involves taking a known weight of cobalt nitrate and/or copper nitrate salts, dissolving them in a known volume of water to produce a specific molar concentration. A weight of promoter such as sodium carbonate may also be added to this mixture to produce the same molar ratio as the catalytic metal nitrate. A promoter serves to alter the chemical behavior of the catalytic metal to control their adsorptive chemistry biased towards a particular reactant. The addition of the promoter forms a co-precipitated salt (termed sol precipitation). The molar concentration of both the catalyst and promoter (termed metals loading) in this solution was on the order of 0.1 and 1.0 moles/ liter. A weighed quantity of substrates such as ZSM-5, Alumina/Silicate (Aerosil) Zirconia, Titania (P-25) or Y Sodium Zeolite is further added to this mixture. This mixture was then heated to remove unbounded or free water by evaporation, yielding a solid composed of the substrate and metal salts. Those catalysts with a 1-1 notation, contained an equal volume fraction of the catalytic metal(s) and sodium promoter deposited on the specified substrate. The solids were then reduced (calcined) at high temperatures under flowing compressed air in an oxidation reactor to oxidize the metal nitrate and sodium carbonate promoter to the catalytic metal and sodium oxide supported on the specified substrate.

8.2 Catalyst Reactor Test Set-up, Results and Discussion

In this section a complete review of the chemisorption, catalyst activity, atmospheric catalyst reactor set-ups and tests is presented. The purpose here is to guide the reader through a systematic explanation of the catalyst reactor development, testing and evaluation process.

8.2.1 *Catalyst Chemisorption Experimental Set-up and Results*

Chemisorption experiments are required to assess the adsorption characteristics of various candidate catalyst materials, a property critical in a heterogeneous catalysis process, as is the case for the NOP rocket catalyst reactor. In the chemisorption experiments, N_2O is adsorbed at the catalyst surface. This means that the gaseous N_2O molecules collect on the catalyst's solid surface, i.e. an external surface phenomenon.

Initial studies on nitrous oxide chemisorption by the catalysts that showed promising activity, based on the literature, were conducted with the experimental setup shown in Figure 28. This typical chemisorption apparatus consists of a glass dosing volume and a quartz catalyst reactor chamber. These volumes are connected by means of a three-way hard vacuum valve. By the appropriate position of this valve, vacuum or N_2O gas can be

easily introduced into the chamber. An additional pressure extension allows the connection to high accuracy pressure transducers that monitor the adsorption process and the final equilibrium pressure. A thermowell built into the catalytic chamber permits the use of a 'K' type thermocouple for temperature recording.

The glassware necessary for adsorption experiments are suspended on an aluminum frame to which all the necessary peripherals are added. These included the pressure transducer with a dynamic range of 0.1 to 1000 torr, and a thermocouple. The two-way valves connect the 5.1966×10^{-5} m^3 dosing volume to a 2.645×10^{-5} m^3 reactor chamber through glass interconnecting tubes. The dosing volume chamber is also connected to a pressure transducer (MKS 12-50062), which has a digital readout. A Hoskins Electrical Furnace is used to heat the catalyst to the appropriate temperature before adsorption. A temperature controller connected to a thermocouple via a Ford Instrument potentiometer controls the catalyst preheat temperature.

In operation, a mg size portion of the catalyst is selected and carefully weighed to a precision of 0.1 mg and loaded into the catalyst chamber. Vacuum is then applied to the entire system to remove air and water vapor that entered during the loading process. In some cases the catalyst is preconditioned by heating under a vacuum to remove surface contaminates. However, since the focus of this research was on catalyst with a minimum of pretreatment, this step was not applied. The catalyst is isolated by closing the valve over the reactor and introducing a measured quantity of gas into the dosing volume. This gas is then allowed to equilibrate and the initial pressure recorded. The valve over the reactor is opened exposing the catalyst to the reactive gas while the pressure in the system is monitored as a function of time until an equilibrium pressure is observed. Knowing the exact volume of each chamber, the moles of adsorbed gas can be determined at a given temperature. The temperature is then increased and the adsorption isotherms determined.

Based on literature reports of copper and cobalt catalytic activity at low ppm levels of nitrous oxide at 150°C and that of commercially available iridium based Shell 405 catalyst, it was decided to focus the chemisorption studies on these catalysts. Results obtained from these initial tests showed that Shell-405 and cobalt based ZSM-5 catalysts had significant chemisorption isotherms. Promoters, typically of alkali metal have been known to enhance the catalytic activity of group VIII transition metals, such as cobalt. Therefore, catalysts were prepared both with and without promoters.
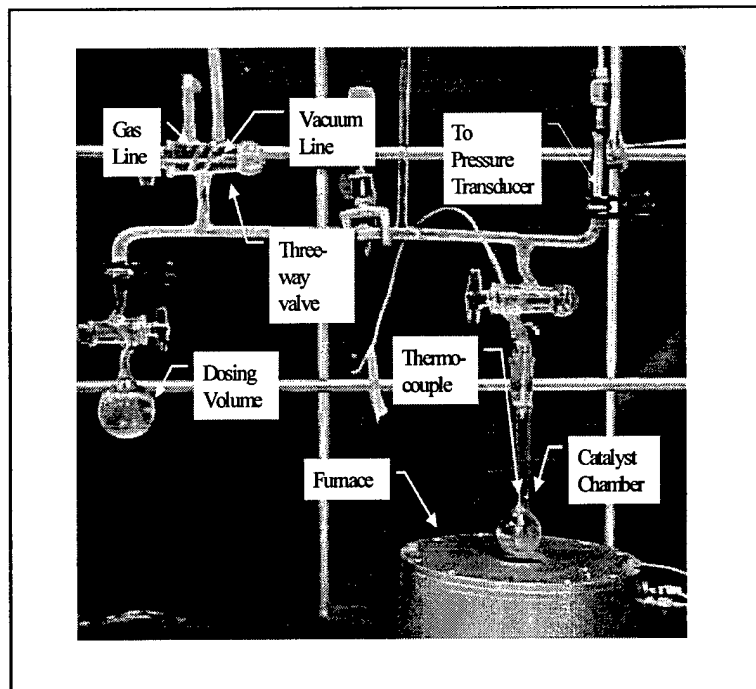
Figure 28: Chemisorption apparatus for nitrous oxide adsorption studies.

Though many studies on the chemisorption behavior of a number of catalysts were attempted, only significant results and their implications to the project goals are presented and discussed below.

Shell-405 was used for the adsorption-decomposition reaction of nitrous oxide. N_2O adsorbs with what is called 'reactive adsorption', a process that involves adsorption of N_2O to the catalyst surface. Later the N_2O dissociates into oxygen and nitrogen via the reaction:

$$N_2O_{(g)} \Rightarrow N_{2(g)} + 1/2 O_{2(g)} + Heat$$
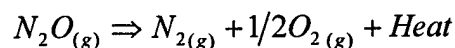
Thus, an initial decrease in pressure is observed, followed by a pressure rise. At equilibrium, the final pressure is 1½ times the initial pressure. The catalyst preheat temperatures were progressively increased from room temperature to 185°C. The decomposition reaction with nitrous oxide was observed at 185°C as shown in Figure 29. This temperature is the minimum temperature required for nitrous oxide to completely decompose on the surface of the catalyst. Using the adsorption results from Figure 29 and Langmuir's isotherm, a calculation of the nitrous oxide active surface area can be made. For the catalytic sample used to generate Figure 29, a surface area of 196.5 m²/gm was calculated. This is within the manufacturer's range of 190-210 m²/gm. This catalyst was later used in activity studies and was eventually key in developing a potential catalytic igniter, as described in Section 8.2.2 and Section 8.2.5.

Shell 405 Gas: Nitrous Oxide

Catalyst Shell-405
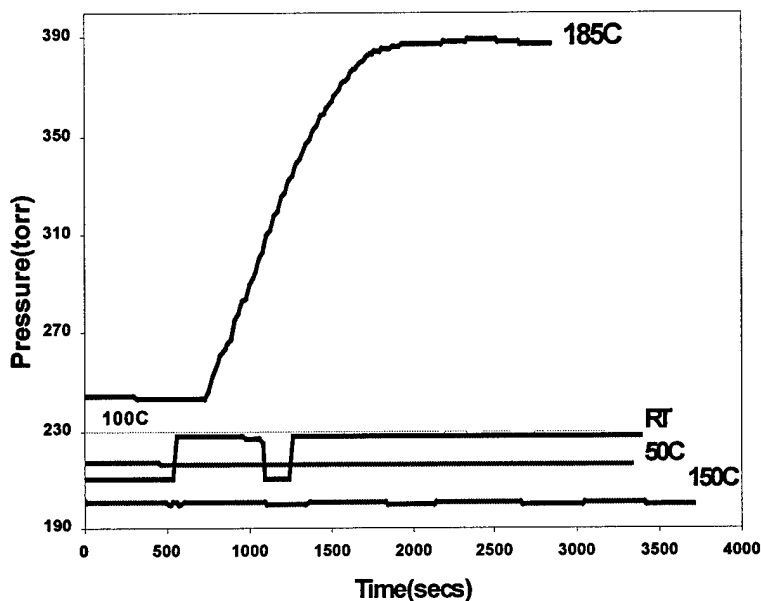
Figure 29: Adsorption isotherms for nitrous oxide on the iridium based Shell-405

Cobalt on ZSM-5 catalysts were also prepared with various promoter metals, such as sodium. Of key importance is the adsorptive behavior with and without the promoter. For the promoted catalysts, sodium at a 1:1 molar ratio relative to the base metal were deposited on ZSM-5. The non-promoted catalyst was prepared and reduced following identical procedures but without the addition of sodium. Figure 30 shows the comparative adsorption profiles of nitrous oxide on these catalysts. From Figure 30 it is seen that addition of promoter has a significant effect on the rate of nitrous oxide adsorption. The promoter enhances the selectivity of the CoZSM-5 catalyst towards the oxygen atoms in nitrous oxide and thus the overall activity of the catalyst towards the thermal decomposition of nitrous oxide. These initial findings were used to develop a series of activity studies using various promoters, as discussed in Section 8.2.2.

Conclusions drawn from the relative adsorption on Shell-405 and Co-ZSM-5 catalysts, lead to a decision to perform reactive flow studies in an experimental combustion reactor. Using the adsorption results for the promoted Co-ZMS-5, a series of promoted catalysts were prepared and their relative activities compared, as described in the following section.
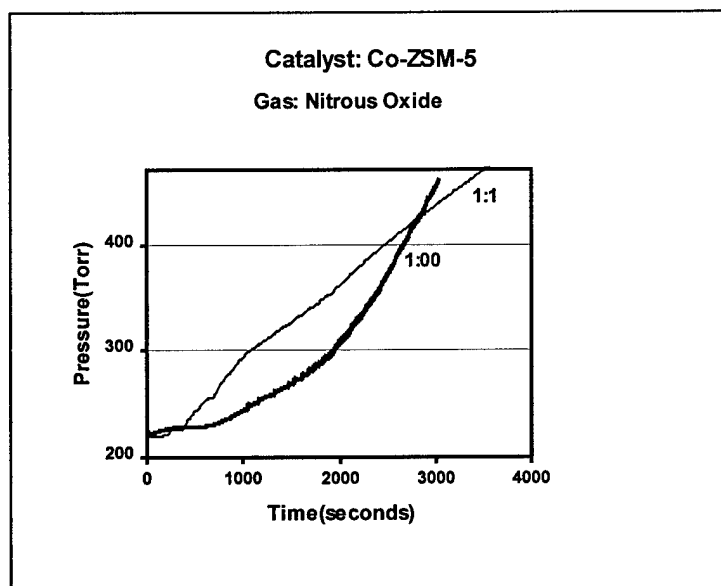
Figure 30: Comparative nitrous oxide adsorption on Co-ZSM-5 catalyst calcined at 275°C with (curve 1:1) and without sodium promoter (curve 1:00) at room temperatures.

8.2.2 Catalyst Activity Studies Set-up and Results

Once the adsorption characteristics of the various candidate catalyst materials were understood, the candidate catalyst materials were tested inside a reactor, in order to measure the activity of the catalyst and gain the information required to build a working reactor for NOP rocket ignition.

The experimental combustion reactor for flow studies is shown schematically in Figure 31. The thermocouples and the 1/16 tubing were introduced through angled slots with suitable fittings on the inlet and exit flanges of the reactor. The fuel (propane or propane with 10% propylene) was also introduced through 1/16 tubing mounted on the inlet side flange of the reactor. Precautions were taken on the inlet side of the reactor by installing variable pressure check valves downstream of a Hoke metering valve on the nitrous line and downstream a Hoke micrometering valve on the propane line. The check valves were required to prevent flame flashback into the inlet lines, an event that had previously damaged a turbine flow meter.

70
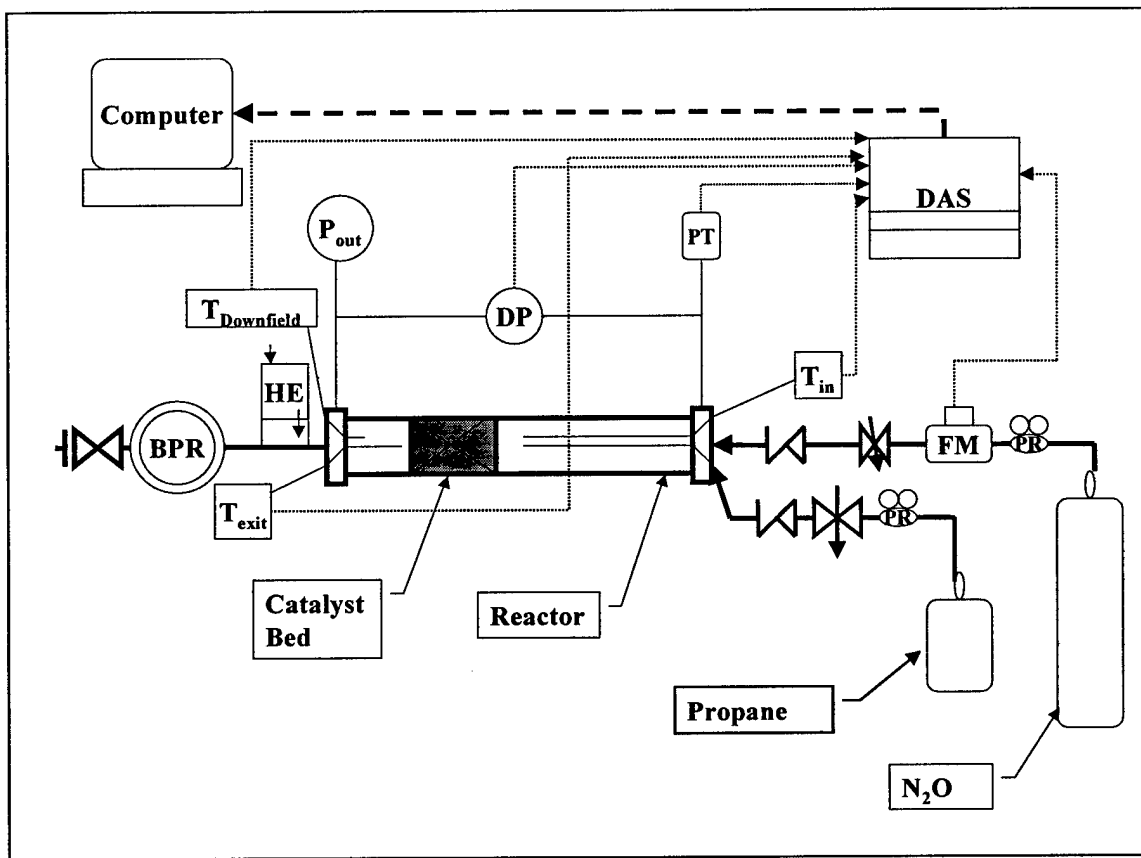
Figure 31: Schematic of the combustion reactor for catalytic activity studies (Note: 'BPR'=Back Pressure Regulator; 'DP'=Differential Pressure transducer; 'PT'=Pressure Transducer; 'FM'=Turbine Flowmeter; 'HE'=Heat Exchanger; 'DAS'=Data Acquisition System; 'PR'=Pressure Regulator

The pressure within the ceramic lined reactor shell was controlled using a Tescom back-pressure regulator 'BPR' connected to a heat exchanger 'HE' downstream of the reactor. The heat exchanger protects the BPR from damage due to high temperature exposure from the catalyst exhaust. Experimental runs were conducted with varying N_2O inlet pressures to determine the pressure at which optimal decomposition of N_2O occurred. The temperatures at the inlet, exit and the downfield side of the reactor were measured with ungrounded 'K' type thermocouples (Medtherm Corporation). Inlet pressure was measured using a Model 280E Setra pressure transducer with a range 0-1000 psig. Differential pressure was measured using a GP:50 differential pressure transducer with a range of 0-100 psig (Saber Corporation). Flow rates were monitored by an Omniflo FTO-5AIXA-GHC-1 turbine flowmeter (Flow Technology, Inc). Frequency information obtained from the turbine flowmeter was conditioned using a CA 51 signal conditioner (Flow Technology, Inc.). To conduct catalyst activity studies, the reactor body was preheated using a Watlow heater, and a Valley Forge linear temperature programmer was connected to an input current controller, in tandem with the heater, to control the catalytic

reactor preheat temperatures. An Iotech Daqbook 260 data acquisition system was used to acquire and record the temperature, pressure and flow rate measured during the experiments. The data acquired were monitored, recorded and saved on a personal computer using Daqview 7.8 software.

In the process of developing a catalytic igniter, multiple candidate catalytic materials were tested, as shown in Table 16. This process served to rule out a number of catalysts and allow focus on others. Shell 405 is being employed for the first version of the catalytic igniter, although several other promising candidates will be tested in the future.

The run ID shown in Table 15 follows a specific labeling system such as Co|ZSm|(1Mol)|T150|T0102, where:

- The first set of characters indicates the metal type on the catalyst.
- The next set of characters indicate the substrate type
- The molar concentrations are indicated within brackets.
- The 'T' followed by numbers indicate the approximate start temperature ($^{\circ}$C) at which the run was conducted. (The run start temperatures in $^{\circ}$F are provided within the text describing the individual runs)
- The next 'T' followed by the numbers indicate the date (mm/dd) on which the run was performed.

Initial Reactor Temperature

Catalyst	Oxdtn. Temp.		70F	122F	212F	302F	392F	Active
Alumina Substrate	NA	Exit T	75F	217F	278F	386F	ND	No
Au – Granular AuT(50,100,150,200)T1027	350C	Exit T	74F	147F	250F	380F	452F	TBD
Shell 405(Ir) – Granular IrT(50,150,200)T1030	NA	Exit T	75F	140F	ND	362F	1100F+	Yes
LCH300(Pt)-Monolith LCH300T(0,50,100,150,200)T1113	NA	Exit T	73F	158F	233F	355F	422F	No
LCH410(Pt) Granular LCH410T(0,50,100,150,200)T1115	NA	Exit T	75F	185F	253F	347F	413F	No
LCH210 LCH210T(50,100,150,200)t1120	NA	Exit T	73F	141F	238F	322F	412F	No
UOP406(Pt) Granular UOP406T(100,150,190100Ox)T1122	NA	Exit T	73F	ND	265F	322F	406F	No
LCH404B(Pt)- Granular D404BT(115,175)T124	NA	Exit T	75F	175F	247F	330F	380F	No
1-1 CoCu(0.1M) on Zsm5 CoCu(0.1M)ZsmT(50,100,150,200)T124	275C	Exit T	74F	195F	272F	362F	441F	Yes
1-1 Co(0.1 M)on Alumina Monolith CoMon(0.1M)T(50,150,200)T125	275C	Exit T	75F	220F	ND	396F	447F	Yes
Co(0.1M) on Zsm5 CoZsm(0.1M)T(50,125,175)126	275C	Exit T	75F	250F	320F	440F	ND	Yes
1-1 Cu(0.1M) on Zirconia CuZr(0.1 M)T(50,100,150,200)T127	275C	Exit T	75F	219F	295F	365F	447F	No
1-1CoCu(0.1M) on P-25(Titania) CoCu,Co(0.1M)P25T(0,50,200)T128	275C	Exit T	76F	236F	ND	ND	417F	Yes
1-1 CuCo(0.1 M) on Y-Na Zeolite CuCoZeY(0.1M)T(50,100,150,200)T1219	275C	Exit T	78F	186F	260F	364F	473F	Yes
1-1 CuCo(0.1 M) on Aerosil CuCo(0.1M)AslT(50,100,160)T1220	275C	Exit T	75F	144F	243F	335F	ND	No
1-1Co(1.0M) on Zsm5 CoZsm(1.0M)T(0,50,150,200,275)T0102	275C	Exit T	80	168	ND	335	404	Yes
1-0Co(1.0M) on Zsm5 CoZsm(1.0M)T(150,200)T0108	275C	Exit T	75	ND	ND	307	397	No
1-0Co(1.0M) on Y-Na Zeolite CoZeY(1.0M)T(150,200,250)T0109	275C	Exit T	ND	ND	ND	310	397	N0
Co(1.M) on Alumina Monolith CoAl(1.0M)T(50,100,150,200)T0116	275C	Exit T	ND	ND	215	315	398	N0
TBD=Promising, ND=No Data								

Table 16: Summary of various catalyst materials tested and their relative activity data.
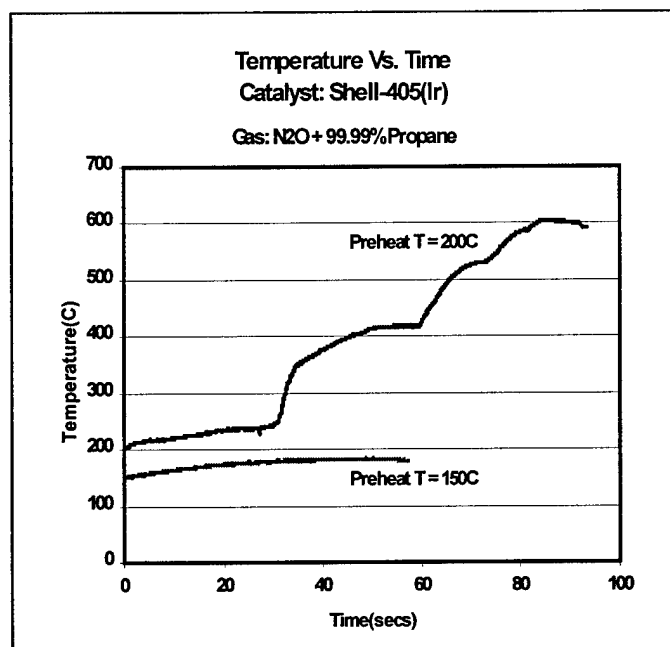
Figure 32: Temperature profiles for nitrous oxide decomposition with 99.99% pure propane, for preheat temperatures of 150°C (302°F) and 200°C (392°F).

The results from these experimental runs suggest that the iridium based catalyst Shell-405, had the highest activity and selectivity towards nitrous oxide decomposition. Initial experimental runs were accomplished using 99.999% propane as the fuel. Thermal decomposition of nitrous oxide occurred at a preheat temperature of about 210°C as shown in Figure 32. In Figure 32 there was not much activity at a catalyst preheat temperature of 150°C. However, at 200°C the exit temperature starts rising. The inlet N_2O pressure was then reduced from 115 to 100 psig and a further temperature rise was recorded. Further reductions in pressure produced an optimum exit temperature (600°C) at an N_2O inlet pressure of 60 psig. The inlet flow rate of the nitrous oxide was 0.015 CFM.

In an effort to reduce the light-off temperature, a premix of 90% mol propane and 10% mol propylene was used. In propylene the C=C bond is nonsymmetrical. This distortion in the structure results in an increased surface reactivity relative to propane. For 90% propane and 10% propylene mix, it was observed that the light-off temperature was 148°C as shown in Figure 33. The inlet nitrous oxide pressure was again adjusted until an optimum pressure of 60 psig was reached. As with the pure propane studies, further reductions in pressure decreased the exit temperature. In Figure 33, the exit temperature was restricted to below the thermal decomposition temperature as a safety precaution. For these studies, the inlet N_2O flow rate was also 0.015 CFM.

74

Comparing Figure 32 and Figure 33, it is clear that the presence of propylene has a dramatic effect on the light-off temperature, reducing it almost 25% with the addition of 10% propylene. Studies at higher propylene concentration are possible, and should be a topic for further studies.

Temperature Vs. Time
Catalyst: Shell-405
Gas: N2O + (90%Propane+ 10%Propylene)
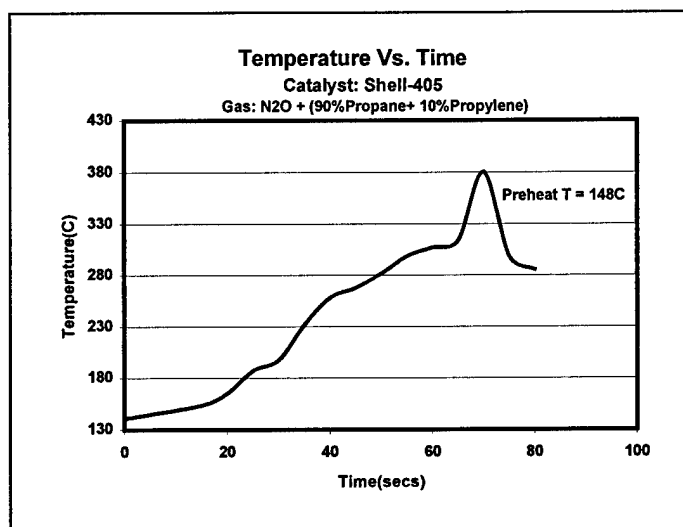
Preheat T = 148C

Figure 33: Temperature profile of nitrous oxide decomposition using a 90% propane and 10% propylene mixture as fuel, at a preheat temperature of 148°C (298°F).

8.2.4 Supported Cobalt and Copper Catalyst Development Results

Experimental results indicate that cobalt based ZSM-5 catalysts with sodium as promoter metal produced high activity toward the thermal decomposition of nitrous oxide in the presence of a propane/propylene mix. Figure 34 shows a typical experimental run. A Co-ZSM-5 catalyst with sodium as a promoter at a 1:1 molar ratio was used for this test. The objective of the test was to determine the activity of the catalyst for N_2O and/or propane/propylene adsorption as a function of exit temperature, metal loading, substrate and promoter effect on adsorption at a catalyst preheat temperature of 275 °C. The reactor bed was preheated to about 275°C with N_2O at very low pressures. At a set temperature the heater was turned off and N_2O gas at 85 psig was passed through the bed. The temperature rose to about 330°C and remained constant. At this point a very small flow rate of the propane/propylene mix was established. This low flow rate of about 2 cc/sec had a major effect on the exit temperature, which rose to above 500°C while the inlet temperature fell to about 315 °C and remained constant. At 500°C the propane/propylene flow rate was increased to 6 cc/sec and then quickly turned off as the decomposition of nitrous oxide temperature was exceeded.

In Table 16, the results are summarized in terms of reactor exit temperatures and an estimate of relative activity. As can be seen, many catalysts had minimal activity when

initially oxidized at 275°C. Addition of propane in the inlet to the nitrous oxide reactor caused carbon deposition on the catalysts and a thick oily substance to appear in the exit of the reactor. Propane injection was therefore moved to the reactor exit immediately after the catalyst for future tests. During recent nitrous oxide reaction studies with propane in the exhaust (Run 55), it was noticed that a 1-1 Cobalt on ZSM5 catalyst heated to 275°C, underwent further oxidation and developed substantial catalytic activity producing an exit temperature of 600°C, as shown in Figure 34 below. This is a very encouraging result and from this it is concluded that the calcining temperature was not high enough to fully reduce both the nitrate and carbonate. The initial oxidation temperature has therefore been increased to 350°C and for future work many of these catalysts will be re-evaluated.
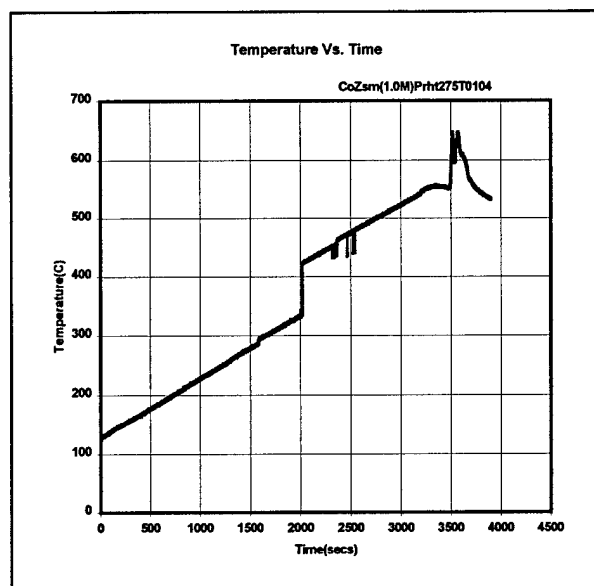
Figure 34: Exit temperature profile of N₂O decomposition with a Co on Zsm (1 molar) catalyst, with sodium carbonate as the promoter. The reactor bed was preheated to 275 °C (527°F).

Figure 34 indicates the activity of the catalyst was dramatically influenced by the presence of the sodium promoter. As shown in Figure 34 the Co on Zsm (1 molar) catalyst, with sodium carbonate promoter, attained an exit temperature of 600 °C (1112 °F), which is adequate for propane autoignition (> 874 °F). At a set temperature the heater was turned off and the N₂O gas was allowed to flow through at 80-97 psig. When the exit temperature reached about 330 °C (626 °F), the propane/propylene mixture was flowed and the exit temperature started rising above 600 °C (1112 °F).

Alkali metals have varying affinity for their outer orbital electron. This affinity decreases as the molecular weight of the alkali metal increases, with Li showing the greatest affinity and Cs showing the least. As such, they can either retain or contribute their electron to alter the oxidation state of the Co catalyst. To investigate how this affinity influenced the catalytic activity of Co, a series of catalysts were prepared and their

76

activities directly compared. The promoters used were lithium, sodium, potassium, rubidium and cesium all added as carbonates at a 1:1 molar ratio. Initial comparative temperature profiles at preheat temperatures of about 100°C, 150°C and 200°C are shown in Figure 35 - Figure 37, where it is seen that there are two routes towards the activity for nitrous oxide decomposition. One is the high temperature route favored by promoters like lithium and the other, the low temperature route favored by promoters such as cesium and potassium. Clearly, cesium and potassium promoters offer potential alternatives to lowering the light-off temperatures for nitrous oxide decomposition.
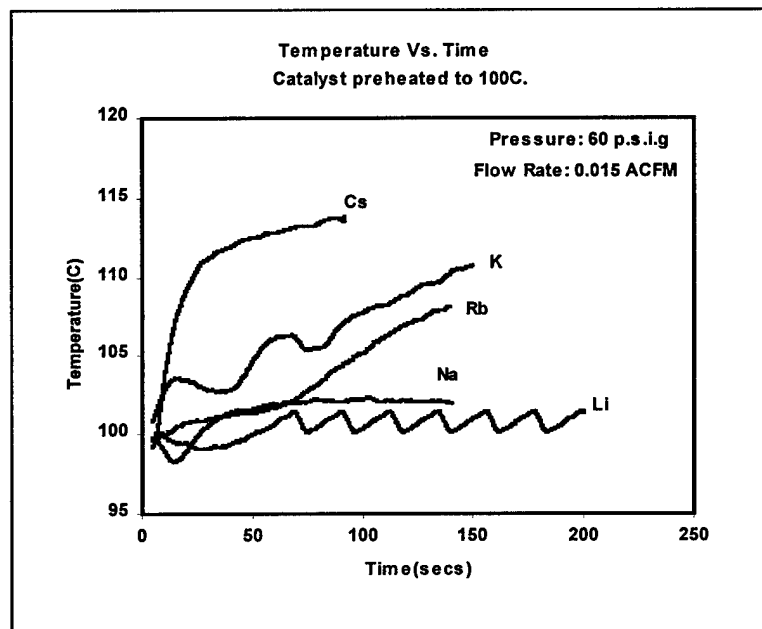
Figure 35: Catalytic activity of various promoters with CoZSM-5 catalyst preheated at 100 °C, (212°F).
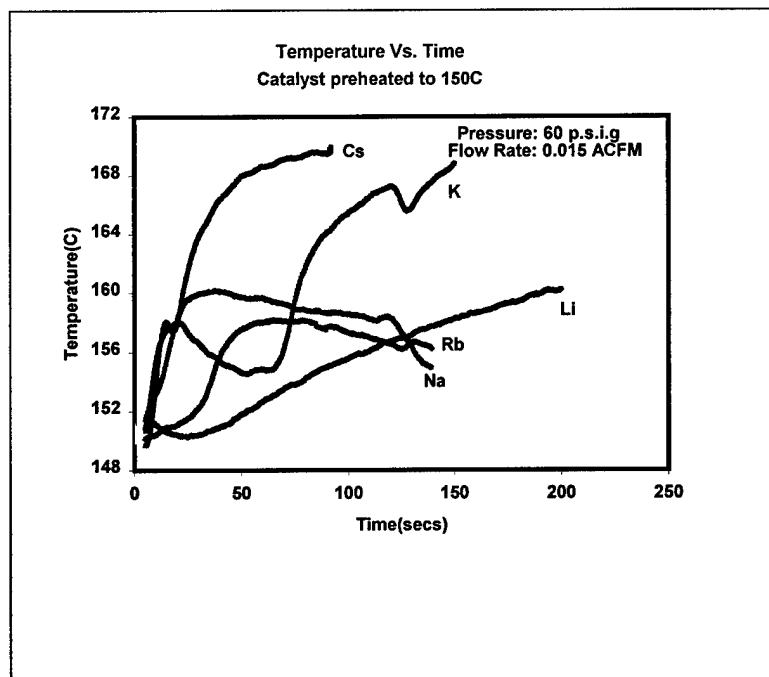
Figure 36: Catalytic activity of various promoters with CoZSM-5 catalyst preheated at 150 °C, (302°F).
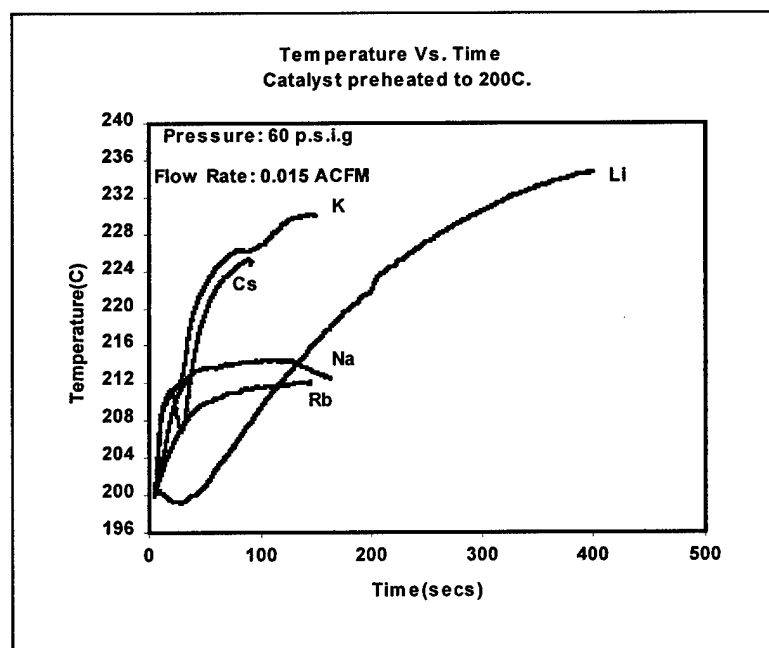
Figure 37: Catalytic activity of various promoters with CoZSM-5 catalyst preheated at 200 °C, (392°F).

8.2.5 Atmospheric Catalyst Reactor/Igniter Set-up and Results

To accommodate the rocket ignition circuit, a catalyst reactor was prepared to exhaust directly to the atmosphere. Further experimentation to optimize the conditions under which the thermal decomposition occurred were carried out in this atmospheric combustion reactor/igniter. A schematic of this experimental setup is shown in

Figure 38. This reactor was designed to simulate and perform experiments in tandem with the experiments at Test Stand 2 at the Johnson Research Center at UAH. Field tests were later carried out under practical conditions at Test Stand 2.
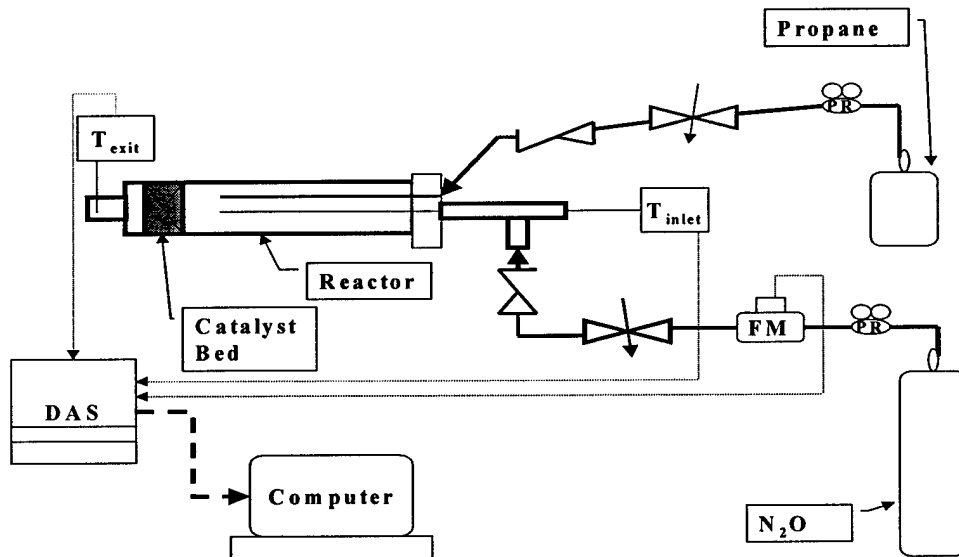
Figure 38: Atmospheric combustion reactor/atmospheric igniter set-up.

Initial experiments with this reactor used an exit choked with a 1/16-inch tubing to permit operation at the optimal pressure of 60 psig, as determined in previous experiments, Sec. 8.2.2. Nitrous oxide flows were established at 0.2 SCFM at the preheat temperature. When propane was added, a high exit temperature was recorded for almost 80 seconds and a flashback occurred damaging a flow meter and data acquisition system, thus terminating these experiments.

The reactor circuit was modified with propane injected at the catalyst exit. Shell 405 catalyst was now used, with a bed length of 1.2", as determined from previous experiments. For these studies, the reactor was preheated to various temperatures, the nitrous flow rate was established at 0.2 SCFM, at an exit pressure of 60-80 psig and the propane flow rate was gradually increased. At a preheat temperature of 200°C, as the propane was increased, a flashback was experienced and the catalyst inlet temperature rose to over 900°C. The internal backfire meant that the choked flow could not handle

79

the rapidly expanding flow. In both cases, the catalyst performed as expected. To direct the flame front in the proper direction, i.e. away from the bed exit in the direction of flow, the catalyst bed length was reduced to ¼ inch and the choke removed from the exit. This resulted in a reactor upstream operating pressure of 1-2 psig with the downstream at essentially atmospheric pressure. Again, the reactor was preheated, and the nitrous oxide flow established at 0.2 SCFM. Propane/propylene was then added to the reactor inlet about ½" from the catalytic bed and the exit and inlet temperatures were recorded. For a Shell 405 catalyst, preheated to 125°C, the instant propane was added at 4-9 cm^3/sec, a flame was established and sustained for over 60 seconds. Termination of both the propane and nitrous oxide was required to extinguish this flame indicating that it resulted from both propane combustion and nitrous oxide decomposition.

Additional studies were accomplished using spent Shell 405 that had seen the extreme temperatures discussed above. At all preheat temperatures studied, the catalyst was found to be deactivated. This may have resulted from the excessively long exposure time to the reactive flows. Details of these tests are summarized in Table 17 below.

Catalyst							Comments
Co(1.0M) on Zsm5 CoZsm(1.0M)T0T275119	Inlet T					527F	Fresh Charge
	Exit T					>1300F	Active
Shell 405(Ir) – Granular IrT(100,150,200)T0124	Inlet T		226F	302F	400F		Fresh Charge
	Exit T		343F	518F	752F		Active
Shell 405(Ir) – Granular IrT(100,125,150)T0131	Inlet T	212F	260F	302F			Spent Charge
	Exit T	212F	264F	305F			No Activity
Shell 405(Ir) – Granular IrT100T0205	Inlet T		212F	239F	257F		Fresh Charge
	Exit T		225F	266F	>1100F		Active

Table 17: Summary of atmospheric catalyst reactor/igniter experiments

8.2.6 Catalyst Reactor/Rocket Ignition Test Results

Experimental runs were conducted at the UAH rocket motor Test Stand 2 at the Johnson Research Center at UAH, in coordination with Dr. Moser and his research team. The focus of these experimental runs was to optimize the procedure and synchronize the catalytic decomposition under nominal operating conditions, in conjunction with the propulsion team's NOP rocket experimental setup. The following describes an ignition sequence using the atmospheric catalytic reactor set-up, as integrated with the NOP Rocket 1.

Shell-405 catalyst weighing about 1.400 grams was loaded into the atmospheric combustion igniter, resulting in a bed length of about ¼ inch. The reactor was preheated to 148°C at the inlet, while the exit temperature was 98°C. Nitrous oxide at a gage pressure of 117 psig was then flowed through the reactor at 0.015 ACFM. A time delay of about 4 seconds was allowed before the propane/propylene mix was injected into the reactor at 103 psig pressure and a flow rate of about 1 cc/sec. At that instant a flame was observed at the exit of the reactor, shown in Figure 39. The flow of the propane mix and nitrous oxide were then shut-off and the reactor purged with N_2. The flows were then restarted and a flame was again observed at the exit. This procedure was repeated 6 times and each time the propane mix was turned on a flame was observed. The exit temperature profile from the exposed type K thermocouple positioned at the reactor exit, shown in Figure 39, is presented in Figure 40. Here the exit temperature was controlled not to exceed 400°C. The profile shown in Figure 40 is a typical example of several ignitions that produced a flame profile consistent with the flame in Figure 39.

To overcome a recurring failure, namely, the oxidation of the stainless steel wire screen, which was used to restrain the catalyst particles inside the reactor, a monolithic screen was incorporated. A platinum monolith with a length of about 1/4 inch, cut to fit inside the reactor diameter, was used to make this modification. The monolith was also used to check for the activity of the platinum catalyst towards the thermal decomposition of nitrous oxide.
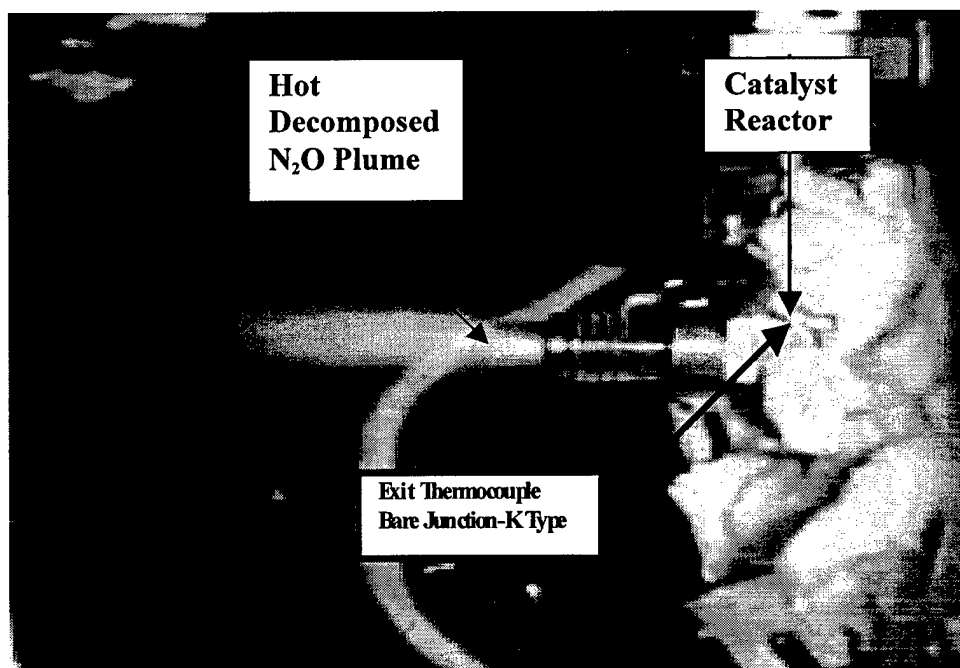
Figure 39: A hot flame of N_2O decomposed gases is shown emanating from the exit of the atmospheric combustion catalytic igniter.

Temperature Vs. Time

Catalyst: Shell-405   **JRC**
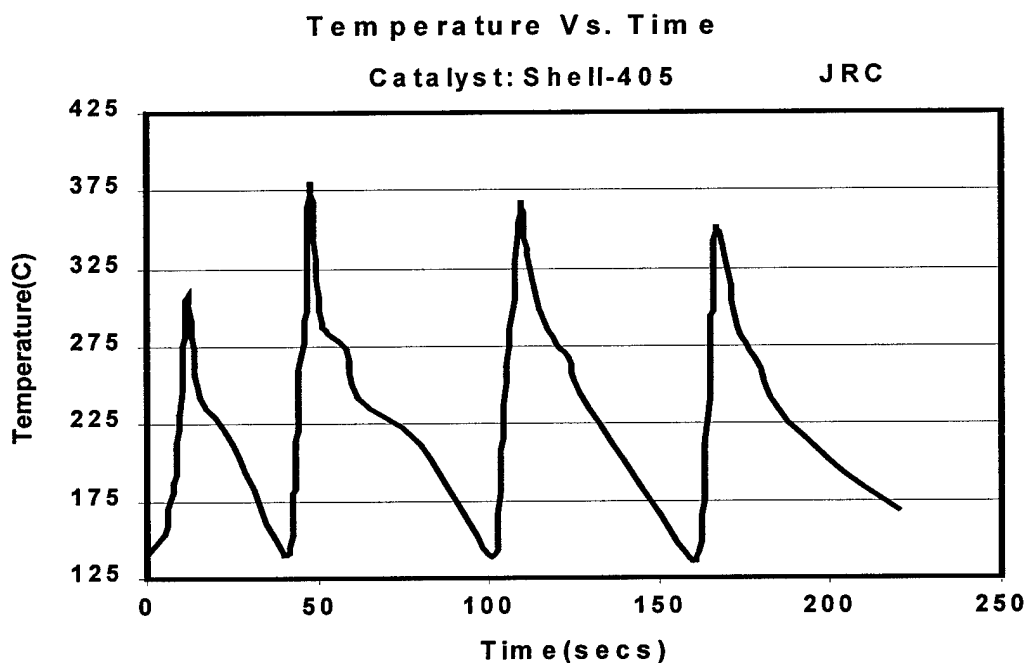
Figure 40: Temperature profiles for Shell-405 catalyst at 150 °C preheat.

The catalyst igniter is shown firing, Figure 39, prior to integration with the NOP Rocket 1. This reactor was fired approximately 15 times in rapid succession, displaying robustness in the catalyst reactor operation.

A hybrid catalyst bed was made up of Shell-405 (1/4 inch bed length) and platinum monolith (1/4 inch bed length) and the experimental runs performed. Exit temperatures greater than 700°C were observed, but it was also observed that these high temperatures burnt and fused the platinum catalysts as shown in Figure 42. The original condition of the platinum monolith is shown in Figure 41, with temperature profiles shown in Figure 43. It was also observed that the flame produced at the reactor exit was almost colorless in comparison to the reddish-yellow flame produced when only Shell-405 catalyst was used, Figure 39, indicating cleaner combustion of the reacting mixtures.
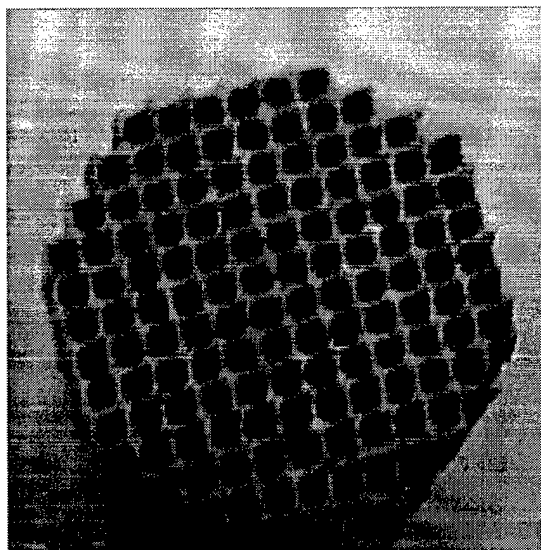
Figure 41: Platinum catalyst before the experimental run.
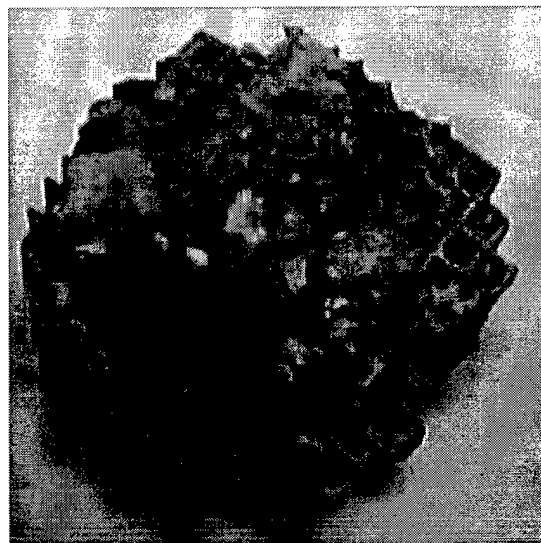
Figure 42: Platinum catalyst after the experimental run.

Using Shell-405 in the laboratory, a reddish flame was observed. This coloration may result from the presence of NO_x due to incomplete combustion, a point that needs further study. In the hybrid catalyst bed, the Shell-405 started the reaction and platinum propagated the nitrous decomposition. In this case, both nitrous oxide and the propane/propylene mix flows had to be turned off to end the reaction.

Since the igniter performed on command, a series of ignition rocket experiments were attempted. In all cases, the igniter performed as expected, however the rocket did not ignite. The cause for the problem is most likely due to the different operating pressure in the igniter (atmospheric) and rocket motor (150 psig) that causes flashback into the igniter before the flame can propagate downstream. The solution is to increase the ignitor's operating pressure to prevent this backflow, a topic for further study.

Temperature Vs. Time

Catalyst: Shell-405 (Iridium)+Pt. Monolith
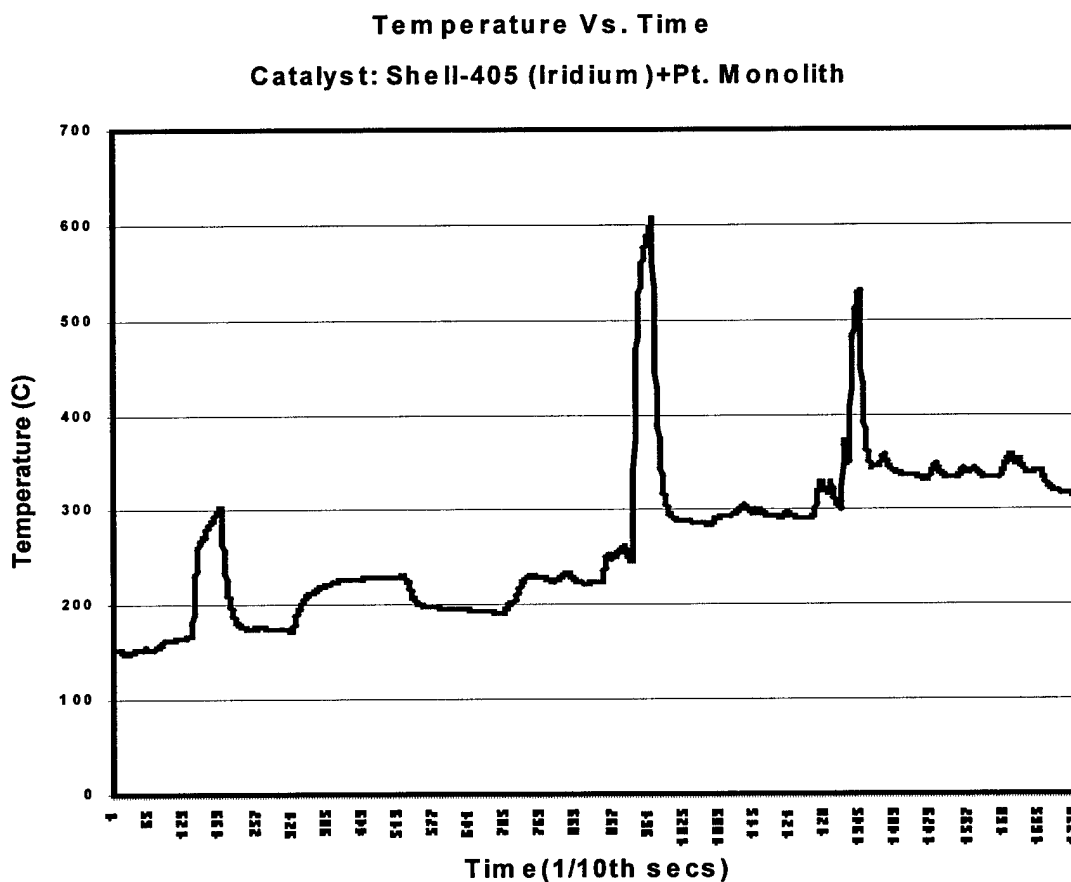
Figure 43: Temperature profiles from (Shell-405 + Pt) catalyst preheated to 150 °C.

9 NOP Rocket Experimental Results

The following sections present the data reduction equations used in assessing the performance of NOP Rocket 1 as well as an overview of a basic uncertainty analysis. Test results for the NOP Rocket 1 are discussed with regards to rocket performance. The analysis of the data involved identifying the steady state time period, then averaging the data set during steady state. The averaging process was a straightforward summation of the data divided by the total number of data points sampled during that period.

9.1 Data Reduction Equations and Uncertainty Analysis

The basic measurements required for assessing rocket performance were discussed in Section 7.2.2. These measurements include chamber pressure, propellant mass flow rates, rocket thrust and nozzle temperatures. One of the most important parameters used to compare different propulsion systems is specific impulse, I_{sp}. There are several different specific impulse calculations that can be made, including the specific impulse, I and $(I_{sp})_{vac}$. These equations are derived from the momentum equation, which results in:

$$Thrust = F = \dot{m}_T u_e + (P_e - P_a)A_e \qquad (9\text{-A})$$

The average specific impulse, I is defined as:

$$I = \frac{F}{\dot{m}_T} = \frac{u_e}{g_c} + \frac{(P_e - P_a)A_e}{\dot{m}_T} = I_{sp} + \frac{(P_e - P_a)A_e}{\dot{m}_T} \qquad (9\text{-}2)$$

where the total propellant flow rate $\dot{m}_T$ is equal to $\dot{m}_{N_2O} + \dot{m}_{C_3H_8}$. The exit area A_e is 0.659 in^2, the nozzle throat area is $A^* = .298$ in^2 and P_a is the ambient pressure. The exit pressure P_e is given by $(P_e/P_c)^* P_c$, where the ratio P_e/P_c is calculated using a NASA chemical equilibrium code[34] resulting in $(P_e/P_c) = 0.1$, and P_c is the measured chamber pressure. The specific impulse I_{sp}, assuming a perfectly matched back pressure (i.e. no drag term in Eqn. (8.1)), is given by rearranging Eqn. (8.2):

$$I_{sp} = I - \frac{(P_e - P_a)A_e}{\dot{m}_T} \qquad (9\text{-}3)$$

where $I = F/\dot{m}_T$. The vacuum specific impulse $I_{sp,vac}$ is obtained from Eqn. (8.2) when the ambient pressure P_a, is assumed to be zero due to vacuum conditions:

$$I_{sp,vac} = I_{sp} + \frac{P_e A_e}{\dot{m}_T} \qquad (9\text{-}4)$$

The thrust coefficient c_f is calculated from:

$$c_f = \frac{F}{P_c A^*} \qquad (9\text{-}5)$$

The characteristic exhaust velocity c*, is given by the following equation:

$$c^* = \frac{(P_c)A^* g_c}{\dot{m}_f}$$ (9-6)

where $g_c = 32.2$ $lb_m ft/lb_f s^2$.

The c* efficiency is calculated by:

$$\eta_{c^*} = \frac{c^* Eq.(8.6)}{(c^*)_{theory}}$$ (9-7)

where $(c^*)_{theory}$ is obtained by using the NASA chemical equilibrium code[34] with the measured P_c and mixture ratio as inputs.

The NASA chemical equilibrium code[34] was used to obtain theoretical values for I_{sp} and $I_{sp,vac}$. The calculations were performed for idealized conditions, as well as for cases accounting for heat transfer to the heat sink test article. Heat transfer was calculated using two different heat transfer models. The first heat transfer model used the analysis of Bartz[35] to relate heat transfer flux $\dot{q}$ with A/A^*. The total heat transferred $\dot{Q}$ was calculated by:

$$\dot{Q} = \int q dA = 87.4 \text{ Btu/sec}$$ (9-8)

where $\dot{Q}$ is calculated at 150 °F average nozzle wall temperature based on nozzle thermocouple data. The enthalpy loss, H_{loss}, was then found by dividing $\dot{Q}$=87.4 Btu/sec by the average total nominal mass flow rate for Pc=150 psia, ~0.149 lb_m/sec to get H_{loss} =586.7 Btu/lb_m=14,330 cal/gmole. This value for enthalpy loss due to heat transfer is used to deficit the enthalpy values for N_2O and C_3H_8 in the NASA chemical equilibrium code[34] input deck.

The second method used to approximate heat transfer losses from the rocket motor was to apply a lumped capacitance model using the following equation for heat transfer, $\dot{Q}$:

$$\dot{Q} = h_c A(T_{af} - T_{wall}) = mC\dot{T}$$ (9-9)

where m is the component mass, C is the specific heat, obtained from experimental C data as a function of temperature, $\dot{T}$ is the time rate of temperature rise of the component mass m, h_c is the convective heat transfer coefficient, T_{af} and T_{wall} are the adiabatic flame and wall temperatures respectively. The total heat transfer is $\dot{Q}_T = \dot{Q}_c + \dot{Q}_n$ where $\dot{Q}_c$ is the heat transfer from the combustor and $\dot{Q}_n$ is the heat transfer from the nozzle.

Due to the fact that the rocket test article was instrumented with a thermocouple only in the nozzle and not in the combustor wall, the $\dot{T}$ for the combustor, $\dot{T}_c$, had to be calculated based on the nozzle measurement, $\dot{T}_n$, for which there was a thermocouple measurement.

Applying Eqn. (8.9) to the rocket nozzle and combustor portions of the motor, and equating the lumped capacitance expression with the convective heat transfer equation, an equation for $\dot{T}_c$ the combustor temperature rise is derived:

$$\dot{T}_c = \dot{T}_n \left(\frac{m_n}{m_c}\right)\left(\frac{C_{p,Cu}}{C_{p,SS}}\right)\left(\frac{h_c A_c T_c}{h_n A_n T_n}\right) \tag{9-10}$$

where the subscripts 'c' and 'n' refer to the combustor and nozzle components of the rocket motor, respectively. The ratio of h_c/h_n is provided by Bartz[35]. Experimental data shows that $\dot{T}_n$ is ~ 147.3 K/sec. Substituting the appropriate data into Eqn. (8.10), the combustor temperature rise is estimated to be ~ 10.9 K/sec. Now, knowing $\dot{q}$ for the combustor and nozzle, the total heat transfer $\dot{q}$ is estimated to be $\dot{q} = \dot{q}_c + \dot{q}_n$ ~17 Btu/sec + 39.3 Btu/sec=56.3 Btu/sec. The enthalpy loss, H_{loss} is (56.3 Btu/sec)/(0.149 lb_m/sec)=377.8 Btu/lb_m=9228.8 cal/gmole. This value for enthalpy loss due to heat transfer is used to deficit the enthalpy values for N_2O and C_3H_8 in the NASA chemical equilibrium code[34] input deck.

The above analysis and data reduction equations (Eqns. 9.1-9.10) were used to analyze the results presented in the following sections, Section 9.2. As with any presentation of experimental data, an uncertainty analysis is required to display the degree of confidence in the data, and track the propagation of these uncertainties to calculated parameters. This basic analysis accounts for the uncertainty in the measurement of each data point. It does not include the uncertainty in the averaging process of the reduced data, which was subject to the large P_c oscillations observed and is also a slight function of how the user determined the steady state time period.

The uncertainty in c* is found from the following equation:

$$u_{c^*} = \left[\left(\frac{\partial c^*}{\partial P_c}u_{P_c}\right)^2 + \left(\frac{\partial c^*}{\partial P_a}P_a\right)^2 + \left(\frac{\partial c^*}{\partial \dot{m}}u_{\dot{m}}\right)^2 + \left(\frac{\partial c^*}{\partial A^*}u_{A^*}\right)^2\right]^{1/2} \tag{9-11}$$

where:

$$\frac{\partial c^*}{\partial P_c} = \frac{A^* g_c}{\dot{m}} = \frac{\left(.298 in^2\right)\left(32.2 lb_m ft/lb_f s^2\right)}{\left(0.23 + 0.043\right)lb_m/s} = \left(35.1\right)\frac{in^2 ft}{lb_f s}$$

87

$$\frac{\partial c^*}{\partial P_a} = \frac{A^* g_c}{\dot{m}_f} = \frac{\left(.298 in^2\right)\left(32.2 lb_m ft/lb_f s^2\right)}{(0.23+0.043) lb_m/s} = (35.1)\frac{in^2 ft}{lb_f s}$$

$$\frac{\partial c^*}{\partial \dot{m}_f} = \frac{-(P_c)A^* g_c}{\dot{m}_f^2} = \frac{-\left(150 psia\right)\left(0.298 in^2\right)\left(32.2 lb_m ft/lb_f s^2\right)}{(0.23+0.043) lb_m/s} = (-19,312)\frac{ft}{lb_m}$$

$$\frac{\partial c^*}{\partial A^*} = \frac{(P_c)g_c}{\dot{m}_f^2} = \frac{\left(150 psia\right)\left(32.2 lb_m ft/lb_f s^2\right)}{(0.23+0.043) lb_m/s} = (17,692)\frac{ft}{in^2 s}$$

The uncertainties in P_c, P_a, $\dot{m}_f$, and A^* are given by:

$u_{P_c} = u_{P_a} = \sim 1\%$ Full Scale range of SETRA pressure transducer = 1.3 psia

$u_{\dot{m}_f} = \sim 2\%$ estimated guess=0.005 lb_m/sec.

The uncertainty in the nozzle throat area, u_{A^*} is given by:

$$u_{A^*} = \left[\left(\frac{\partial A^*}{\partial d^*}u_{d^*}\right)^2\right]^{1/2} = \left[\left(\frac{\pi}{4}2d^*u_{d^*}\right)^2\right]^{1/2} = \frac{\pi d^*}{2}u_{d^*} \qquad (9\text{-}12)$$

where the uncertainty in throat diameter, u_{d^*} is +/- 0.005", so that $u_{A^*} = 0.00484$ in^2, from Eqn. (8.12). Knowing all the constituent uncertainties, Eqn. (8.11) is used to calculate the overall uncertainty in the c* data, $u_{c^*} = +/-144.3 ft/sec$.

To calculate the uncertainty in the I$_{sp}$ data, $u_{I_{sp}}$ Eqn. (8.3) is used to obtain:

$$u_{I_{sp}} = \left[\left(\frac{\partial I_{sp}}{\partial F}u_F\right)^2 + \left(\frac{\partial I_{sp}}{\partial \dot{m}_f}u_{\dot{m}_f}\right)^2 + \left(\frac{\partial I_{sp}}{\partial (P_e/P_c)}u_{(P_e/P_c)}\right)^2 + \left(\frac{\partial I_{sp}}{\partial P_c}u_{P_c}\right)^2 + \left(\frac{\partial I_{sp}}{\partial P_a}u_{Pa}\right)^2 + \left(\frac{\partial I_{sp}}{\partial A_e}u_{A_e}\right)^2\right]^{1/2}$$

$$(9\text{-}13)$$

The third and fourth terms are considered negligible as determined from the experimental and numerical data using the NASA chemical equilibrium code.[34] The other terms in Eqn. (8.13) are calculated as follows:

$$\left(\frac{\partial I_{sp}}{\partial F}\right) = \frac{1}{\dot{m}_f} = 3.66 \sec/lb_m$$

$$\left(\frac{\partial I_{sp}}{\partial \dot{m}_f}\right) = \frac{-F}{\dot{m}_f^2} + \left[\frac{P_e}{P_c}P_c - P_a\right]\frac{A_e}{\dot{m}_f^2} = -668.3 \text{ lb}_f\text{s}^2/\text{lb}_m^2$$

$$\left(\frac{\partial I_{sp}}{\partial P_a}\right) = \frac{A_e}{\dot{m}_f} = 2.41 \text{ in}^2\text{sec/lb}_m$$

$$\left(\frac{\partial I_{sp}}{\partial A_e}\right) = -\left[\frac{P_e}{P_c}P_c - P_a\right]\frac{1}{\dot{m}_f} = -1.1 \text{ lb}_f\text{sec/in}^2\text{lb}_m$$

The uncertainties in the thrust, mass flow rate, atmospheric pressure and exit area data are:

$u_F = +/- 0.1\%$ full scale of compression load cell $= +/- 0.1$lbs$_f$. (Full Scale=100 lbs$_f$)

$u_{\dot{m}_f} = 0.005$ lb$_m$/sec

$u_{P_a} = +/- 0.1$ psia (educated guess)

$u_{A_e} = \frac{\pi d_e}{2}u_{d_e} = +/- 0.0072$ in^2, where the uncertainty in the machining of the nozzle exit diameter is +/- 0.005".

Upon substitution of the above information into Eqn. (8.13), the uncertainty in the I_{sp} data is $u_{I_{sp}} = +/- 3.4$ sec.

Knowing the uncertainty in the performance data c* and Isp, as well as how to account for heat losses, the rocket data can now be analyzed as described in the following section.

9.2 NOP Rocket Performance Test Results

During this development program, experiments were conducted for the purpose of assessing rocket performance, determining the optimum L* for the given injection scheme, and evaluating rocket ignition using catalytic decomposition of nitrous oxide. These steady state performance tests were performed in the atmospheric test stands (Test Stand 1 and 2) at UAH on a rocket with a truncated nozzle (NOP Rocket 1 and 2). The rocket test article was a copper heat sink design consisting of a preliminary injector design, combustor and nozzle components. To compensate for the non-optimal injector, combustor L* was set sufficiently large to accommodate atomization, evaporation, mixing and combustion.

It should be noted that the NOP Rocket 2 was tested at Test Stand 2, but combustion instabilities, perhaps due to inappropriate L*, coupled with a non-optimal injector,

mitigated use of this rocket in favor of NOP Rocket 1. The performance data presented in this section is therefore for the NOP Rocket 1 test article evaluated on Test Stand 2.

The rocket engine (NOP Rocket 1) was tested with L*= 1, 2, and 3m. At L*=1m, NOP Rocket 1 showed degraded performance. The L*=3 m was used for this injection scheme, and L* can only be reduced by improving the injector design. The swirl injector was chosen for these concept development tests since it provides reasonable performance without the expense of complex machining processes. A more elaborate injection scheme will be developed as a step to higher technical readiness levels (TRLs).

Heat transfer losses experienced during ground testing will be mitigated in a prototype rocket by designing to maintain a higher wall temperature. By using flight materials instead of heat sink copper, proper use of coatings and insulation, and possibly regeneratively heating the fuel, a c* efficiency of 96% should be achievable, along with correspondingly higher specific impulse approaching that of the theoretical values.

Figure 44 shows a NOP rocket firing in Test Stand 2 at UAH. Also shown in this figure is a traversing pitot rake used for the AEDC thrust measurement technique. Tests were performed to assess rocket performance over a range of mixture ratios (4.9-8.7) and L* (2m and 3m). A compilation of results from these tests is shown in Figure 45 through Figure 50, and Table 18. These plots display some of the performance data and typical rocket performance parameters generated from the reduced data. For comparison purposes, plots of the theoretical vacuum $I_{sp,vac}$, I_{sp}, and c*, obtained from a NASA chemical equilibrium code[34], are presented. Initial results are promising, showing rocket performance consistent with theoretical prediction taking into account the effects of heat transfer and nozzle area ratio.

Figure 45 shows a plot of specific impulse versus mixture ratio. The data are displayed with symbols and uncertainty bars, while theoretical predictions are displayed by various colored lines. Heat loss was calculated by two methods as discussed in Section 9.1 and included with the theoretical predictions. One method used the Bartz analysis[35], where a heat loss of 586.7 Btu/lb_m for N_2O and C_3H_8 each was calculated for a wall temperature of 150°F and used to generate the heat loss curves in Figure 45-Figure 48, and Figure 50. The second method assumed a lumped capacitance model for the combustor and rocket nozzle, with an estimated 377.8 Btu/lb_m for the heat loss, for N_2O and C_3H_8 each. It is evident from these plots that heat loss to the cold heat-sink rocket model can account for the difference between the ideal rocket performance and that measured. Other losses not accounted for in the theoretical predictions include total pressure loss in the combustion chamber, non-axial thrust losses due to flow angularity at the exit of the truncated nozzle, and incomplete combustion.

Figure 45 shows the I_{sp} as a function of mixture ratio for L*=2m and 3m for both Test Stand 1 and 2. The L*=3m NOP Rocket 1 tested on Stand 2 displays about a 7% drop in I_{sp} compared with the Test Stand 1 tests with the same rocket. Reasons for this difference may be attributed to uncertainties in mass flow rate and thrust measurement taken at Test Stand 1. The maximum I_{sp} measured at Test Stand 1 is 181.5 sec at an MR=4.89, compared with a maximum I_{sp} of 171.85 sec at MR=6.83, measured at Test Stand 2.

From Figure 46, the maximum $I_{sp,vac}$ measured at Test Stand 1 (210.4 sec) was at a L*=2m and MR=5.44, with a fairly "clean" chamber pressure trace, without large pressure oscillations and chugging observed at the higher mixture ratios (6<MR<8.68). The maximum $I_{sp,vac}$ measured at Test Stand 2 (204.1 sec) was at a L*=3m and MR=6.83.

Figure 47 shows that at the A/A* of 2.21, the experimental data is within 18% of the theoretical curves, which do not account for heat losses, and within 11% of the theoretical data that does account for heat losses, as calculated by using Bartz analysis.[35] At the design area ratio of 50, for space propulsion applications, the NOP rocket, with lower heat losses than the heat sink test article, and improved injector design should approach the theoretical vacuum I_{sp} of 312 sec for MR=8.3.

Figure 48 shows a plot of c* versus the mixture ratio where the c* varied from 4460 ft/sec at MR=4.89 to 4866 ft/sec at MR=8.68. Heat loss calculations (via the Bartz analysis[35]) used in adjusting the theoretical c* curves, correlate well with the experimental c* data for the Test Stand 2. The c* efficiencies, between 82% and 93%, reflect a combination of all system losses, including heat loss and non-optimal propellant injection (affecting atomization, vaporization, mixing, and combustion). As shown in Figure 49 for Test Stand 1, η_{c*} varied from 87.9% at MR=4.89 to 92.7% at MR=5.44; and for Test Stand 2, η_{c*} varied from 81.8% at MR=6.82 to η_{c*}=93.2% at MR=8.68.

Figure 50 shows the variation in the NOP Rocket 1 thrust coefficient (article 1, evaluated on test Stand 1 and 2) as a function of mixture ratio for two combustor lengths, L* (2m and 3m). The average thrust coefficient measured on Test Stand 1 is 1.21, compared with a theoretical value (neglecting heat losses) of 1.27, and a measured value of 1.14 on Test Stand 2, compared with a theoretical value (neglecting heat losses) of 1.26. Table 18 presents a summary of the relevant performance data (thrust, I_{sp}, I, $I_{sp,vac}$, c* and P_c) as a function of mixture ratio and L*.

Data is shown for L* of 2m and 3m and indicates no real change in performance between the two combustor lengths, with respect to I_{sp}, $I_{sp,vac}$, c* and η_c. However, L* and mixture ratio are not the only factors affecting engine performance. Increasing N_2O mass flow rate above a given value leads to larger chamber pressure oscillations and a decrease in c* efficiency, as shown in Figure 51 - Figure 52. As the mass flow rate of N_2O increases from $\dot{m}_{N2O}$=.232 lb_m/sec (η_{c*}=.887) to $\dot{m}_{N2O}$=.265 lb_m/sec (η_{c*}=.818), P_c oscillations increase from ~17 Hz (+/- 4.55 psia standard deviation) to ~ 28 Hz (+/- 13.1 psia standard deviation).
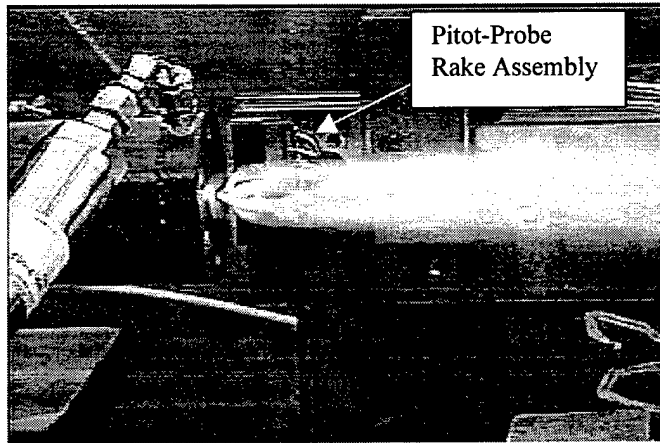
Figure 44 NOP rocket firing at newly built atmospheric test stand at UAH with pitot rake assembly foreground.
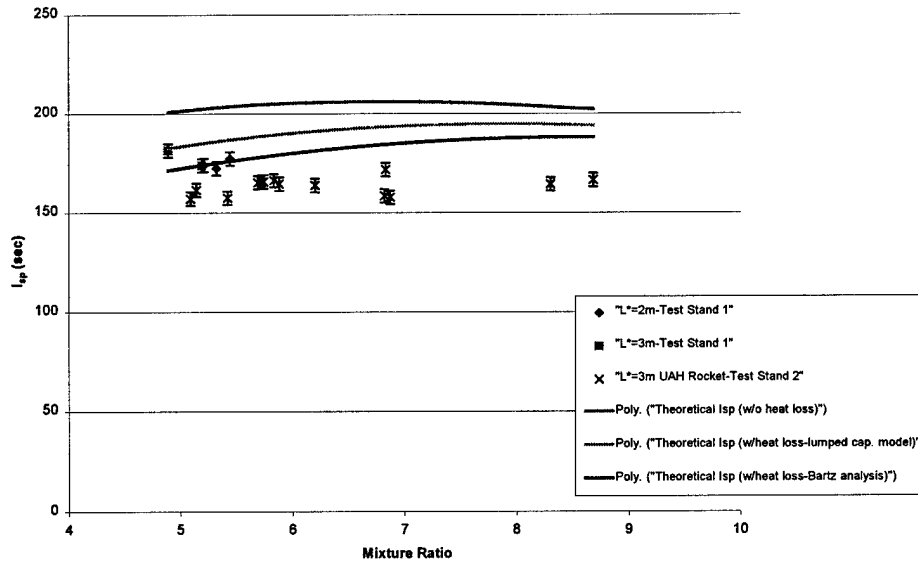
Figure 45: Specific impulse I$_{sp}$ as a function of mixture ratio for two different combustor L*.
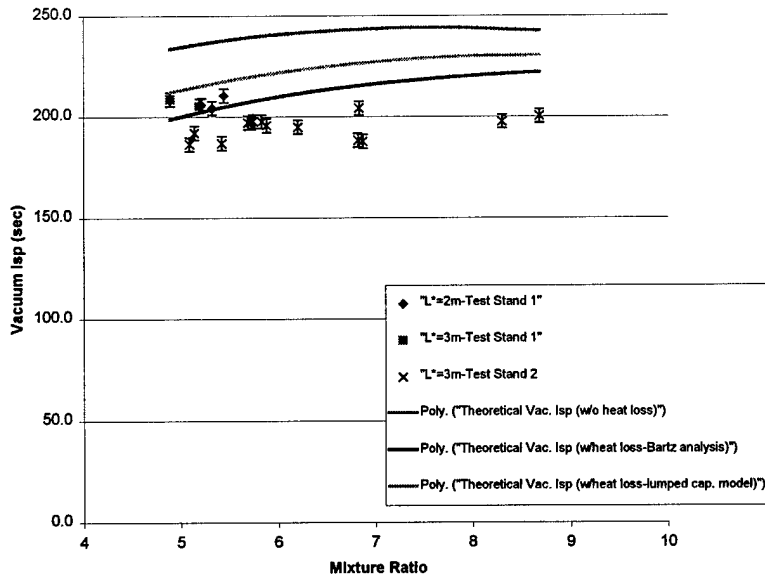
Figure 46: Vacuum I_{sp} versus mixture ratio for two different combustor L*.

$$I_{sp\,vac} = I_{sp} + P_{amb}A_{exit} / Mdot$$
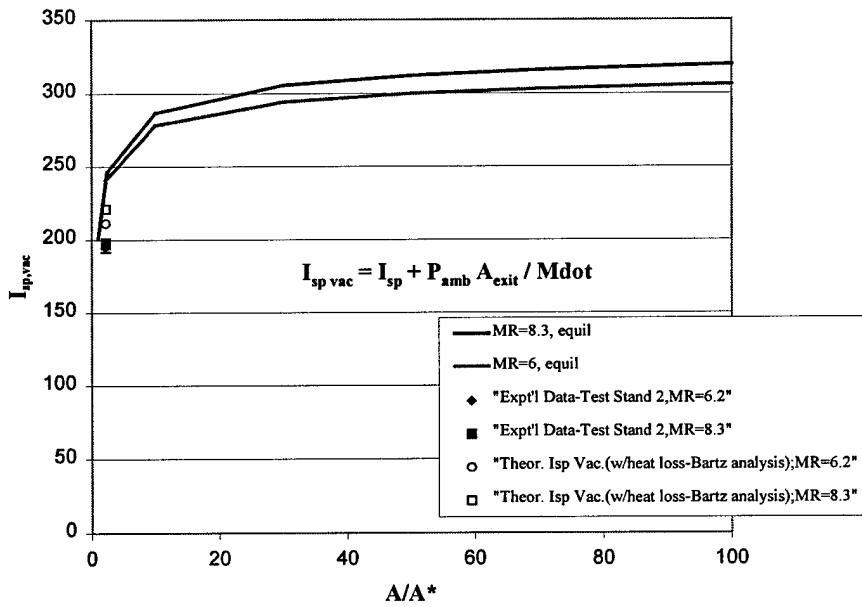
Figure 47: Theoretical and experimental data for vacuum I_{sp} as a function of A/A*.
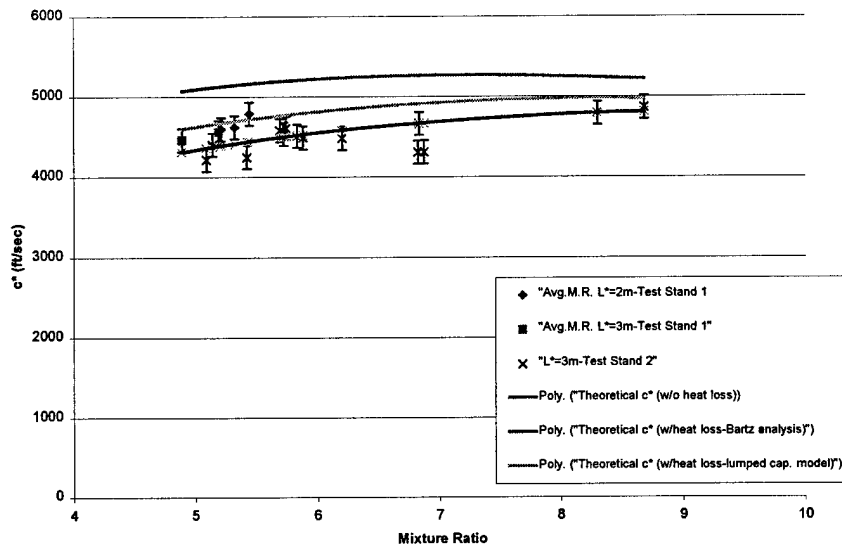
Figure 48: Rocket c* as a function of mixture ratio for two different combustor L*.
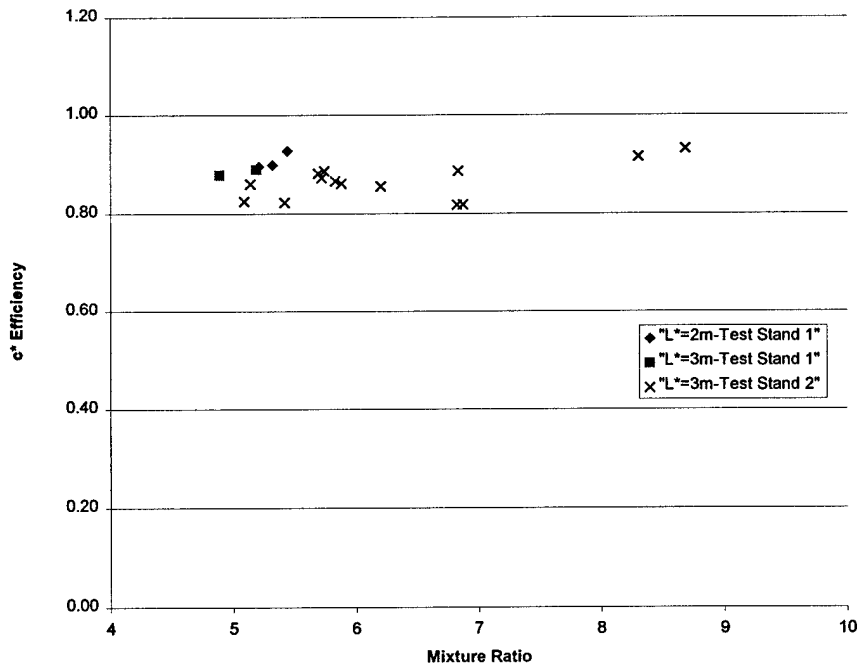
Figure 49: Rocket c* efficiency as a function of mixture ratio for two different combustor L*.

94
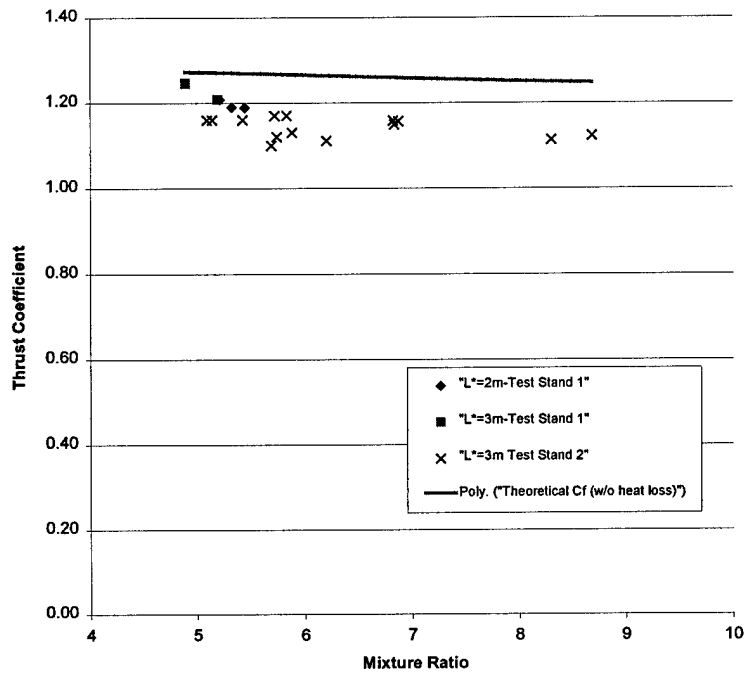
Figure 50: Rocket thrust coefficient as a function of mixture ratio for two different combustor L*.

L*	Avg. M.R	Avg. Thrust	Avg. I$_{sp}$	Avg. I	Avg. I$_{sp}$ Vac.	Avg. c*	Avg. P$_c$
(m)		(lb$_{sf}$)	(sec)	(sec)	(sec)	(ft/sec)	(psia)
2	5.44	52.5	177.4	177.5	210.4	4788.1	148.2
2	5.21	50.2	174.1	172.3	205.7	4594.8	139.5
2	5.32	50.0	172.5	170.9	204.2	4620.3	140.9
3	5.19	48.9	173.9	171.2	205.3	4562.4	136
3	4.89	46.6	181.5	172.5	208.5	4460.3	125.5
1	5.88	27.5	114.3	99.7	135.0	3522.5	101.2
1	5.29	37	146.2	132.4	167.	3621.0	104.6
3	6.87	48	157.8	155.7	187.6	4310.6	139.2
3	6.82	47.4	158.5	155.9	188.2	4308.4	137.3
3	6.2	39.0	163.8	155.6	194.8	4481.9	117.9
3	6.83	45	171.8	167.5	204.1	4666.4	131.4
3	8.68	56.9	166.5	170.7	200.2	4865.7	170.0
3	8.3	53.1	164.4	166.7	197.5	4794	160.1
3	5.14	46.4	161.5	158.4	191.9	4402.6	135.2
3	5.09	45.02	157.1	153	186.3	4218.7	130.2
3	5.42	45.18	157.5	153.5	186.8	4248.5	131.12
3	5.88	41.53	164.6	158.2	195.6	4489.6	123.55
3	5.69	39.6	165.3	157.9	197	4579.2	120.47
3	5.74	44.04	165.7	161.6	197.6	4609.7	131.73
3	5.83	48.21	166.3	164.1	197.5	4513.3	139.02
3	5.72	52.64	165.6	166	197	4537.9	150.82

Table 18: Summary of performance data for NOP rocket tests.

Legend:
- (MR=5.72;N2O mdot=.270 pps,C3H8 mdot=.047 pps, c*eff=.873)
- (MR=5.74;N2O mdot=.232 pps, C3H8 mdot=.04 pps,c*eff=.887)
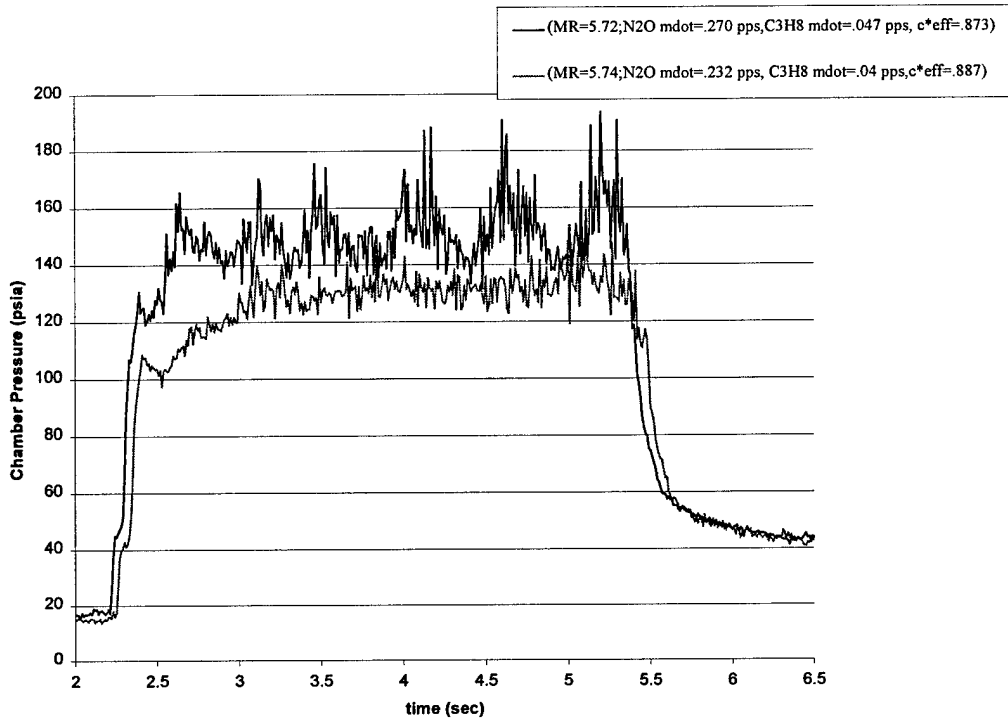
Figure 51: Shown above is a plot of chamber pressure profile for fixed average MR=5.73 and C_3H_8 flow rate=.044 lb_m/s for varying N_2O flow rate.

The chamber pressure profiles displayed in Figure 51 show that there are larger rocket chamber pressure oscillations (for approximately the same MR and propane fuel flow rate) at higher N_2O flow rates. This result shows that the engine test hardware operates smoother for N_2O flow rates less than 0.270 lb_m/s, and an MR range of 5-6. Also, notice from Figure 51 that for a fixed MR, as N_2O flow rate increases by 16%, the c* efficiency decreases by 17.7%. These combustion instabilities are related to several factors, which include: (1) injector design; (2) sufficient L* for appropriate injector design; and (3) possible injection of N_2O in a two phase flow state. All these factors will require further study to attain a more optimal design.

The residence time inside the combustor scales directly with L^{*2} and inversely with mass flow rate. Therefore, as the N_2O flow rate is increased the residence time for an N_2O molecule (for a given L*) decreases as $1/\dot{m}$. Figure 51 implies that there may be incomplete combustion or insufficient mixing, as well as oscillating fluid flow and acoustic interactions, causing the increased P_c oscillations, as the N_2O flow rate increases from .232 lb_m/sec to .270 lb_m/sec.

Similarly, Figure 52 displays the chamber pressure profiles for three mixture ratios and c* efficiencies, for a fixed propane flow rate of 0.040 lb_m/sec. From this data, we can

97

deduce that as mixture ratio increases by 19%, the c* efficiency decreases by 8%, the chamber pressure oscillations increase 65%, leading to a degradation in I_{sp} by about 4% (from 165.7 sec at MR=5.74 to I_{sp} = 158.5 sec at MR=6.82). The P_c oscillations increase from ~17 Hz, ± 4.55 psia at MR=5.74 to 28 Hz, ± 13.1 psia at MR=6.82. This data, in conjunction with the information in Figure 51 clearly demonstrates that $\dot{m}_{N2O}$ (and indirectly a residence time and L* effect) plays a critical role with regards to rocket combustor instabilities and performance, in addition to mixture ratio.
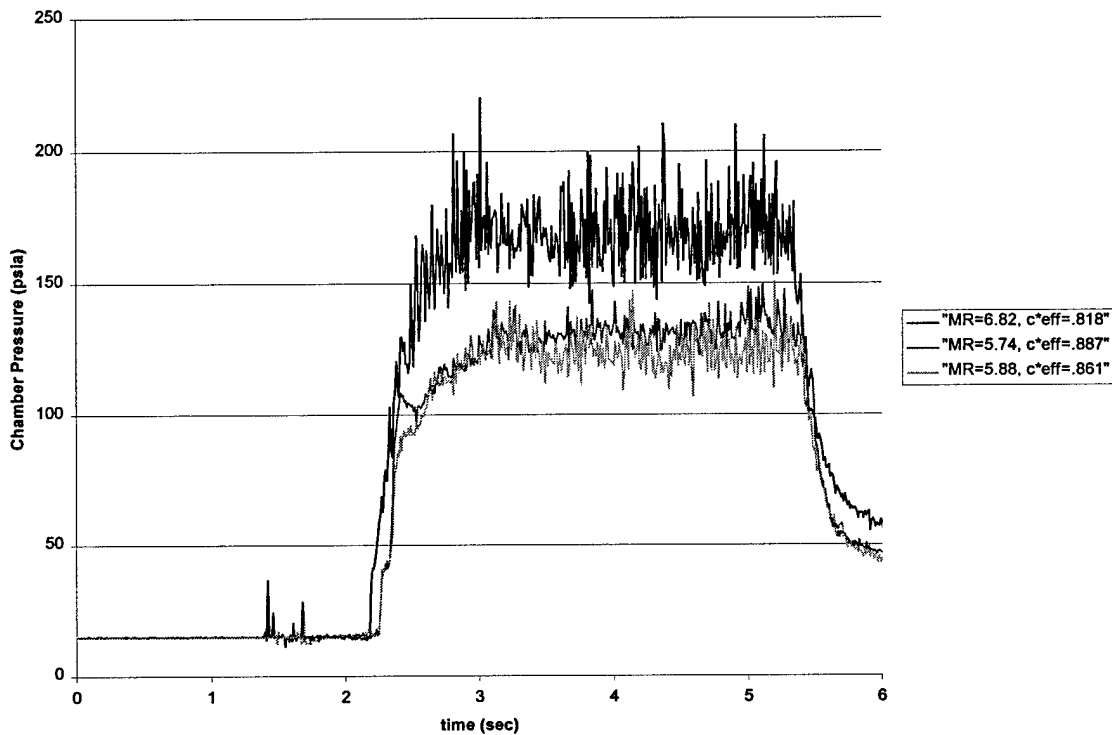
Figure 52: Chamber pressure profiles for variable mixture ratio and c* efficiency and a fixed propane flow rate of 0.040 lb$_m$/sec.

9.3 Pitot Pressure measurements and the Determination of Thrust

9.3.1 Introduction

A pitot pressure system was designed, fabricated, and deployed for the UAH test series on 15 March 2001. The pitot pressure measurements were used to determine the thrust of the rocket engine. This was intended as a technology demonstration and as a back-up to the UAH thrust stand.

9.3.2 Theory

The vacuum thrust (F_v) of a jet propulsion device, assuming ideal one-dimensional flow, can be shown to be [36,37]

$$F_v = \dot{m} u_e + P_e A_e \qquad (9\text{-}14)$$

where u_e, P_e, and A_e are the exit plane velocity, static pressure and area, and $\dot{m}$ is the mass flow. Since the mass flow may be written as

$$\dot{m} = \rho_e u_e A_e \qquad (9\text{-}15)$$

where ρ_e is the exit plane density, Equation (9-14) becomes

$$F_v = \left(\rho_e u_e^2 + P_e \right) A_e \qquad (9\text{-}16)$$

where the term within the parentheses is referred to as the stream thrust. Applying the ideal gas law yields

$$F_v = \left(\frac{P_e}{R T_e} u_e^2 + P_e \right) A_e \qquad (9\text{-}17)$$

where R is the specific gas constant and T_e is the exit plane static temperature. Multiplying and dividing the first term by the ratio of specific heats (γ) yields

$$F_v = \left(\gamma \frac{u_e^2}{\gamma R T_e} + 1 \right) P_e A_e \qquad (9\text{-}18)$$

Recognizing that the exit plane speed of sound (a_e) is given by

99

$$a_e = \sqrt{\gamma R T_e} \qquad (9\text{-}19)$$

and the exit Mach number (M_e) by

$$M_e = \frac{u_e}{a_e} \qquad (9\text{-}20)$$

Equation (9-18) may be written as (see Reference 38)

$$F_v = \left(\gamma M_e^2 + 1\right) P_e A_e \qquad (9\text{-}21)$$

Equation (9-21) could be used to infer thrust from an exit plane static pressure measurement. However, it is obvious that this relation is sensitive to errors both in γ and M_e – both quantities that would have to be approximated by either calculations or other measurements – in addition to measurement errors in P_e. The thrust varies essentially linearly with γ and goes approximately as the square of the Mach number. Therefore, small errors in either γ or M_e would contribute large errors to the inferred thrust. For example, the probe method recommended in Reference 39 requires measurement of both static and total pressures.

However, if we measure pitot pressure (P_{02}) rather than the static pressure, Equation (9-21) may be written as

$$F_v = \left(\gamma M_e^2 + 1\right) \frac{P_e}{P_{02}} P_{02} A_e \qquad (9\text{-}22)$$

where (assuming now a constant γ) the ratio of the static pressure to the pitot pressure is given by

$$\frac{P_e}{P_{02}} = \left[\frac{2}{(\gamma+1)M_e^2}\right]^{\frac{\gamma}{\gamma-1}} \left[\frac{2\gamma M_e^2 - (\gamma-1)}{\gamma+1}\right]^{\frac{1}{\gamma-1}} \qquad (9\text{-}23)$$

for supersonic ($M_e \geq 1$) conditions and

$$\frac{P_e}{P_{02}} = \left[1 + \frac{\gamma-1}{2}M_e^2\right]^{\frac{-\gamma}{\gamma-1}} \qquad (9\text{-}24)$$

for subsonic ($M_e < 1$) flow.

Equation (9-22) may now be written as

$$F_v = P_{02} A_e f\left(\gamma, M_e\right) \qquad (9\text{-}25)$$

100

where

$$f(\gamma, M_e \geq 1) = \left[\frac{2}{(\gamma+1)M_e^2}\right]^{\frac{\gamma}{\gamma-1}} \left[\frac{2\gamma M_e^2 - (\gamma-1)}{\gamma+1}\right]^{\frac{1}{\gamma-1}} (\gamma M_e^2 + 1) \qquad (9\text{-}26)$$

or

$$f(\gamma, M_e < 1) = \left[1 + \frac{\gamma-1}{2}M_e^2\right]^{\frac{-\gamma}{\gamma-1}} (\gamma M_e^2 + 1) \qquad (9\text{-}27)$$

for supersonic or subsonic flows, respectively. The function f is termed the pitot pressure thrust function.

It will be shown that $f(\gamma, M_e)$ is relatively insensitive to both γ and M_e. This is one of the advantages of using pitot pressure rather than static pressure. The thrust measured on a static test stand (F) would be given by

$$F = P_{02} A_e f(\gamma, M_e) - P_\infty A_e \qquad (9\text{-}28)$$

where P_∞ is the ambient atmospheric pressure.

The relations above all assume uniform one-dimensional flow. If instead we assume axisymmetric (radially-varying) flow, Equation (9-28) becomes

$$F_v = 2\pi \int_0^{R_e} P_{02} f(\gamma, M_e) r \, dr - P_\infty A_e \qquad (9\text{-}29)$$

where R_e is the nozzle exit radius.

The function $f(\gamma, M_e)$ given by Equations (9-26) and (9-27) exhibits an absolute maximum at $M_e = 1$, which is given by

$$f(\gamma, M_e = 1) = \left(\frac{2}{\gamma+1}\right)^{\frac{\gamma}{\gamma-1}} (\gamma+1) \qquad (9\text{-}30)$$

The high Mach number asymptote of the function $f(\gamma, M_e)$ is given by

$$f(\gamma, M_e \to \infty) = \left(\frac{2}{\gamma+1}\right)^{\frac{\gamma+1}{\gamma-1}} \gamma^{\frac{\gamma}{\gamma-1}} \qquad (9\text{-}31)$$

The low Mach number limit is given by

$$f(\gamma, M_e = 0) = 1 \qquad\qquad (9\text{-}32)$$

The function given by Equations (9-26) and (9-27) is plotted as a function of Mach number for several different ratios of specific heat in Figure 53. Note that the value of the function varies less than 30% over the entire range of Mach number and γ. For any supersonic Mach number, the function varies less than 5% with γ. This demonstrates that the pitot pressure thrust function (f) is relatively insensitive to both M_e and γ, and for a sufficiently high Mach number, the function is completely insensitive to Mach number. These sensitivities will be discussed in more detail below.
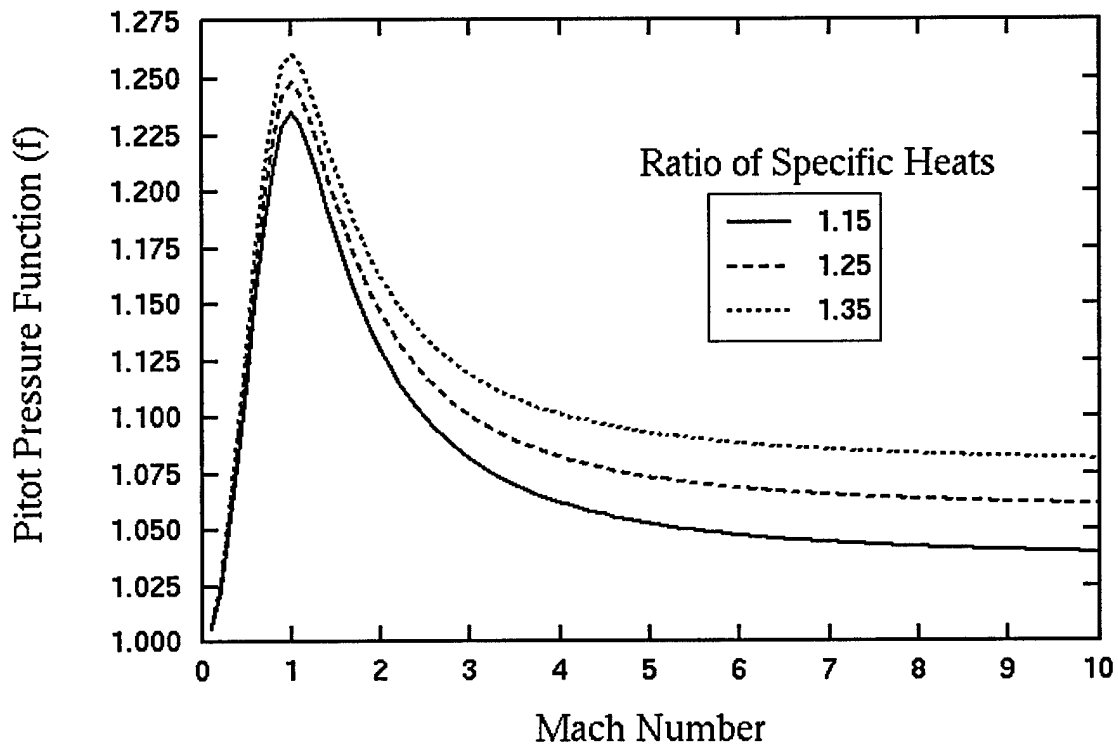
Figure 53: Pitot Pressure Thrust Function as a Function of Mach Number and Ratio of Specific Heats

Figure 54 shows the allowable error in Mach number if a +/-2% uncertainty in the pitot pressure thrust function is desired. For example, the figure shows that, at a nominal Mach number of 3, the allowable uncertainty in the actual Mach number ranges from – 20% to +40%. That is, the Mach number can actually be between 2.4 and 4.2 and the function f would vary only 2% from its value at Mach 3. Therefore, even a rough estimate of the local Mach number can provide a sufficiently small uncertainty in the pitot pressure thrust function.
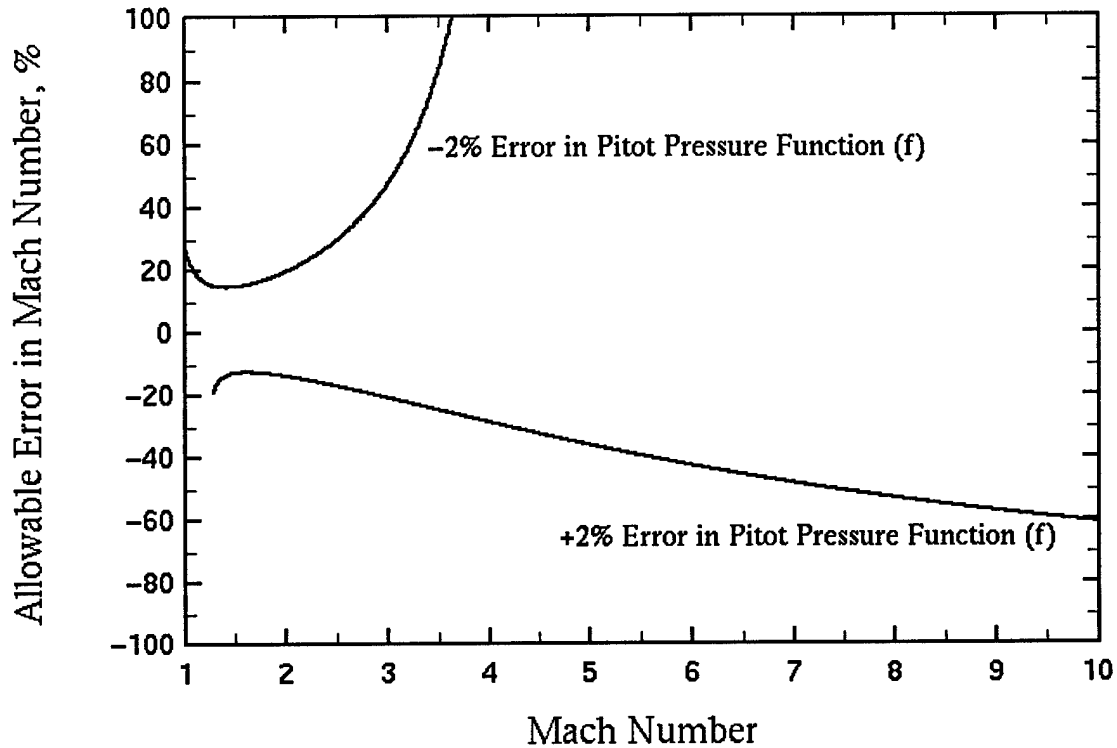
Figure 54: Allowable Error in Assumed Mach Number to Achieve +/-2% Error in the Pitot Pressure Thrust Function

As another example, Figure 55 shows the allowable error in Mach number to achieve +/- 0.5% error in the pitot pressure thrust function for Mach numbers between one and two. This region is relevant for application to turbine engines, where the exhaust is typically mildly supersonic. Note that, at a Mach number of 1.2, the allowable Mach number error is +/- 5% to achieve +/- 0.5% error in the pitot pressure thrust function – an effective lever arm of 10:1.

Allowable Error in Mach Number to Achieve +/– 0.5% Error
in Stream Thrust Function
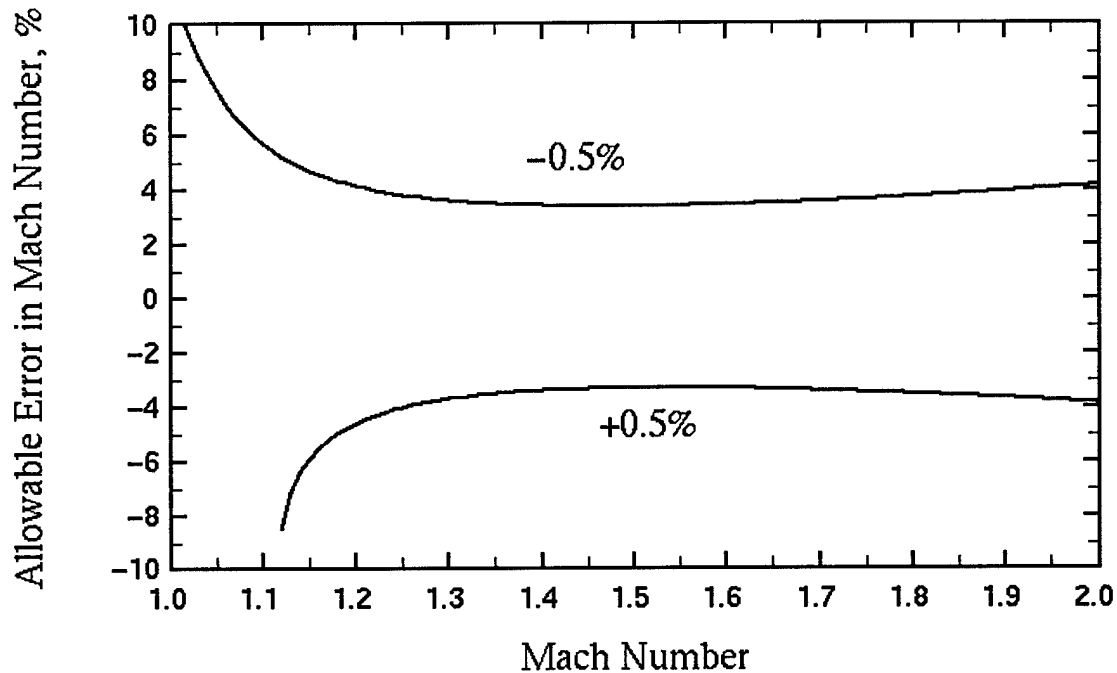
Figure 55: Allowable Error in Assumed Mach Number to Achieve +/-0.5% Error in the Pitot Pressure Thrust Function

9.3.3 Effect of Thermochemistry

The theoretical development above assumed ideal gas behavior – i.e. constant specific heats. In this section, the effect of variable specific heats is addressed computationally. As shown above, the stream thrust (σ) is given by

$$\sigma = P + \rho u^2 \quad (9\text{-}33)$$

Multiplying and dividing Equation (9-33) by the pitot pressure (P_{02}) yields

$$\sigma = P_{02}\left[\frac{P + \rho u^2}{P_{02}}\right] \quad (9\text{-}34)$$

The term in the brackets is the pitot pressure thrust function, but, unlike above, no assumption has been made about thermochemistry.

An axisymmetric, viscous, chemically reacting CFD model[40] was used to execute a series of nozzle flowfield calculations for a hydrocarbon-fueled rocket engine. Nine cases were executed – nominal chamber pressure and mixture ratio, and +/- 10% variations in chamber pressure and mixture ratio. The model also includes the capability of computing the pitot pressure assuming frozen composition but allowing variable specific heats in the normal shock process. This will allow the computation of the bracketed term in Equation (9-34). For this particular nozzle, the nominal computed exit plane Mach number distribution is shown in Figure 56. For every point in the nine computed exit planes, both the stream thrust and the frozen pitot pressure were calculated. The ratio of these quantities (i.e. the bracketed term in Equation (9-34) is plotted as a function of Mach number in Figure 57. Also included on the figure is the pitot pressure thrust function computed for a constant ratio of specific heats of 1.23.

Note that the results from then nine computed cases are indistinguishable from each other, indicating that the pitot pressure thrust function is insensitive to rather large changes in chamber pressure and mixture ratio. Note also that the constant and variable specific heat results are separated at most by 2%.
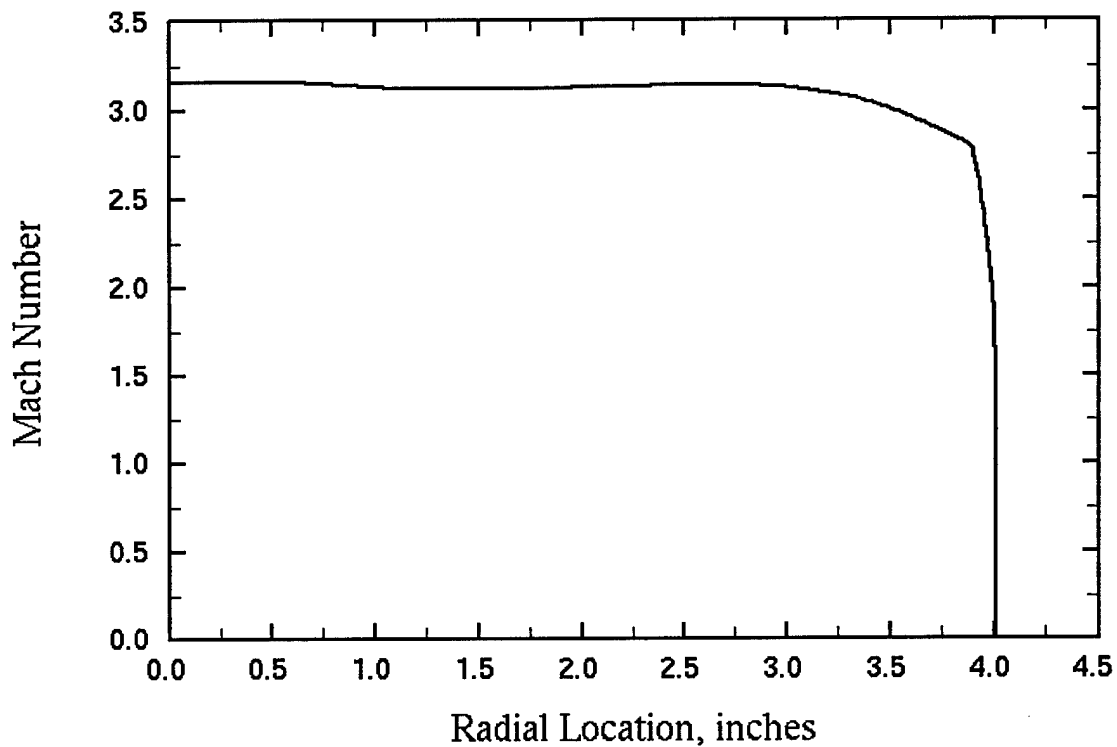
Figure 56: Computed exit plane Mach number distribution
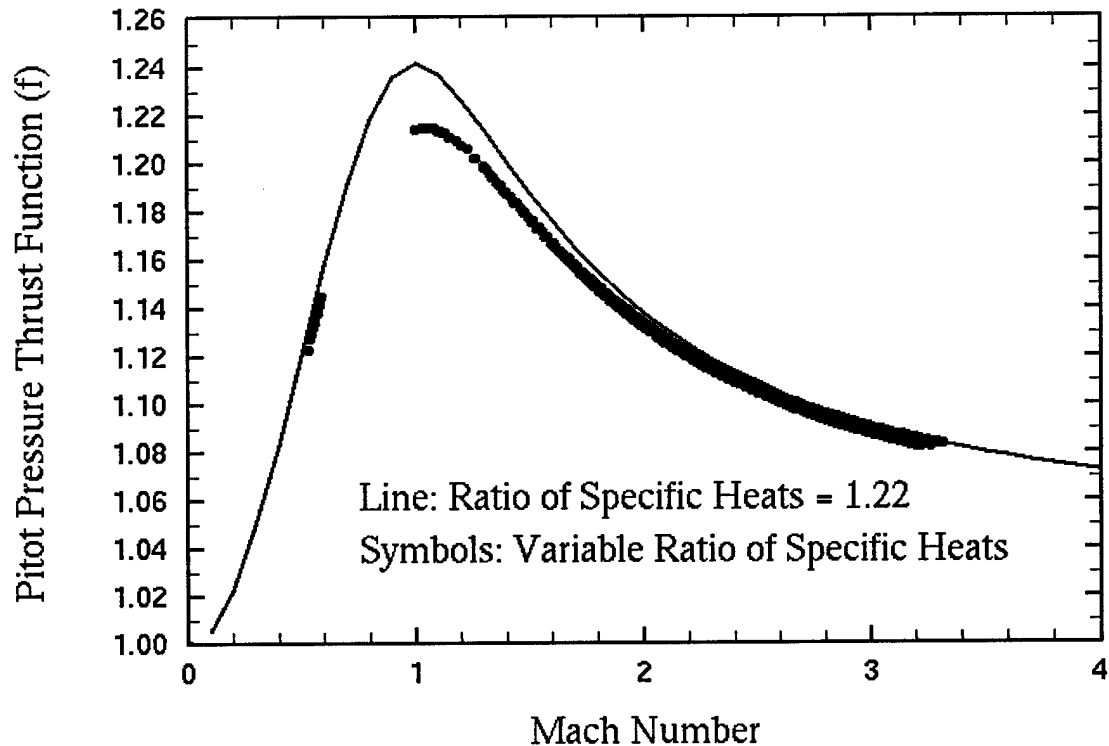
Figure 57: Pitot pressure thrust function for constant and variable specific heats

The results in Figure 57 allow specific heats to vary, but the composition remains fixed. If chemical reactions are allowed take place in the shock/stagnation processes in front of the pitot probe, and those reactions proceed to completion, then the indicated pitot pressure is the equilibrium pitot pressure, which is typically somewhat higher than the frozen pitot pressure. This is indicated schematically in Figure 58. The figure also shows the effect of probe size on the sensed pitot pressure. The figure shows the ratio of the sensed pitot pressure (P_{02}) to the equilibrium pitot pressure ($P_{02, equil}$) as a function of probe diameter. For large probes, the shock stands a large distance away from the probe tip, allowing more time for reactions to proceed between the shock and the probe tip. Therefore, a large enough probe will sense the equilibrium pitot pressure. As the probe size is decreased, the reactions will not have time to proceed to equilibrium, and kinetic rates become important. As the size is decreased further, a frozen plateau is reached. If the probe size is decreased even further to the point that the probe size is on the order of the mean free path, rarefaction effects can bcome inportant. An optimum probe size may be selected by computing the chemically reacting flow field about the probe tip for varying tip sizes. More information on this technique is available in References 41 and 42.

1.

$P_{02}/P_{02,}$

| Rarefaction Effects | Frozen Limit | Kinetic Effects | Equilibrium Limit |
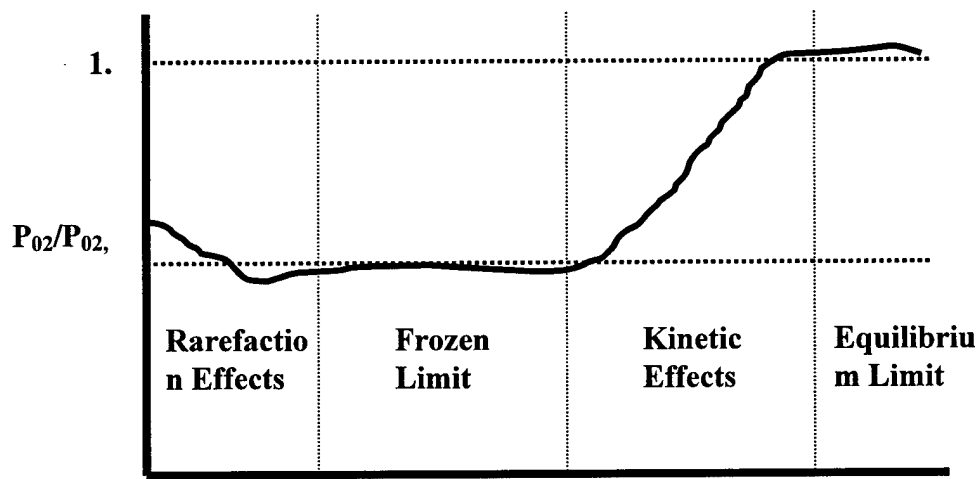
1.1.1   Probe Diameter

Figure 58: Probe Size Effects on Thermochemistry

9.3.4   Apparatus

A traversing, water-cooled rake with a single, integral spherical nose tip designed with a stagnation point pressure sensing tube was used to obtain pitot pressures. The rake and pitot sensing tube were fabricated from copper to accommodate the high heat transfer rakes expected. The rake was assembled by brazing. The pitot probe tip protruded 3/32 inch upstream of the leading edge of the rake in order to eliminate any potential interference from the rake. The pitot probe tip was designed with a 3/32 inch spherical nose diameter to provide a compromise for the conflicting requirements of good spatial resolution and no more than the maximum heat flux that the thermal/cooling design of the rake could tolerate. The spherical pitot tip was designed with a relatively small nose diameter and pitot sensing tube diameter to provide good spatial resolution of pitot pressure during the traverse across the nozzle exit plane. Cooling water for the probe was provided by two piston-pumps with 4 gpm flow rate at 1000 psia.

Dimensioned sketches of the probe tip assembly are shown in Figure 59 and Figure 60 below. Photographs of the probe and probe tip assembly are shown in Figure 61 through Figure 65.

Prior to testing at UAH, the probe was subjected to an acetylene/oxygen torch test. A photograph taken during that test is shown in Figure 66. The probe survived the maximum temperature reducing flame with no damage. A captured video frame taken during a test at

UAH showing the probe immersed in the plume is shown in Figure 67.
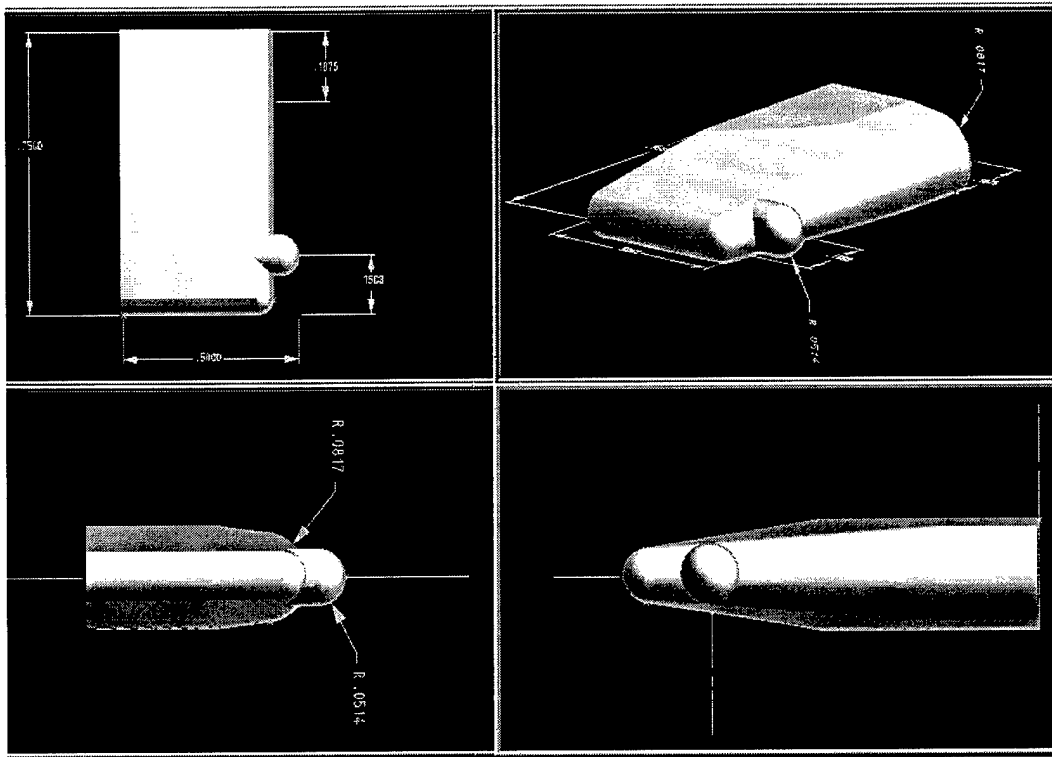
Figure 59: Three View and Three Dimensional Sketches of Probe Tip
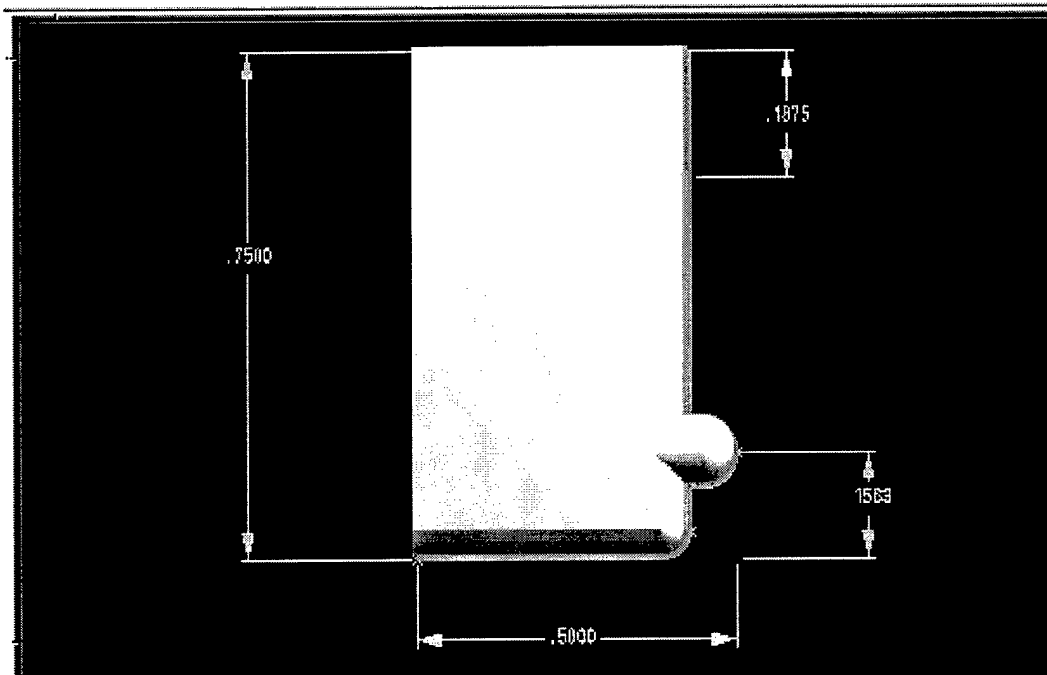
Figure 60: Top View of Probe Tip Assembly
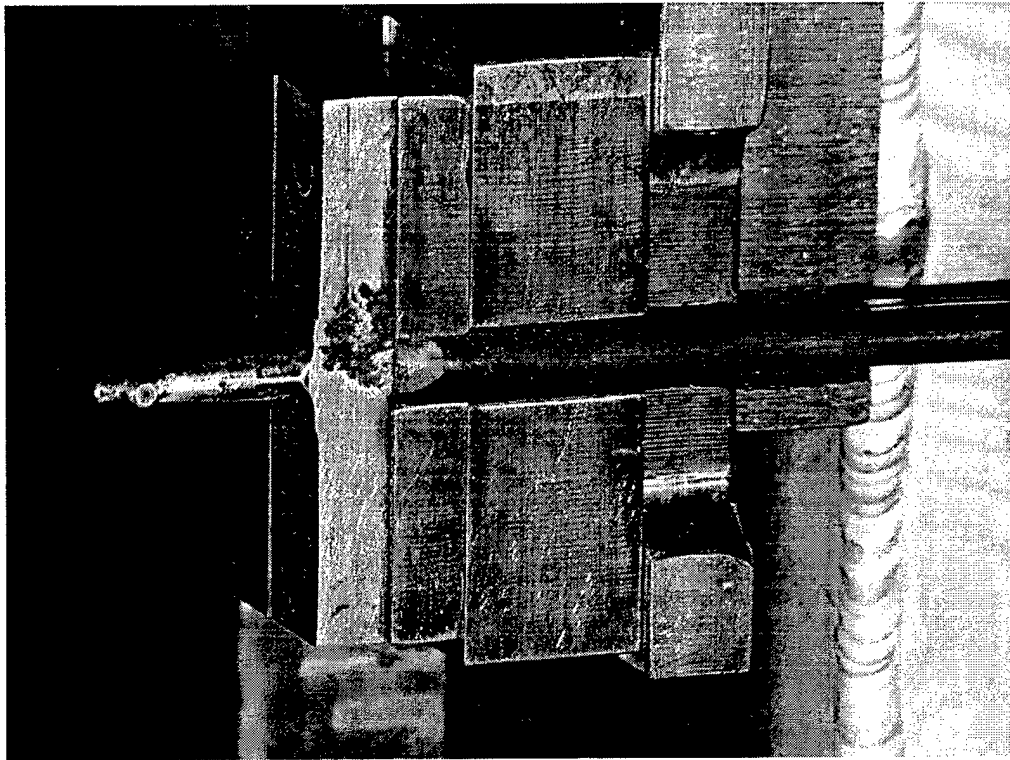
Figure 61: Oblique View of Probe Tip Assembly
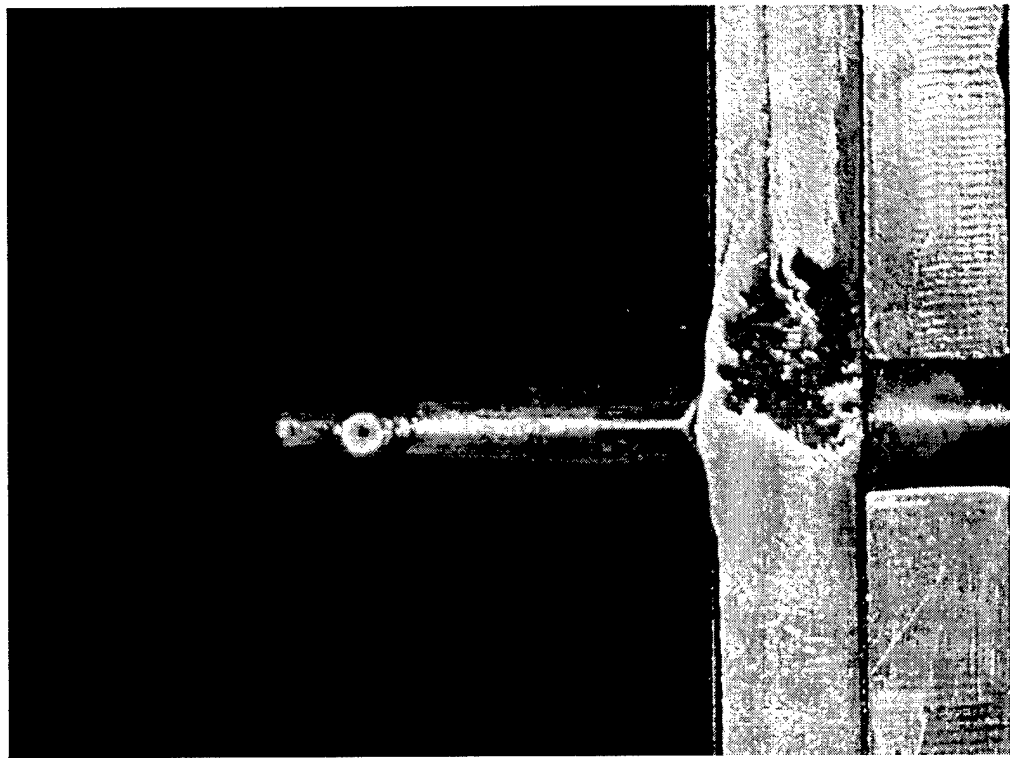
Figure 62: Front View of Probe Tip Assembly
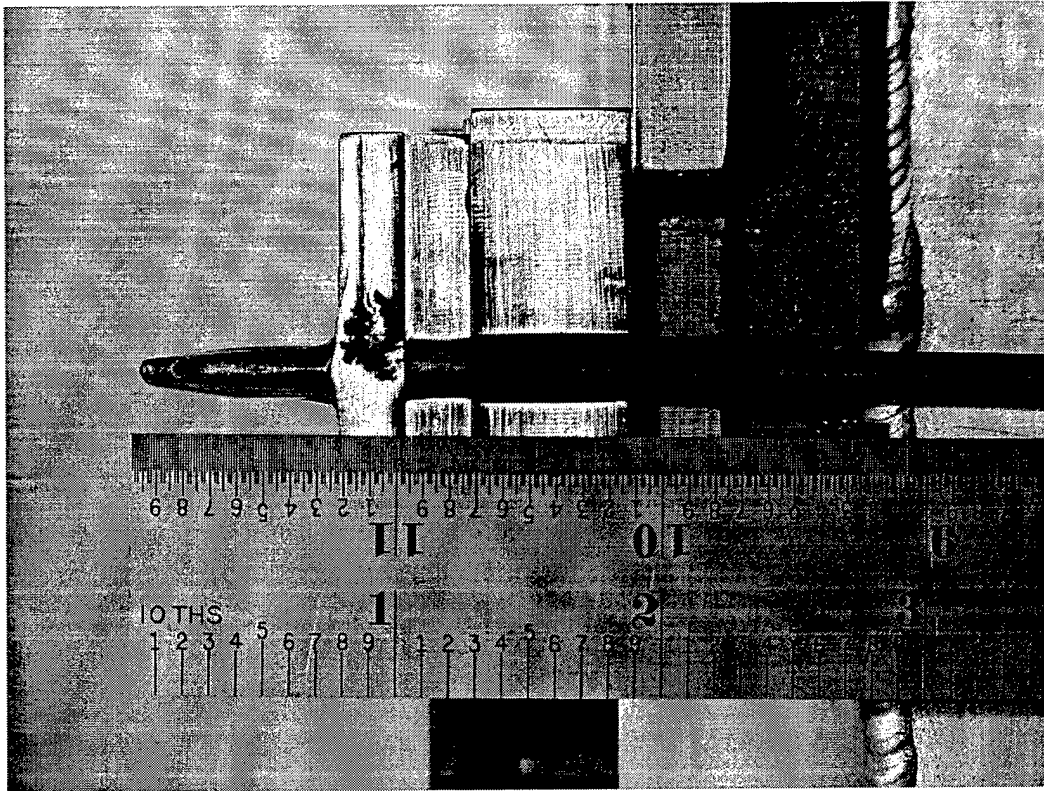
Figure 63: Front View of Probe Tip Assembly with Scale
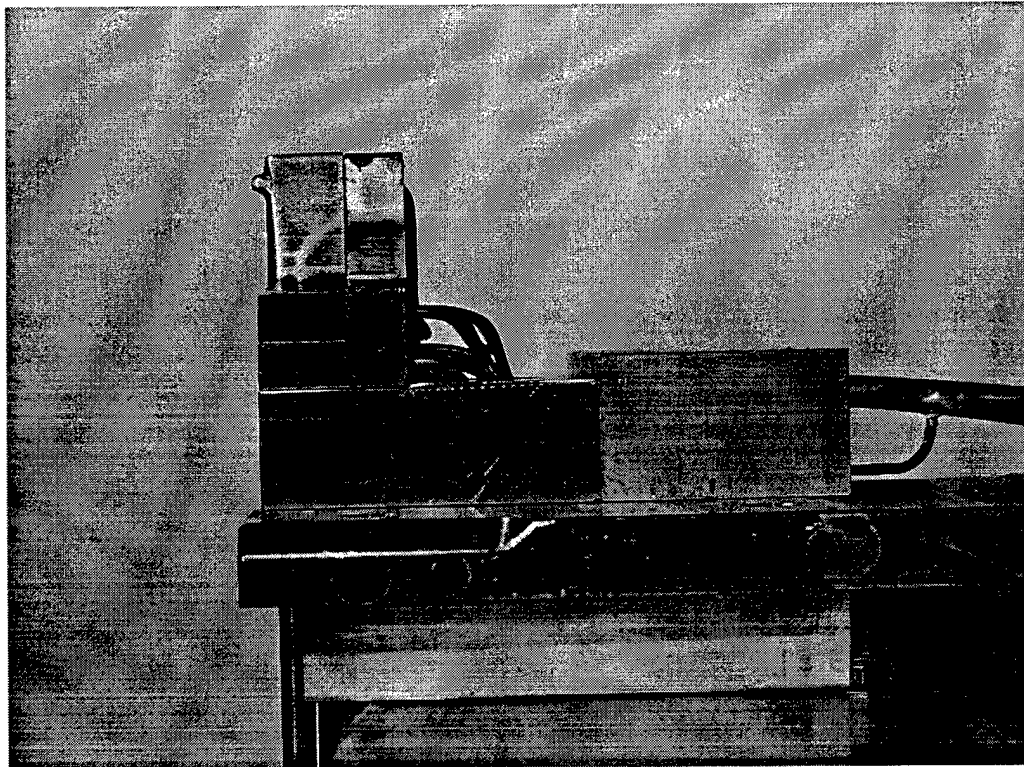
Figure 64: Side View of Probe Assembly

110
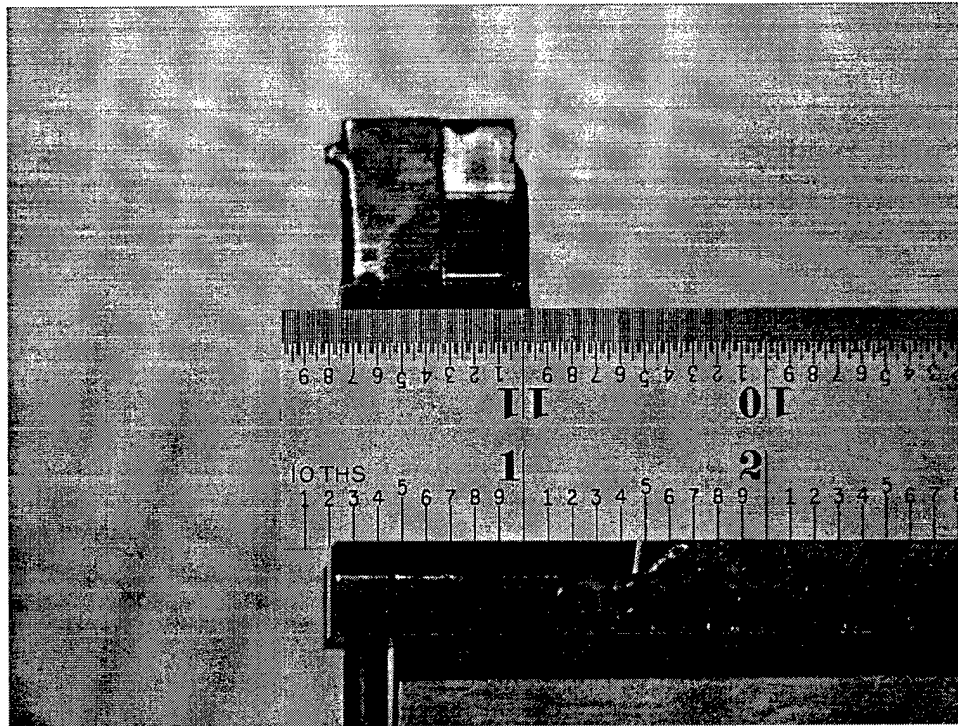
Figure 65: Side View of Probe Assembly with Scale
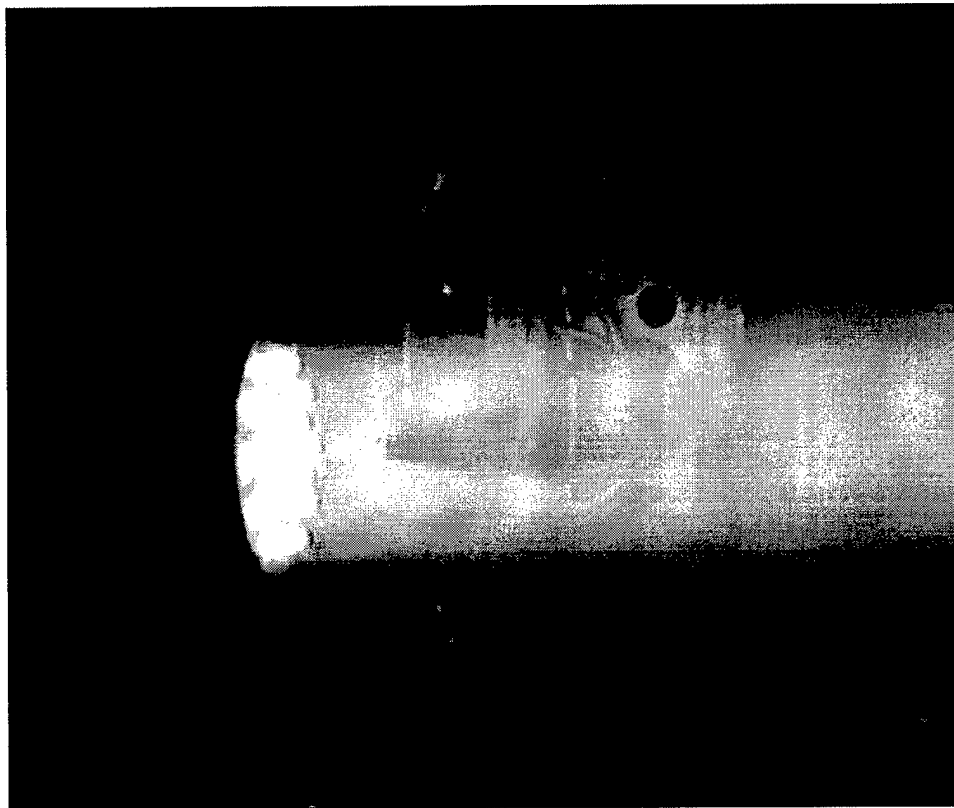
Figure 66: Photograph of Acetylene/Oxygen Test of Probe Assembly
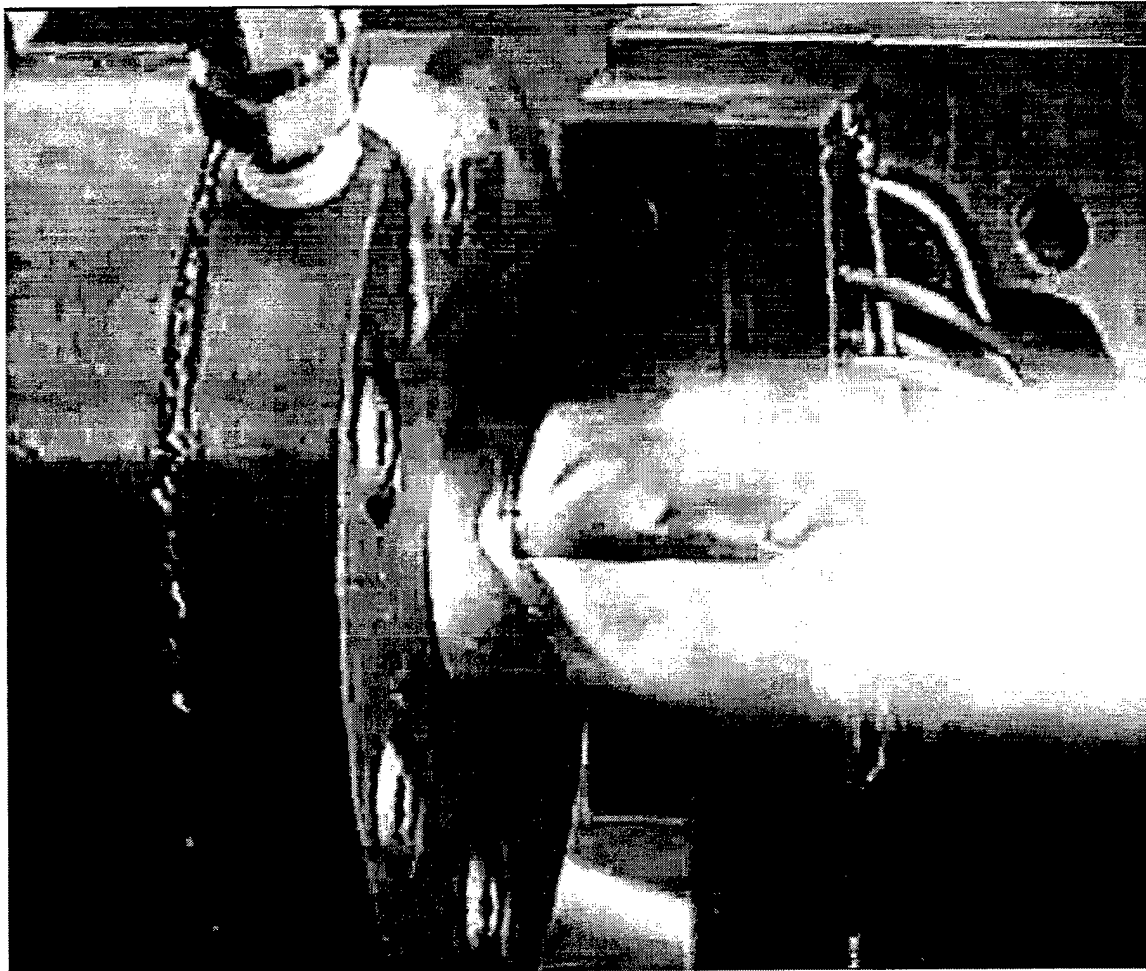
Figure 67: Video Frame of Probe Immersed in NOP Rocket Plume During UAH Test

An electrically driven linear actuator table was used to traverse the pitot rake across the exit plane. The rake was mounted on the traversing actuator table so that the spherical pitot probe tip would traverse a plane of symmetry through the axis of the rocket nozzle. The probe tip was positioned as close as practical to the nozzle exit plane – about 1/16 inch downstream.

The pitot pressure was sensed with a Scanivalve Corporation Model DSA 3217/16Px electronic pressure scanner. A 200 psi module was used to obtain these data. Data were acquired at a rate of 60 Hz. The rocket motor stagnation pressure was acquired simultaneously on a separate Scanivalve channel in order to be better able to align the facility and probe data. The Scanivalve pressure module was close-coupled to the pitot pressure sensing orifice with approximately 12 inches of tubing. The total pressure measurement uncertainty of the Scanivalve instrumentation was estimated to have been 0.1% of the full-scale value. A photograph of the Scanivalve system is shown in Figure 68.
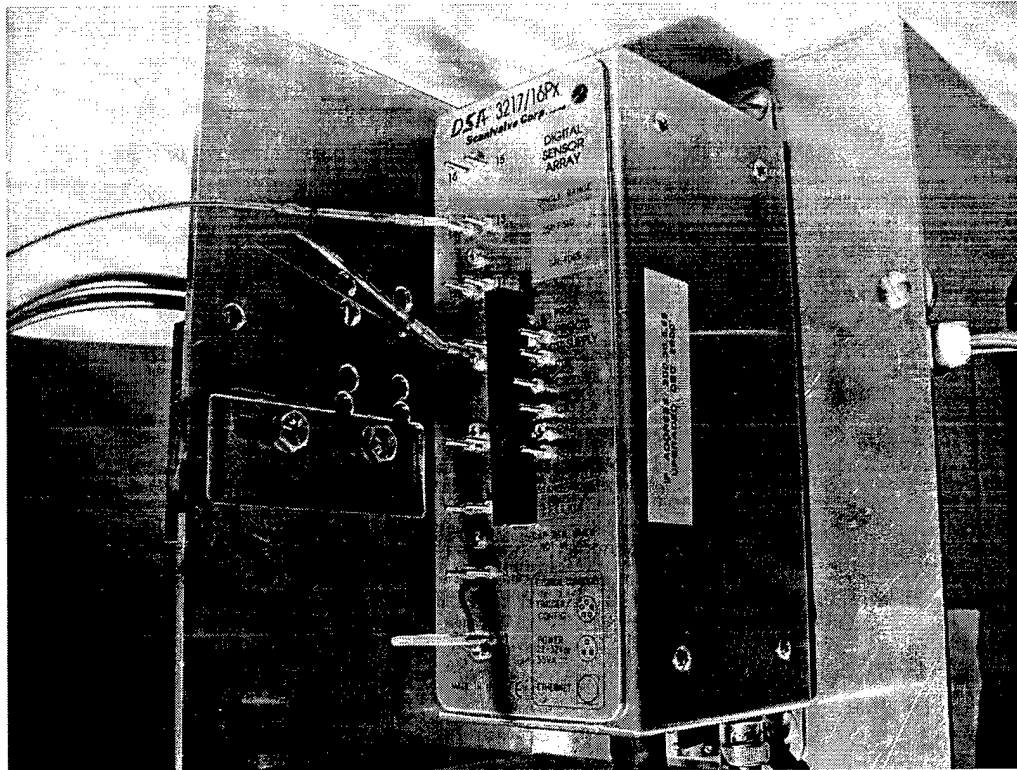
Figure 68: Scanivalve Pressure Module

9.3.5 Time Response

The time response of the pressure module and tubing system was measured by applying "step" changes in pressure to the system at the sensing orifice. The response closely approximated a first order system, so time constants were extracted from the response of the pressure system to these step change forcing-functions.

Rocket nozzle pitot pressure distributions are characterized by large pressure gradients at the nozzle lip. Consequently, the effects of the finite time constant of the pressure system on the measured pressure is greatest at the nozzle lip. In order to minimize the errors in the measured pressure data due to the finite response of the pressure system, the drive system for the rake was programmed to traverse this region at a rate of about ¼ of that used to traverse the core region of the rocket exhaust. The result was found to be a generally negligible contribution to the uncertainty of the pressure measurement caused by the finite response of the pressure measuring system through out the traverse across the nozzle.

A typical sequence for a test was to initially park the pitot probe about 1.0 inch below the lower lip of the nozzle. Then upon a signal from the facility controller the probe was traversed at high speed to just outside the plume. The traversing system was programmed to slow to minimum speed to minimize pressure error as the probe traversed the high pressure gradients in the nozzle lip region. As the probe entered the relatively

113

constant pressure core region the traversing system was programmed to speed up in order to traverse the nozzle exit plane within the allotted rocket motor burn time. This high speed traverse was limited in order not to induce pressure response errors into the data. The traverse was slowed as the probe again penetrated the nozzle lip area and finally speeded up to a post test park position about 1.0 inch above the nozzle. The traverse through the plume was programmed to occupy about 3.0 seconds of the nominal 5.0 second available rocket burn.

In order to assess the impact of the finite time response, the pressure system was modeled as a first order system with a time response τ. The governing differential equation is

$$\dot{f} + \frac{1}{\tau} f = \frac{1}{\tau} p \qquad (9\text{-}35)$$

where f is the system response and p is the forcing function. In this case, p would be the actual pitot pressure and f is the indicated pressure. The differential equation can be numerically solved so that the impact of traverse speed on the indicated pressure can be assessed. Discretizing the differential equation to first order yields

$$\frac{f_{i+1} - f_i}{\Delta t} + \frac{1}{\tau} f_i = \frac{1}{\tau} \left(\frac{p_{i+1} + p_i}{2} \right) \qquad (9\text{-}36)$$

which, when solved for the system response at the advanced time step yields

$$f_{i+1} = f_i \left(1 - \frac{\Delta t}{\tau} \right) + \frac{\Delta t}{\tau} \left(\frac{p_{i+1} + p_i}{2} \right) \qquad (9\text{-}37)$$

The time constant for the pneumatic response of the pressure system was experimentally determined to be 15-20 msec.

Figure 69 below shows the expected pitot pressure distribution for the nozzle for a chamber pressure of 150 psia (rather than the ~85 psia chamber pressure used in the UAH test series). This pitot pressure distribution was computed using the VIPER model (Ref. 40). Figure 70 shows the difference between the pitot pressure and the pressure system response for several different probe traverse speeds – 0.01, 0.1, and 1inch per second. Also shown on the figure is the pressure system response for a programmed traverse schedule which goes slowly through steeply varying pressure at the edge of the plume and then progresses more rapidly through the more gradually varying center of the plume. The traverse rate is 0.01 inches per second until the radius is less than 0.3 inches and is 0.05 inches per second thereafter. This is the actual traverse schedule chosen for the tests at UAH. This traverse schedule was chosen as the best compromise – slow enough to minimize the error in the pressure measurement, but also fast enough to meet the constraint of the test time limit of the motor.
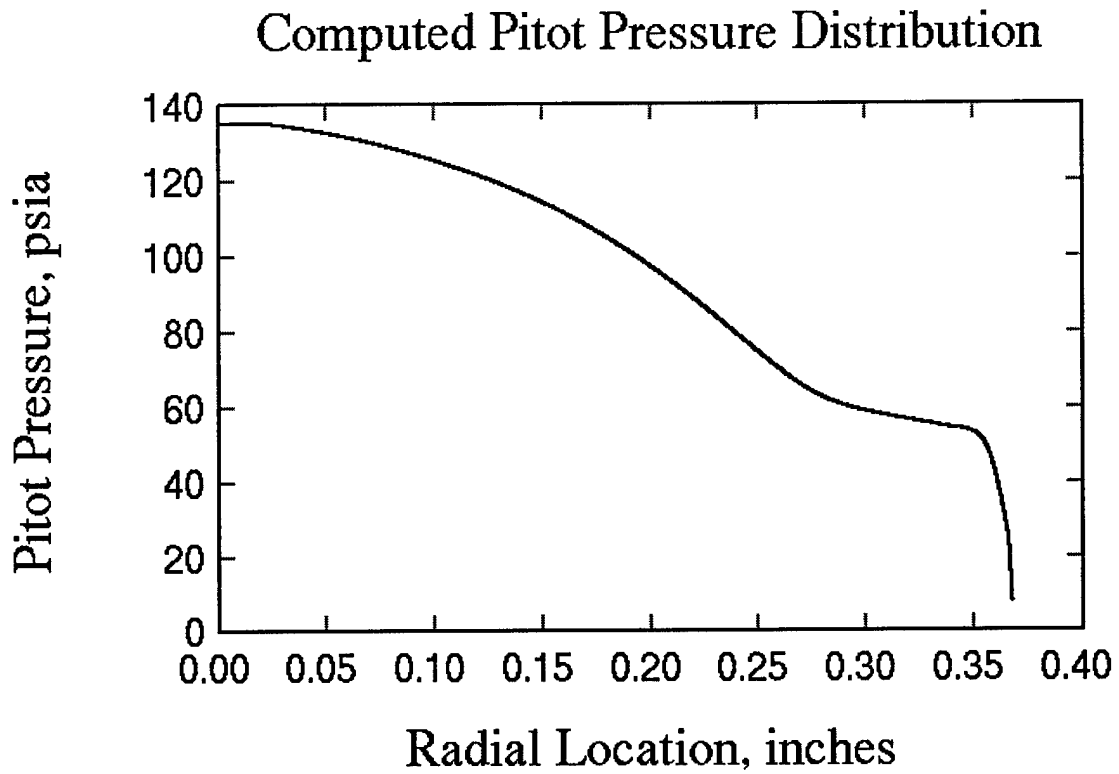
Computed Pitot Pressure Distribution

Figure 69: Computed Pitot Pressure Radial Profile

Pressure System Response
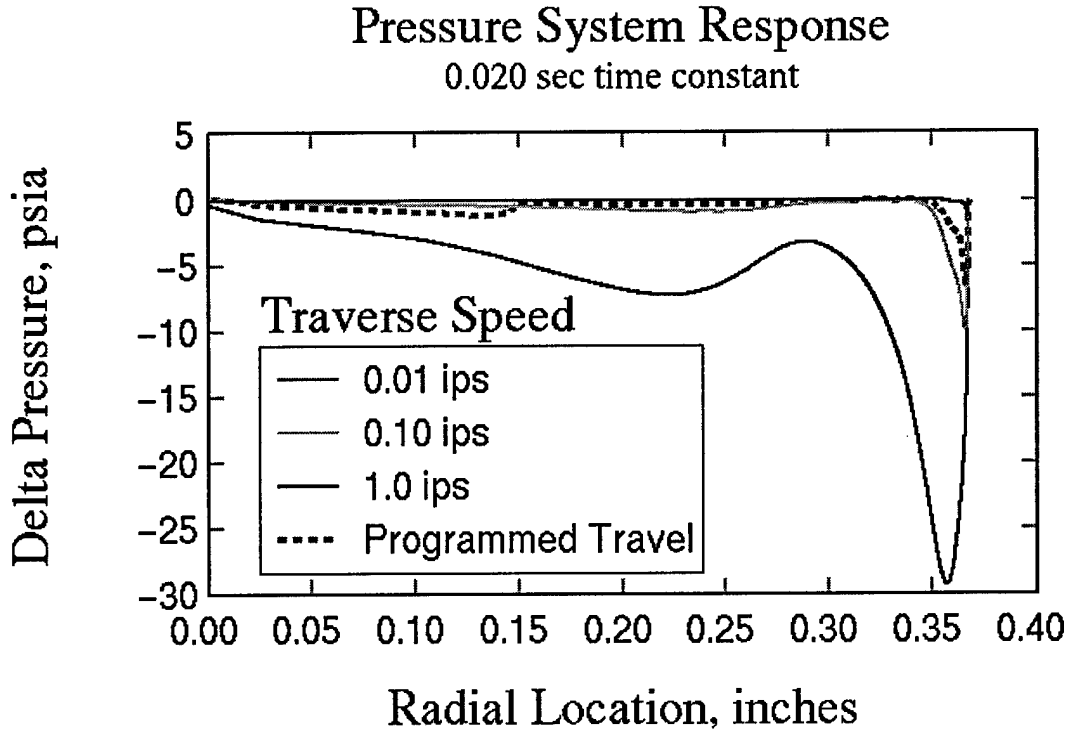### 0.020 sec time constant

Figure 70: Error in Indicated Pressure as a Function of Traverse Speed

9.3.6   Test Data

Pitot pressure data were acquired on UAH Run numbers 2, 4, 8, 9, and 10 on 15 March 2001. Figure 71 through Figure 75 show the time histories for the chamber pressure data acquired by the UAH facility system and the AEDC Scanivalve system, the facility thrust stand indicated thrust, as well as the AEDC pitot pressure data. The thrust stand data is shown both raw (unsmoothed) as well as smoothed using a 0.05 sec wide Savitzky-Golay filter. Note that the AEDC and UAH chamber pressure data agree quite well, in spite of the somewhat noisy signal. For Runs 2, 4, and 8, the chamber pressure changes too much during the probe insertion time to allow reliable thrust computations without extensive analysis. However, the chamber pressure excursions during the thrust insertion time for Runs 9 and 10 are relatively small. These data will be used to determine thrust using the method described in the Theory section above.
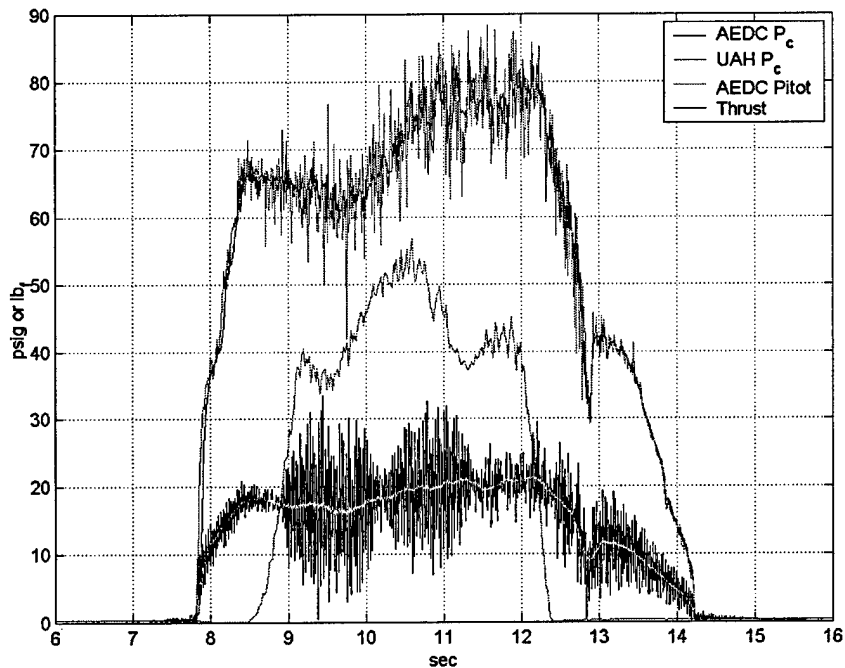
Figure 71: Chamber Pressure, Pitot Pressure, and Thrust Data for Run #2

116
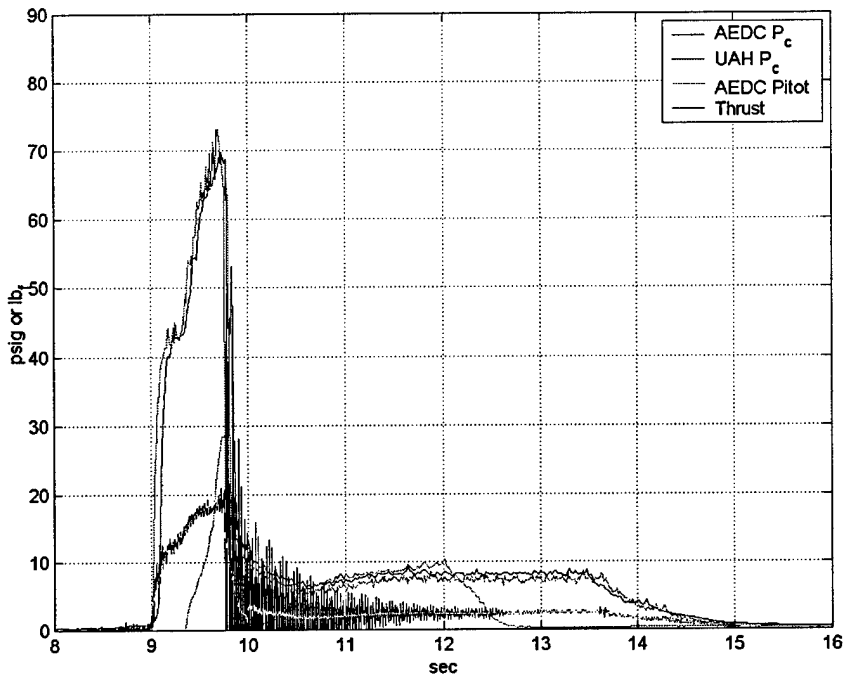
Figure 72: Chamber Pressure, Pitot Pressure, and Thrust Data for Run #4
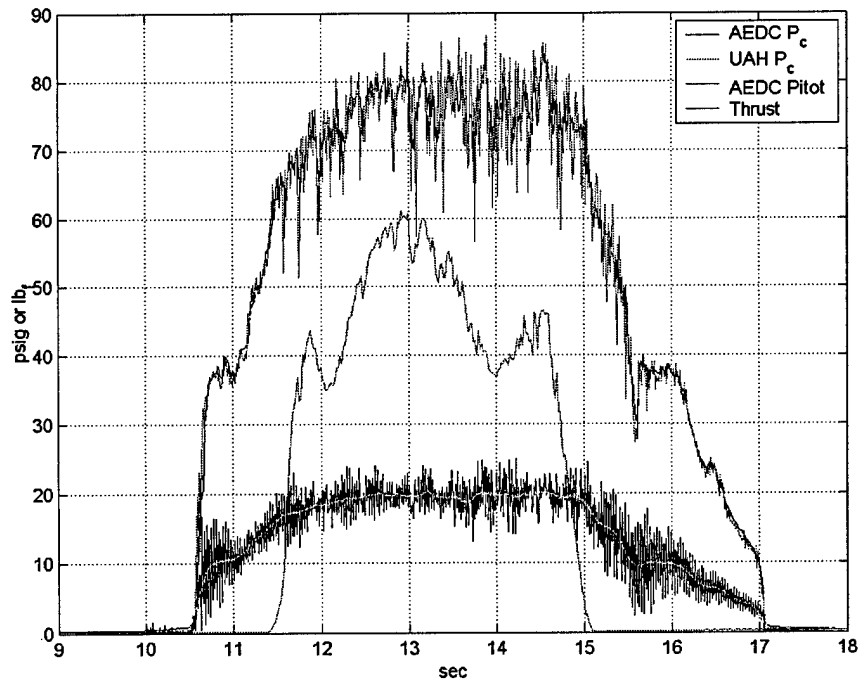
Figure 73: Chamber Pressure, Pitot Pressure, and Thrust Data for Run #8
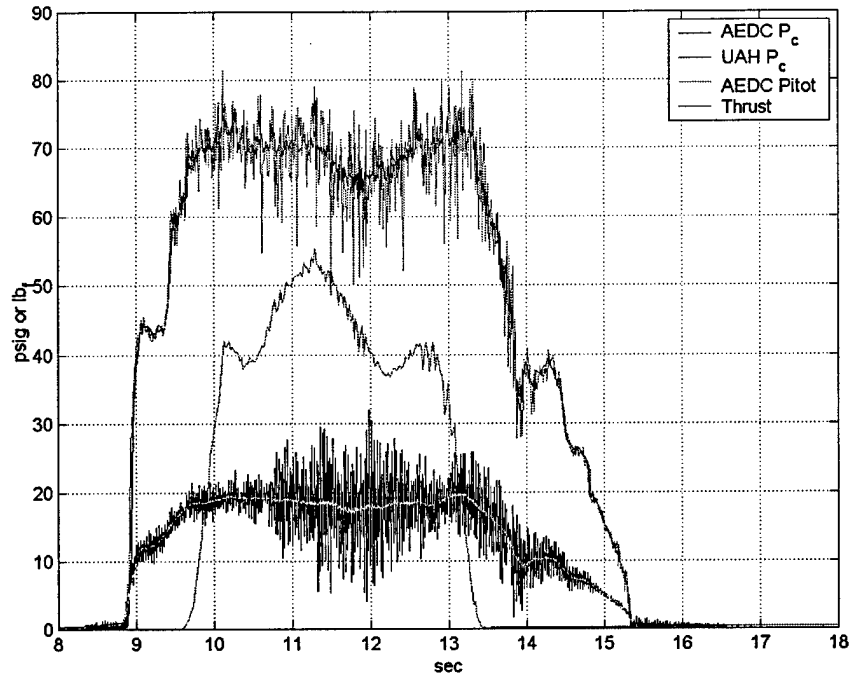
Figure 74: Chamber Pressure, Pitot Pressure, and Thrust Data for Run #9
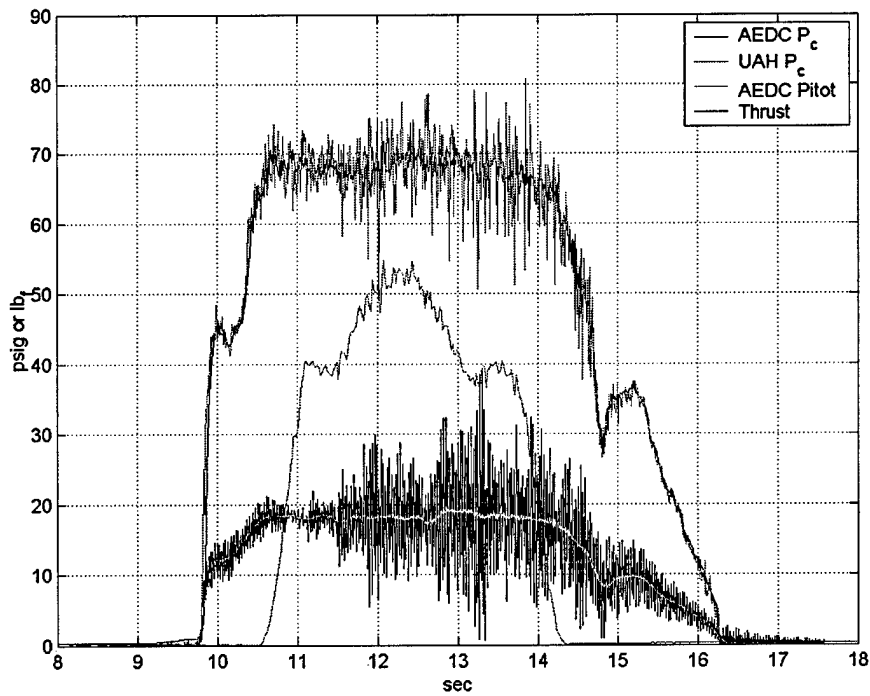
Figure 75: Chamber Pressure, Pitot Pressure, and Thrust Data for Run #10

9.3.7 Analysis And Thrust Computations

The pitot pressure data from Runs 9 and 10 were used to compute thrust. Since the pitot pressures (p_{02}) were recorded as gage pressure (psig), Equation (9-29) above can be modified as

$$F = 2\pi \int_0^{R_e} P_{02} f(\gamma, M_e) r\, dr \qquad (9\text{-}38)$$

where F is the thrust recorded by the thrust stand – i.e. approximately sea-level thrust. The vacuum thrust could then be obtained by adding in the pressure/area term as shown in Equation (9-39).

$$F_v = F + P_\infty A_e \qquad (9\text{-}39)$$

The ratio of specific heats (γ) was chosen as 1.2, based on nozzle exit plane temperature and composition. However, as shown in the Theory section above, the computed thrusts are relatively insensitive to changes in γ. The computed Mach number profile shown in Figure 76 below was used to evaluate the integral in Equation (9-38).
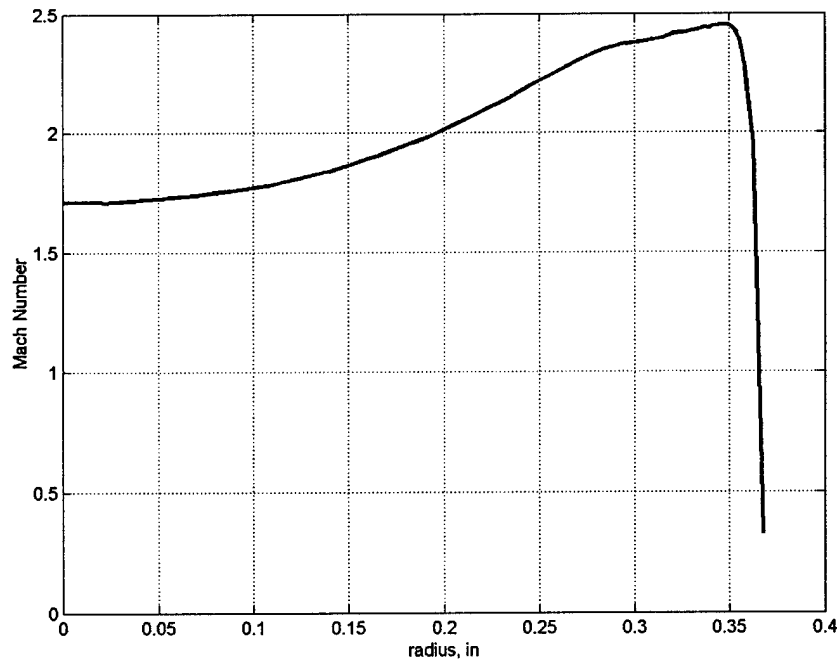
Figure 76: Computed Mach Number Radial Profile

119

Figure 77 and Figure 78 show the radial distribution of pitot pressure for Runs 9 and 10, respectively. The profile for Run 9 is markedly asymmetric. This is due to the reduction in chamber pressure, and consequently thrust, during the time that these data were acquired. This will be borne out by the thrust computations below. The pitot pressure profile for Run 10 is more symmetric than Run 9, but the pitot pressure for the positive radial locations is still somewhat lower than the corresponding negative radial locations. The pitot pressure profiles will be integrated separately for each side of the plume – that is, the data from negative radial positions will be treated separately from data from positive radial positions. Thrust will be computed using the pitot pressure data from the negative radial positions using Equation (9-38) above, and will then be compared to the thrust data acquired at the same time as the pitot pressure data. This will somewhat account for the time variation in chamber pressure and thrust. Thrust will then be computed from the positive radial position pitot pressure data. This procedure was used for Runs 9 and 10. The results are shown Table 19 for Run 9 and Table 20 for Run 10.

The results indicate that in all four cases (Runs 9 and 10, negative and positive radii), the pitot pressure derived thrust lies between the minimum and maximum unsmoothed thrust stand values. In both Run 9 and 10 positive radii cases, the pitot pressure derived thrust results lie between the minimum and maximum smoothed thrust results – which, due to the varying chamber pressure and thrust, is about the best that can be expected. The negative radii results for the pitot pressure derived thrust lie above the maximum smoothed facility values – however, only by about 5.1% for Run 9 and 3.2% for Run 10. It should be noted that since the integral being evaluated in Equation (9-38) is weighted by the radial location, it should not be expected that the pitot pressure derived thrust will match the average thrust over the same time integral. The pitot pressure derived thrust will be biased toward the large-radii values. Also, it should be noted that, as mentioned above, the thrust for the positive side of the exhaust is lower than the thrust for the negative side – both for the pitot pressure results and the thrust stand data. This indicates that the asymmetry observed in the pitot pressure data is real, and indicates a temporal change, not flow asymmetry in the nozzle.
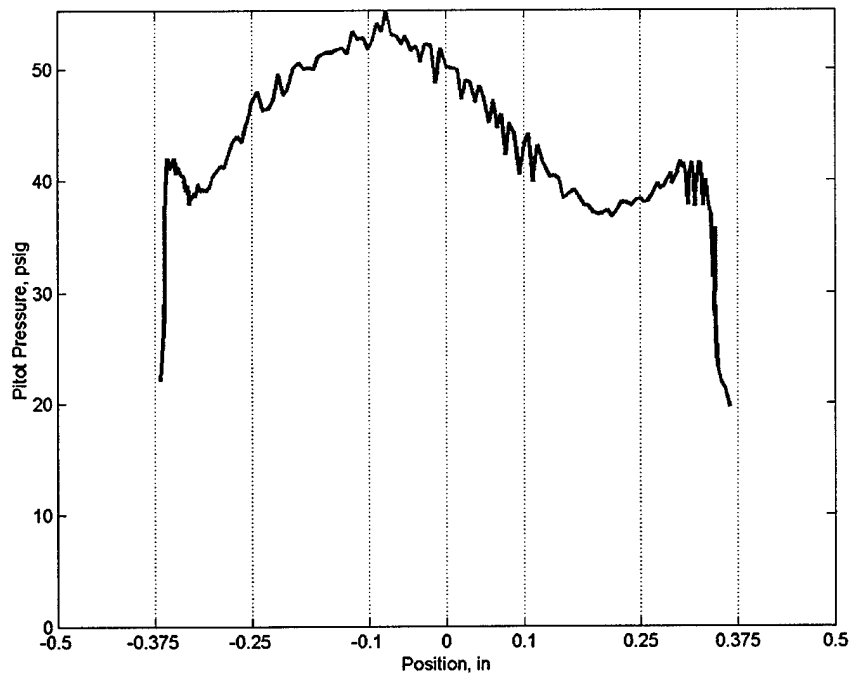
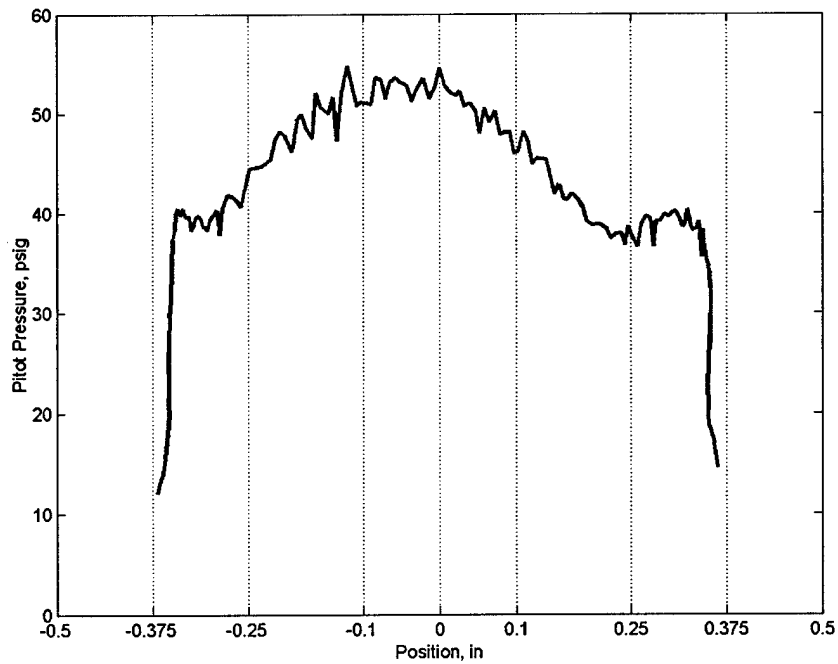**Figure 77: Radial Distribution of Pitot Pressure for Run 9**

Figure 78: Radial Distribution of Pitot Pressure for Run 10

121

Table 19: Comparison of Facility and Pitot-Pressure Derived Thrust for Run 9

Thrust Method	Run 9			
	Negative Radial Locations		Positive Radial Locations	
Pitot Pressure Derived, lbf	20.5		17.8	
Facility Average, lbf	19.0		18.3	
	Minimum	Maximum	Minimum	Maximum
Facility Smoothed, lbf	18.0	19.5	16.9	19.9
Facility Unsmoothed, lbf	10.6	27.7	4.1	31.9

Table 20: Comparison of Facility and Pitot-Pressure Derived Thrust for Run 10

Thrust Method	Run 10			
	Negative Radial Locations		Positive Radial Locations	
Pitot Pressure Derived, lbf	19.2		18.3	
Facility Average, lbf	18.2		18.3	
	Minimum	Maximum	Minimum	Maximum
Facility Smoothed, lbf	17.6	18.6	17.2	19.6
Facility Unsmoothed, lbf	5.5	29.9	0.6	39.0

9.3.8 Effect of Base Pressure

The nozzle configuration tested at UAH had a large base region – the nozzle exit diameter is 0.745 inches, while the base diameter is 2.5 inches. This yields a base area (A_b) of 4.47 in^2. For the UAH test configuration, a base pressure is lower than atmospheric will reduce the thrust indicated by the thrust stand. A base pressure higher than atmospheric will increase the thrust indicated by the thrust stand. The thrust derived from the pitot pressure measurement is independent of the base pressure. Therefore, a more valid comparison will result if the thrust stand measurements are corrected for the base pressure. Typically, the base pressure will be somewhat less than atmospheric due to flow separation and entrainment effects. This is the origin of "base drag." It should be noted that the base pressure was measured using a single static pressure tap. This measured base pressure will assumed to be uniform over the entire base area, whereas there is probably some non-uniform distribution. The corrected thrust is derived using Equation (9-40)

$$F_{corrected} = F_{measured} - P_{b,gage} A_b \qquad (9\text{-}40)$$

where the base gage pressure ($P_{b,gage}$) is determined from the absolute gage pressure (P_b) by

$$P_{b,gage} = P_b - P_\infty \qquad (9\text{-}41)$$

where the local atmospheric pressure (P_∞) may be obtained by using the base pressure reading before ignition. Since the base pressure during the firing is lower than P_∞ the gage pressure will be negative, and the correction shown in Equation (9-40) will result in a corrected thrust higher than the measured thrust. The base pressure data from Runs 9 and 10 are shown in Figure 79 and Figure 80, respectively. The raw data are relatively noisy, so a 0.05 sec wide Savitzky-Golay smoothing algorithm was applied. The smoothed results are also shown on the Figure 79 and Figure 80. The pre-fire data indicate an atmospheric pressure of approximately 14.59 psia. The average base pressure for both runs is approximately 14.565 psia, which yields an average correction to the measured thrust of 0.1 lbf – or about 0.5% of the indicated thrust. This effect is sufficiently small that it is justifiably neglected in the face of the much larger thrust excursions seen in the raw and smoothed thrust data. The base pressure correction is also small enough that its inclusion would not change any of the comparisons of the facility and pitot derived thrust results discussed above.
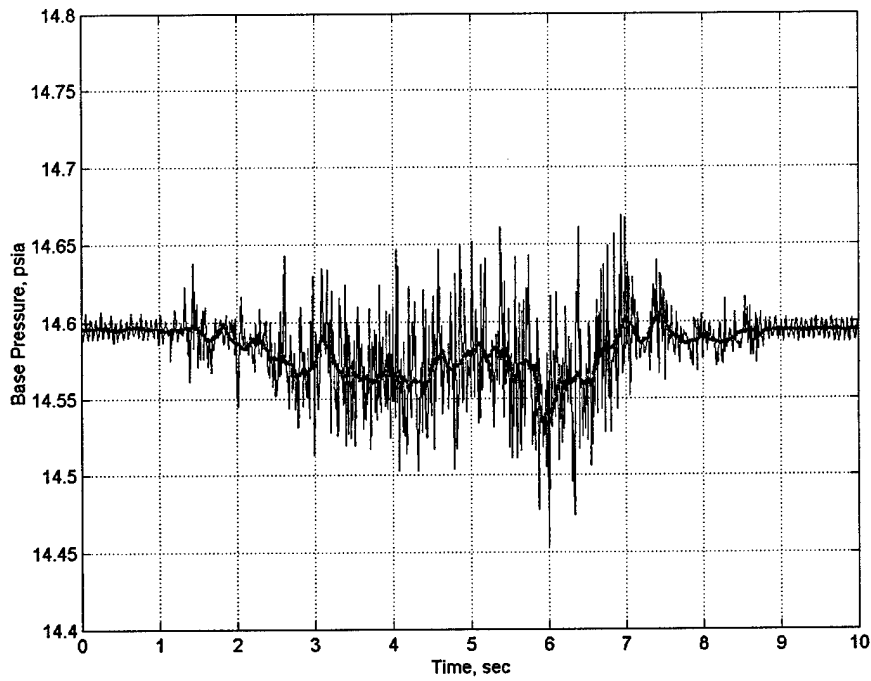
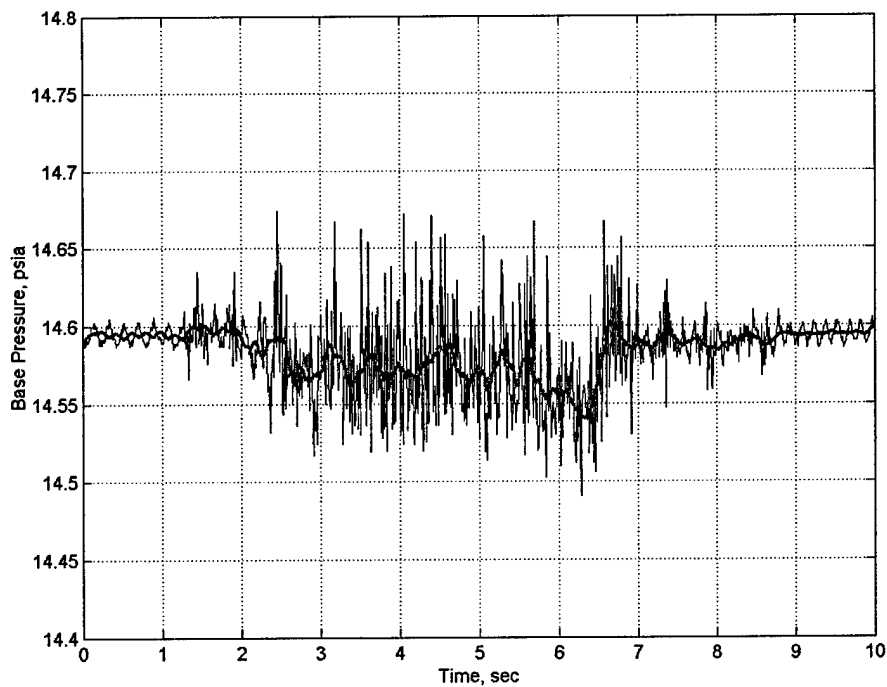**Figure 79: Measured and Smoothed Base Pressure for Run 9**

Figure 80: Measured and Smoothed Base Pressure for Run 10

124

9.3.9 Vacuum Thrust Correction

The comparisons above are presented in terms of thrust at local atmospheric pressure conditions, since this is what the thrust stand indicates. The pitot pressure measurements can directly give vacuum thrust, since

$$F_v = F + P_\infty A_e$$

where F_v is the vacuum thrust. For the UAH nozzle and ambient pressure, the pressure/area correction term is on the order of 6.36 lbf. The vacuum thrust is therefore in the range $24 - 26$ lbf, as compared to the $18 - 20$ lbf range shown in Tables 1 and 2 for the thrust at local atmospheric pressure.

9.4 Nonintrusive Measurements of Exhaust Plume

Two IR imagers, one infrared spectrometer, and two UV/VIS spectrometers collected data during the NOP rocket test series on 27 March, 2001. A test matrix showing the data collected for each test is shown in Table 21. Tests for which the particular instrument acquired data are marked with a 'X'. The instrumentation was arranged around the test article as shown in Figure 81.

Table 21: Optical Data Test Matrix.

Date	UAH Run	AEDC Run	Type	IR Imager-MWIR	IR Imager-LWIR	IR Spectrometer	UV OMA	UV/VIS Zeiss
3-27		1	Catalyst			X		
3-27		2	Catalyst	X		X		
3-27		3	Catalyst	X		X		
3-27		4	Catalyst	X		X		
3-27		5	Catalyst	X	X	X		X
3-27	Run1	6	Spark Plug	X	X	X		X
3-27	Run2	7	Spark Plug	X	X	X		X
3-27	Run3	8	Spark Plug	X	X	X		X
3-27	Run4	9	Spark Plug	X	X	X	X	X
3-27	Run5	10	Spark Plug	X	X	X	X	X
3-27	Run6	11	Spark Plug	X	X	X	X	X
3-27	Run7	12	Spark Plug	X	X	X	X	X
3-27	Run8	13	Spark Plug	X	X	X	X	X
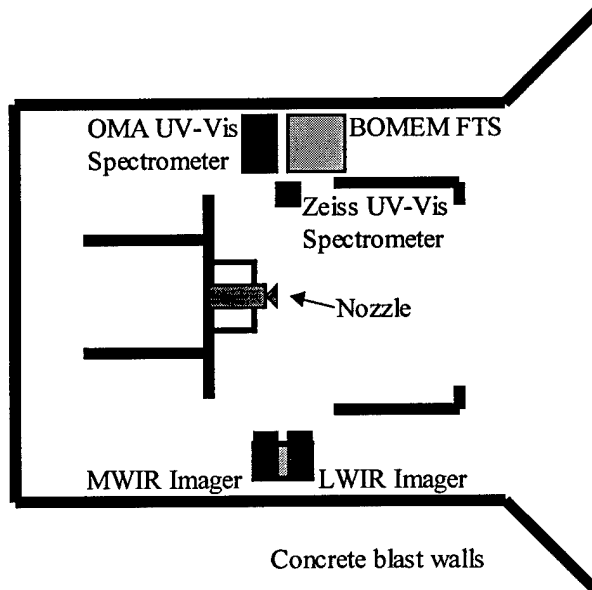
Figure 81: Instrumentation setup for NOP ROCKET test.

An image from a facility video camera during a firing is shown in Figure 82. The exhaust emanates from the ¾-inch diameter nozzle and forms the luminous plume shown. The approximate fields-of-view of the AEDC optical instruments are shown on the figure.
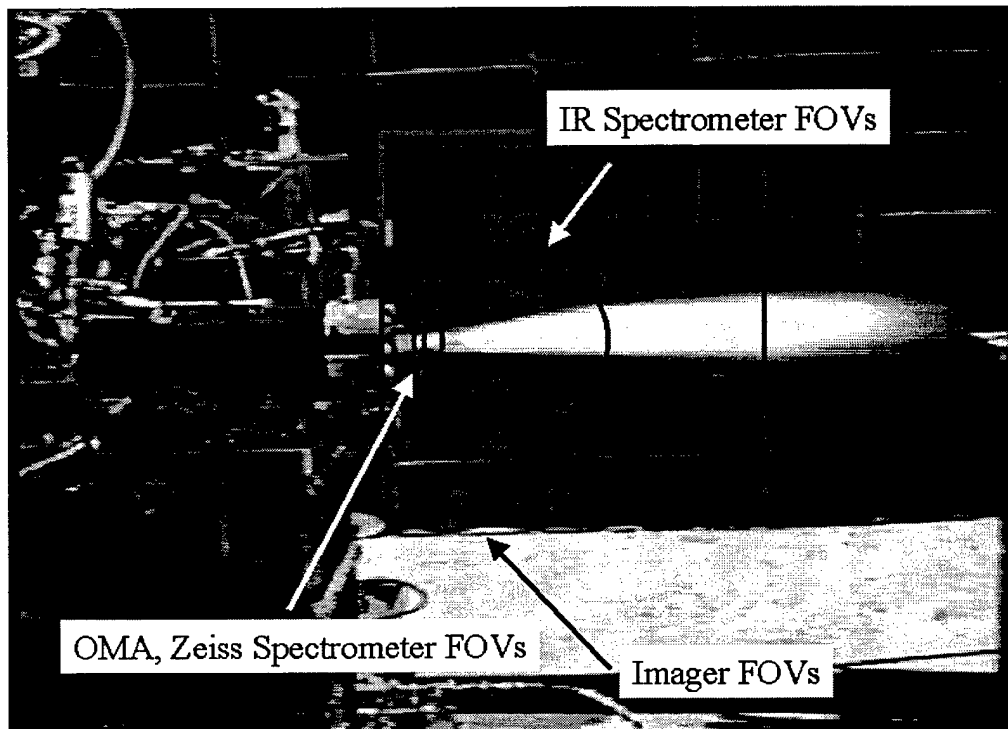
Figure 82: Facility video frame of the NOP ROCKET engine and exhaust plume showing AEDC optical instrumentation FOVs.

A description of the instrumentation and sample data from each instrument follows.

9.4.1   IMAGERY

9.4.1.1   Santa Barbara Focal Plane Imager#1

The MWIR Santa Barbara Focal Plane imager is a custom ImagIR system manufactured by Lockheed\SBFP in Goleta, CA. The camera utilizes a model SBF125 InSb focal plane

array with windowing capabilities. The full (unwindowed) size of the array is 320H x 256V pixels. The array consists of 30 μm square detectors on 30 μm centers. For this application, the array was operated in a 'windowed' mode to provide 256x256 pixel images at 54 frames per second with 14-bits/pixel resolution. A 50mm focal length lens was used to obtain a 8.8° total field-of-view with 0.6 mrad pixels. An optical bandpass filter was cold mounted in the camera dewar to achieve a bandpass of 3.84-4.14μm. Data was collected for 10 seconds on each trial. The MWIR imager was set up at 90° to the nozzle exit at about 80 inches away to observe approximately one foot of plume. The spectral response of this system is shown in Figure 83.
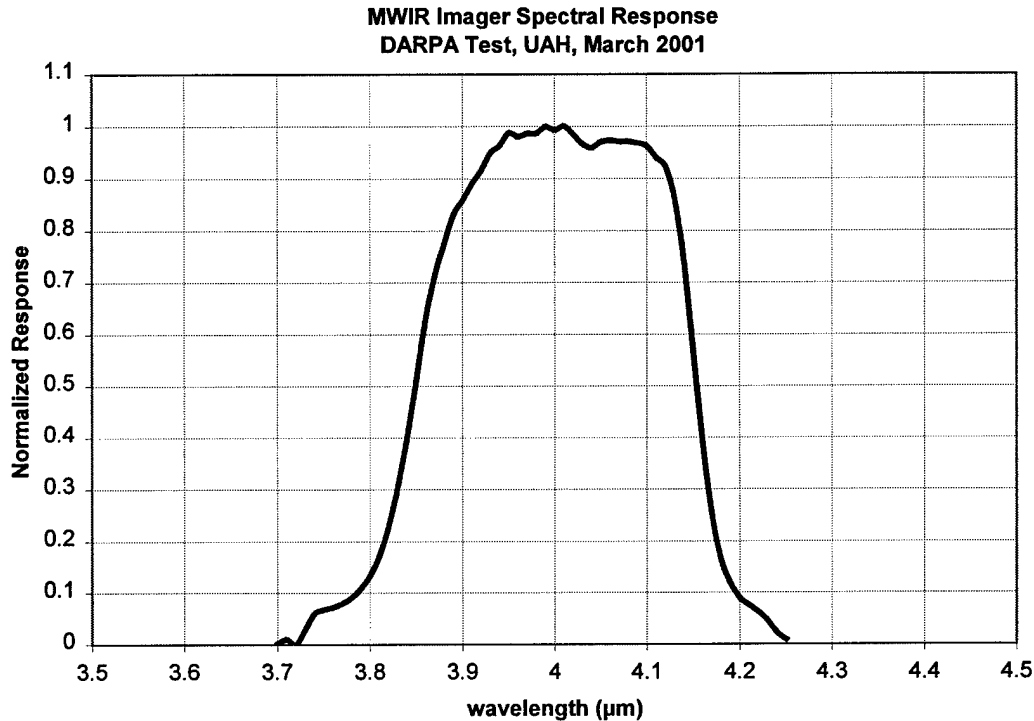
Figure 83: Santa Barbara MWIR imager spectral response.

9.4.1.2 Indigo Systems Merlin Uncooled Bolometer Imager

The AEDC LWIR imager is an uncooled microbolometer focal plane array manufactured by Indigo Systems. The focal plane size is 320H x 240V with 50μm pixels. The camera operates at a frame rate of 60 Hz. A 100mm focal length f/2.0 lens was used giving a 9.3°H x 7.0°V field-of-view. The unfiltered bolometer has an optical bandpass of 7.5-13.5μm. The LWIR imager was set up at 90° to the exit nozzle next to the MWIR imager. The spectral response of this system is shown in Figure 84. The LWIR imager had approximately the same FOV as the MWIR imager.

128

LWIR Imager Spectral Response
DARPA Test, UAH, March 2001
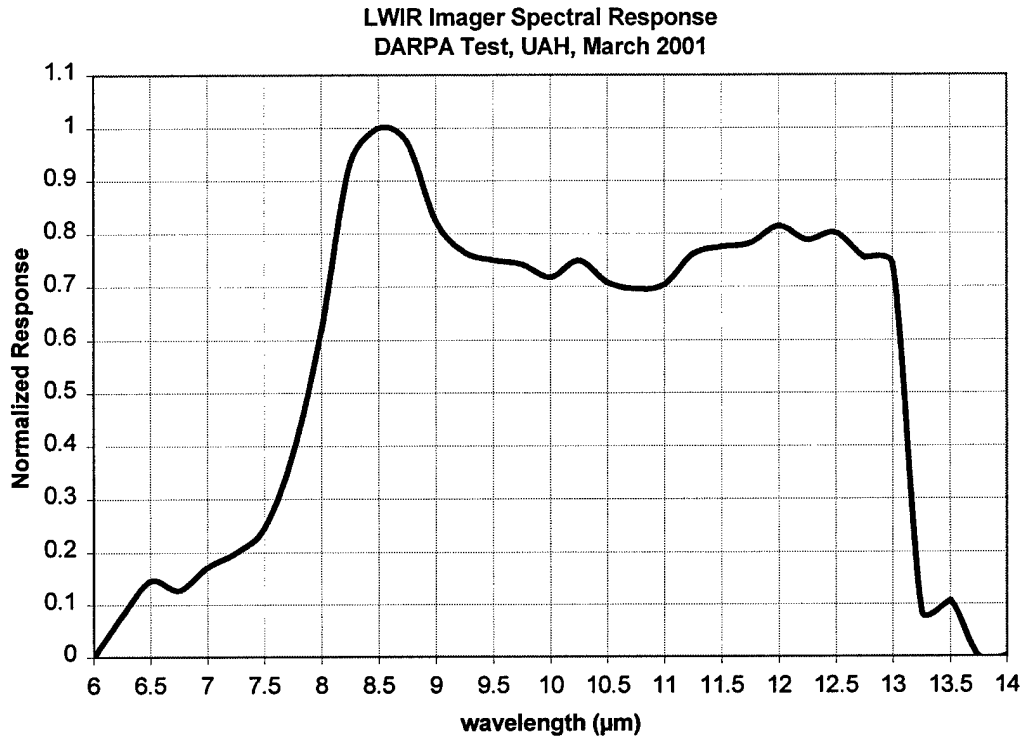
Figure 84: Indigo LWIR imager spectral response.

9.4.1.3 Data Acquisition

Both imager data systems use AEDC custom data acquisition software with a standard frame grabber card in a rack mount computer system.

9.4.1.4 Imager Calibration

Each imager is calibrated using a NIST-traceable blackbody standard. The blackbody has a known calibrated output that is used to convert the raw camera data into radiometric units of radiance (W/cm^2-sr) and intensity (W/sr). Both imagers were calibrated in the AEDC laboratory as well as on site prior to the test.

9.4.1.5 Imagery Sample Data

Samples of IR imagery in the MWIR and LWIR bands are shown in Figure 85. In these figures, the nozzle flow is from left to right. The radiation in the MWIR band is principally due to CO_2, CO and soot (continuum) and the primary radiators in the LWIR band are H_2O and soot. The luminous flame seen in the visible imagery of the exhaust

plume (Figure 82) is supporting evidence for the presence of soot as an exhaust product. Note the shock structure typical of an underexpanded rocket plume is evident in both bands. The continual brightening of the plume as it progresses downstream (left to right in the figures) is indicative of the afterburning of the fuel-rich exhaust with the ambient air, and the resultant rise in temperature. The bright periphery of the plume indicates a fuel-rich region near the chamber and nozzle wall. No marked plume asymmetry is present in either band and there is no streaking, either of which can indicate significant lack of mixing in the chamber.
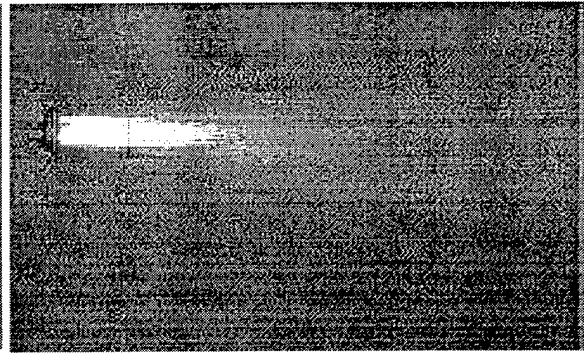
MWIR Image T+0s   LWIR Image T+0s
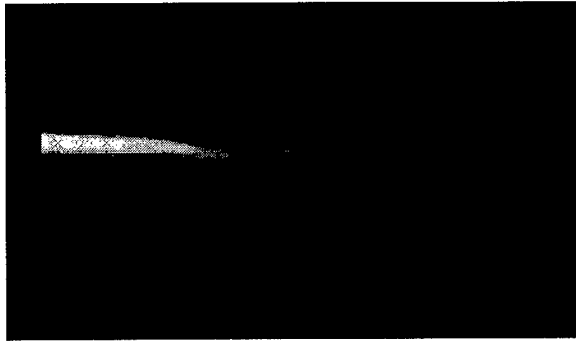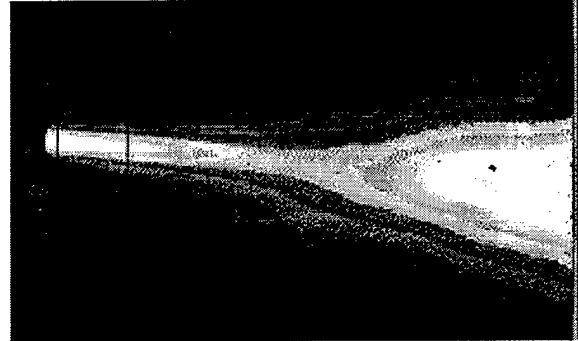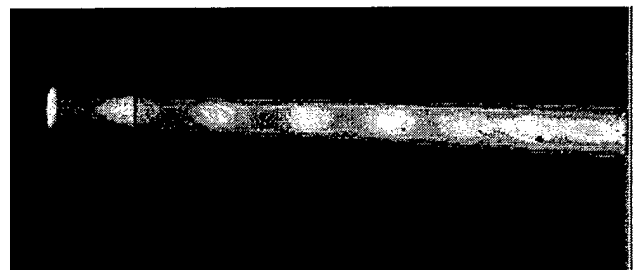
MWIR Image T+0.02s   LWIR Image T+0.02s
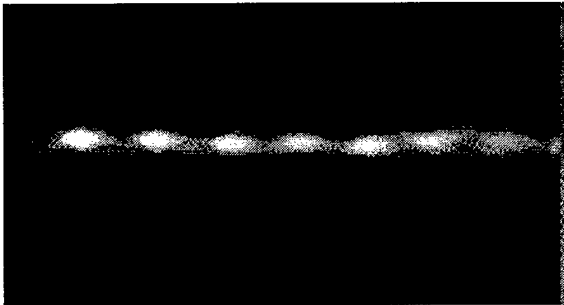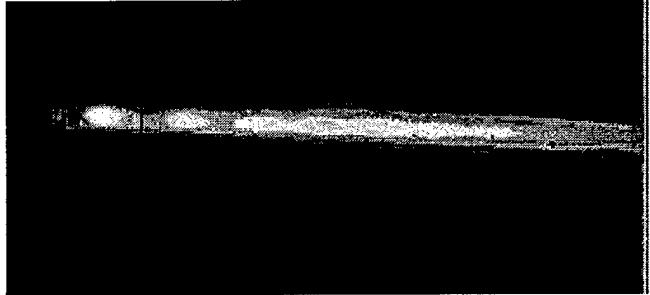
MWIR Image T+0.2s   LWIR Image T+0.2s
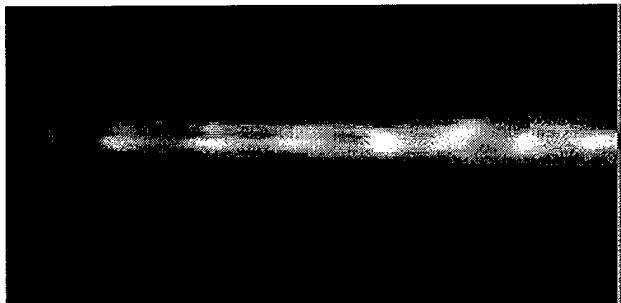
MWIR Image T+1.47s   LWIR Image T+1.47s

Figure 85: Typical IR imager data, AEDC Run 11.

Centerline intensity profiles are shown in Figure 86. The repeating Mach disk/shock structure is clearly evident in these profiles, as is the intensity increase due to afterburning.
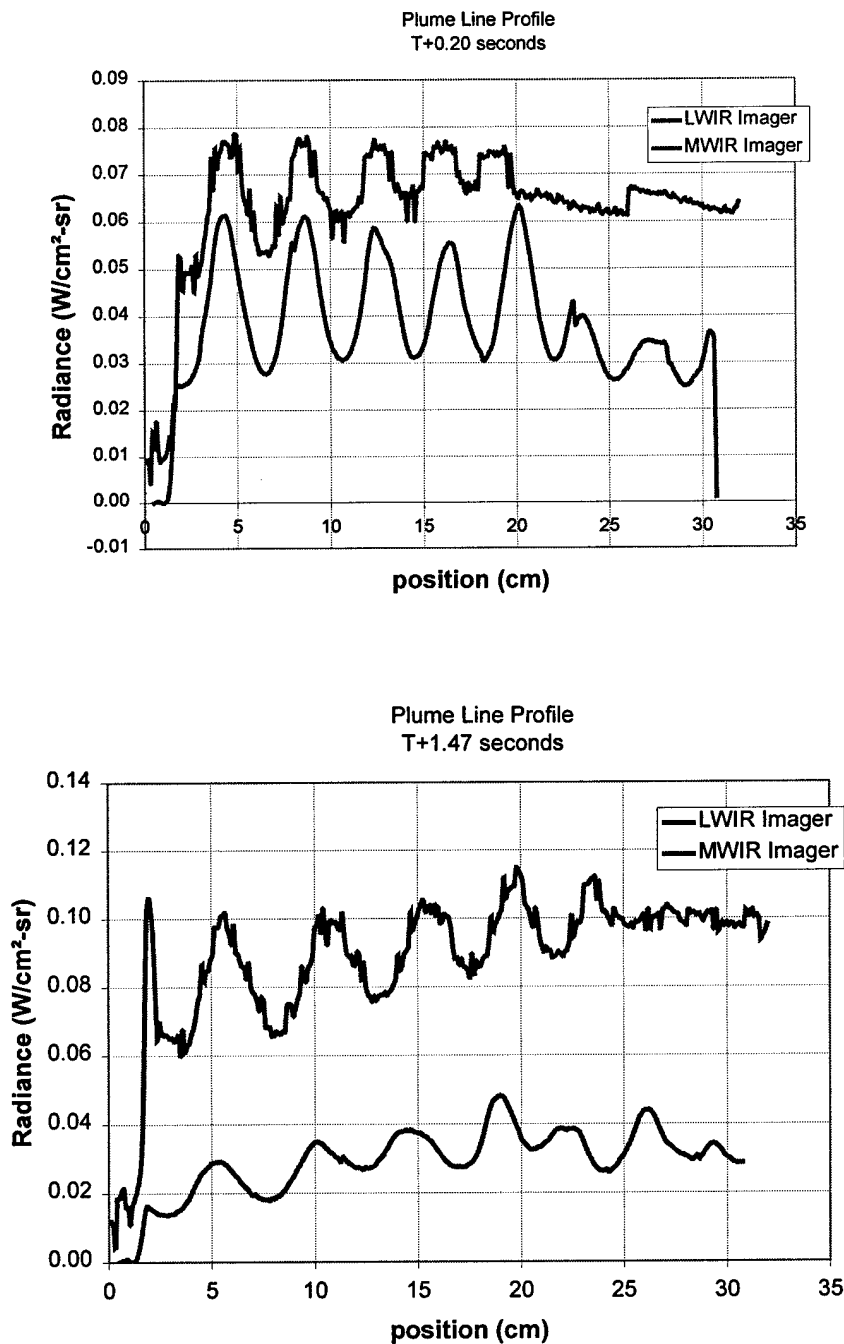
Plume Line Profile
T+0.20 seconds

Plume Line Profile
T+1.47 seconds

Figure 86: Radiance line profile through the plume at T+0.2 seconds and T+1.47 seconds, AEDC Run 11.

Lateral profiles of the MWIR imagery are shown in Figure 87. The locations of the profiles in relation to the nozzle exit plane are indicated on the figure; the 1cm station corresponds approximately to the nozzle exit plane, the 3.5cm station is at the first Mach disc, and the 6cm station is between the first and second Mach discs. Because of its small radial extent and broadside viewing aspect, the exhaust plume is approximately optically thin for axial stations other than at the Mach discs (starting 3.5cm). That is, for a line of sight thru the plume centerline, the emission is additive along that line of sight (i.e. the nearside of the plume does not appreciably attenuate the emission from the far side). For optically thin plumes, the emission profile is related to the underlying emitter concentration thru Abel's equation[43]. The emission profile shapes shown in Figure 87 indicate an emitter (soot) concentration profile which is slightly biased toward the nozzle wall.
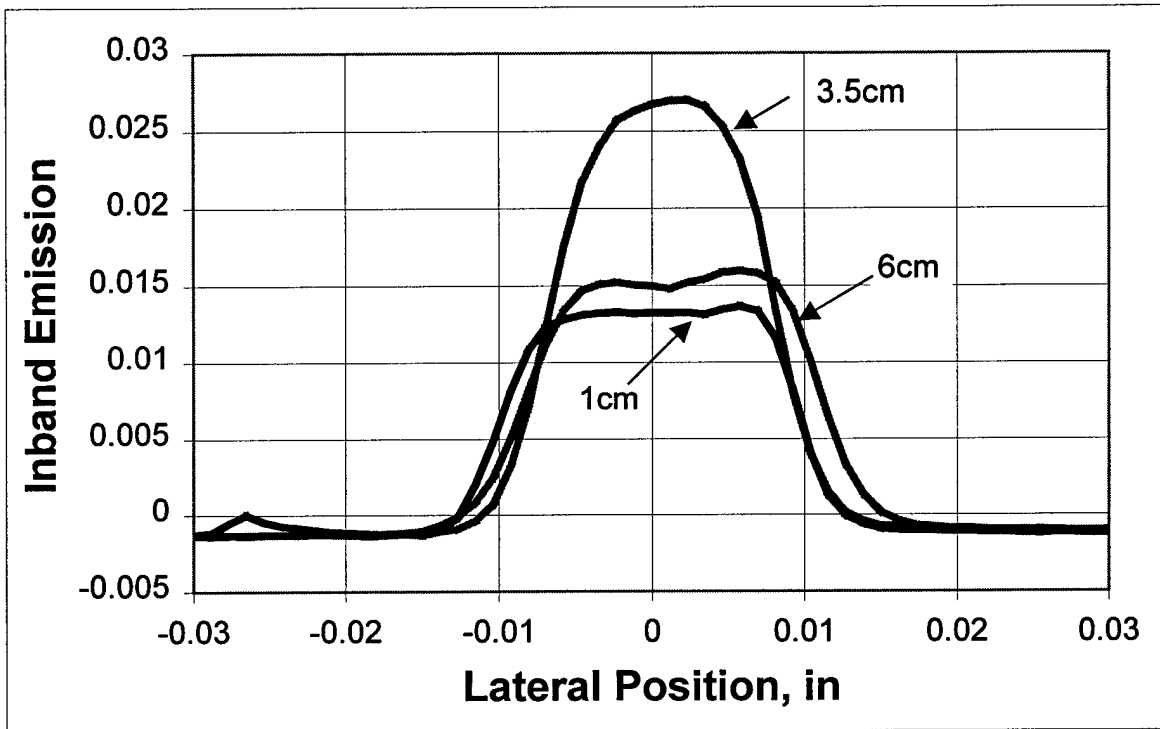

Figure 87: MWIR imagery lateral emission profiles.

9.4.2 SPECTRAL DATA

Spectral data from approximately 0.2 to 5.5 μm were acquired by AEDC during the NOP ROCKET engine tests at UAH. The spectral data were not calibrated for absolute values, but the relative spectral intensity of emission features is correct.

9.4.2.1 MWIR Spectra

Spectra from 2.0-to-6.0 μm were acquired using a Bomem MR200 Fourier transform spectrometer (FTS). The FTS had an approximate 6-inch Field of View (FOV) that was centered vertically on the nozzle axis, with the left edge of the FOV situated 1 inch downstream of the nozzle exit plane. MWIR spectral data were acquired during both the catalyst and spark plug igniter tests.

Although the catalyst bed tests did not result in successful rocket ignition, spectra acquired during these tests typically show CO_2 present in the exhaust. A typical MWIR emission spectrum acquired during a catalyst test is shown in Figure 88. Emission from hot CO_2 , as well as absorption features caused by cold atmospheric CO_2 are readily apparent. Also present around 4.5μm are absorption features that are possibly due to hot N_2O oxidizer in the exhaust. No H_2O emission (2.5μm) is seen in these spectra.
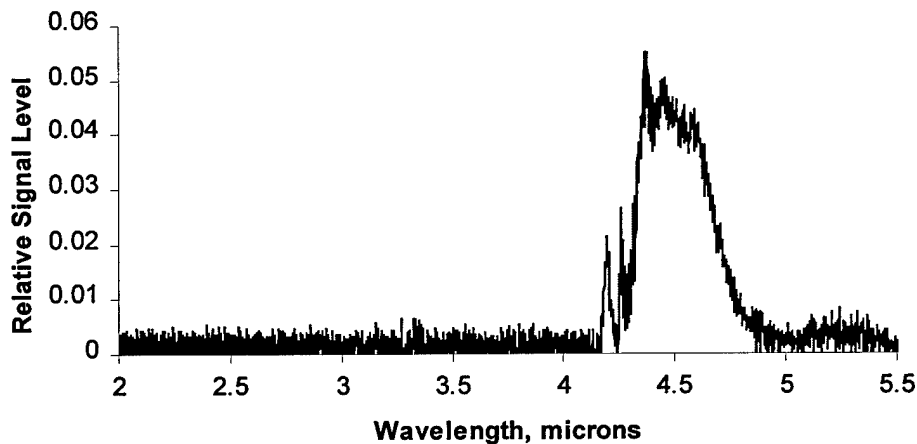

Figure 88: Spectrum acquired during catalyst test.

A MWIR spectrum acquired during the test designated AEDC Run 6, where a spark plug was used to initiate combustion, is shown in Figure 89. Comparison of Figure 89 to Figure 88 shows the intensity of the CO_2 emission resulting from the spark plug initiated combustion is orders of magnitude higher than that seen from the catalyst ignition test. Emission features caused by CO_2 and H_2O emission dominate this spectrum, and absorption features caused by cold atmospheric CO_2 are again readily apparent.
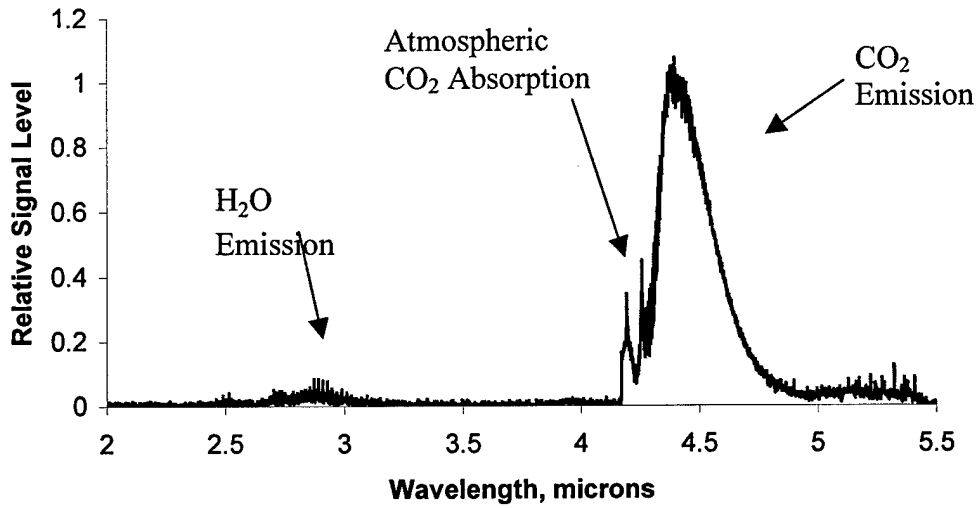
Figure 89: Spectrum acquired during spark plug igniter test designated AEDC Run 6.

MWIR spectral data acquired during runs designated AEDC Run 6 through AEDC Run 9 are similar in content to the spectrum shown in Figure 89. Spectra acquired during AEDC Run 9, shown in Figure 90, appear to contain an emission feature indicative of hydrocarbon emission in the C-H stretch region around 3 μm.
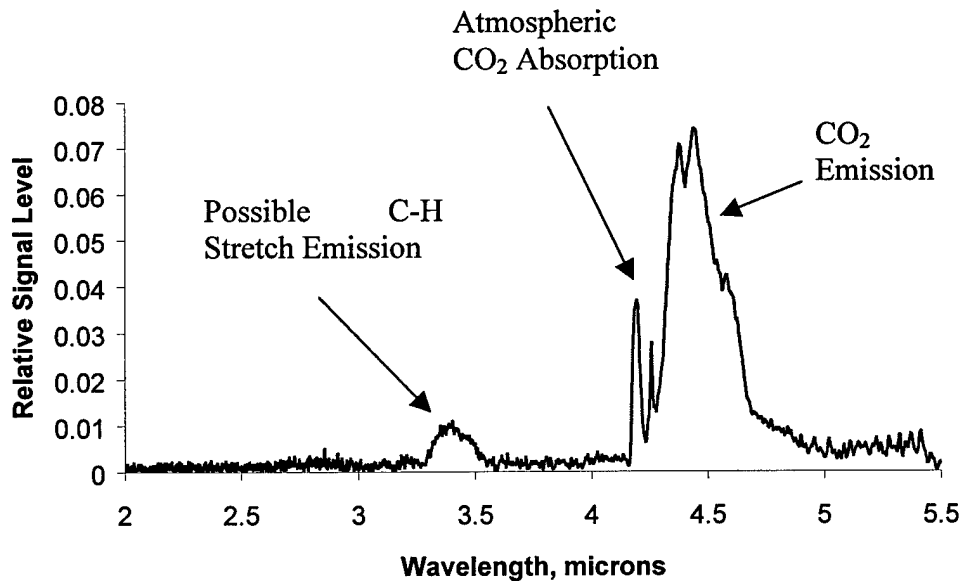

Figure 90: Spectrum from AEDC Run 8 showing C-H possible stretch emission.

Spectra acquired during AEDC Run 11 through AEDC Run 13 contain a feature that has been attributed to N_2O absorption. This feature is most apparent in spectra acquired during AEDC Run 13, which is shown in Figure 91.
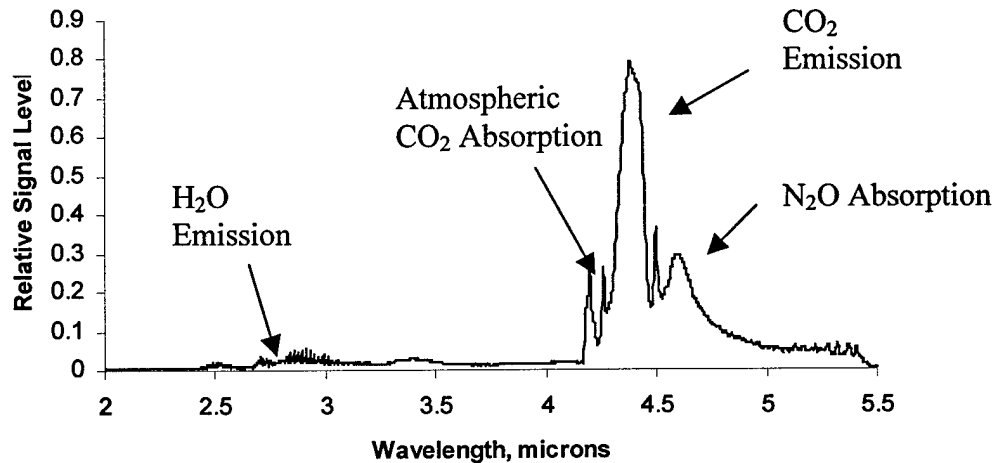

Figure 91: Spectrum from AEDC Run 13 showing N_2O absorption.

9.4.2.2   UV/VIS/NIR Spectrometer

A ZEISS MMSPC spectrometer equipped with a 1024 element silicon diode array was used to provide wide spectral coverage from 0.25-to-0.95 μm at a nominal 2.5 nanometer (nm) spectral resolution in order to provide a survey of UV/VIS/NIR emission from the exhaust.   The 2-inch diameter circular FOV of this spectrometer was located approximately 1-inch from the nozzle exit. No emission features were detected by this spectrometer during the catalyst igniter tests. A spectrum acquired by the ZEISS spectrometer after combustion was initiated by a spark plug, shown in Figure 92, indicates the emission from the exhaust in this spectral region is dominated by emission at roughly 912 nm, possibly due to H_2O, on top of continuum emission. The continuum emission is probably due to soot.
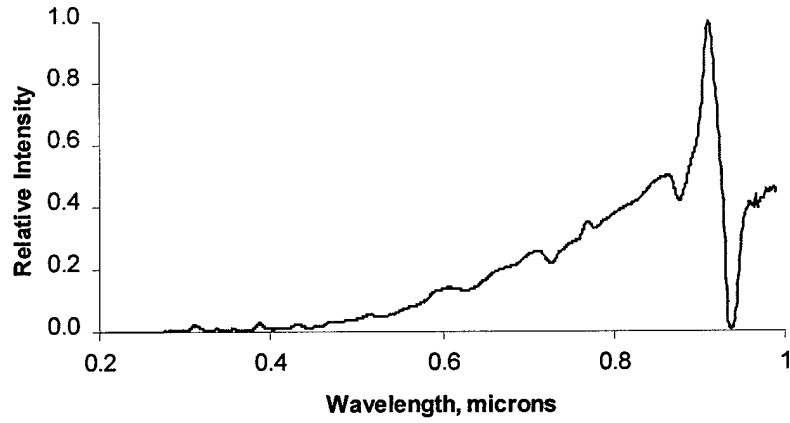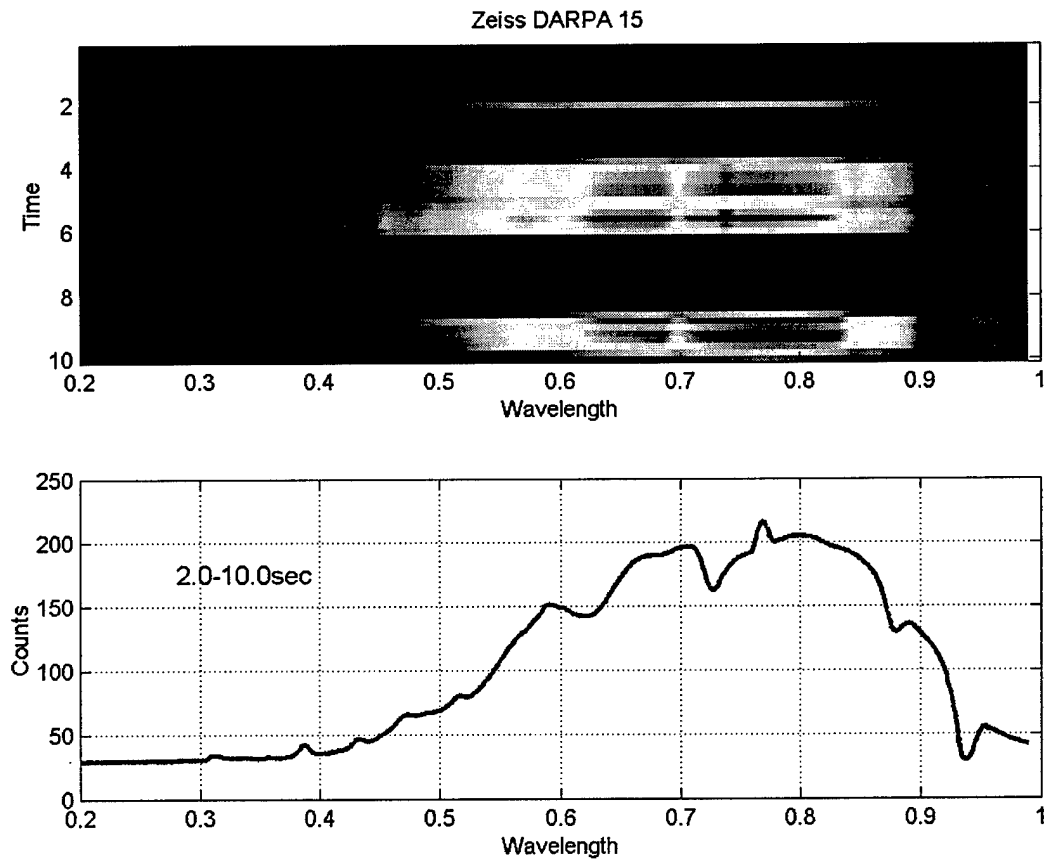
136

Figure 92: UV/VIS/NIR spectrum.

Figure 93: Visible wavelength spectra time history and average spectra.

137

Figure 93 shows a visible wavelength spectra time history and averaged spectra from 2-10sec.. The spectra are dominated by a continuum with a few molecular and atomic features. The decrease of the spectra beyond 0.8μm is due to decreasing instrument response and does not reflect the true spectra. The underlying continuum is probably due to a combination of soot and the NO+O radiative recombination continuum, which has been observed in N_2O/hydrocarbon flames[44,45].

Weaker emission features are also present in spectra acquired by the ZEISS spectrometer, are shown in Figure 94. Although the spectral resolution is only moderate, features tentatively attributed to molecular emission features from OH, CH, and C_2, are identified.
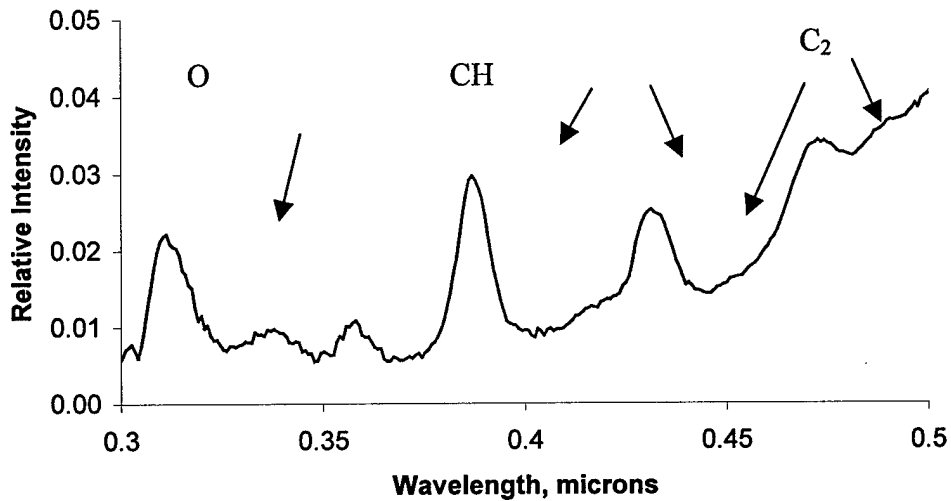

Figure 94: Weak emission features in Zeiss Data.

Spectra acquired when combustion is starting and shutting down, shown in Figure 95, exhibit atomic emission lines that are apparently overridden by the continuum radiation during full combustion.
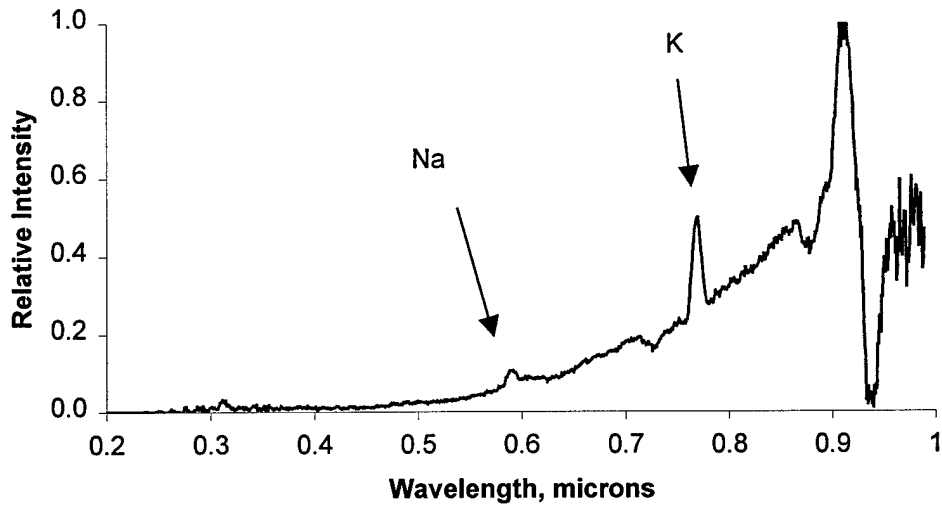
138

Figure 95: Spectrum showing atomic emission lines present at startup and shutdown.
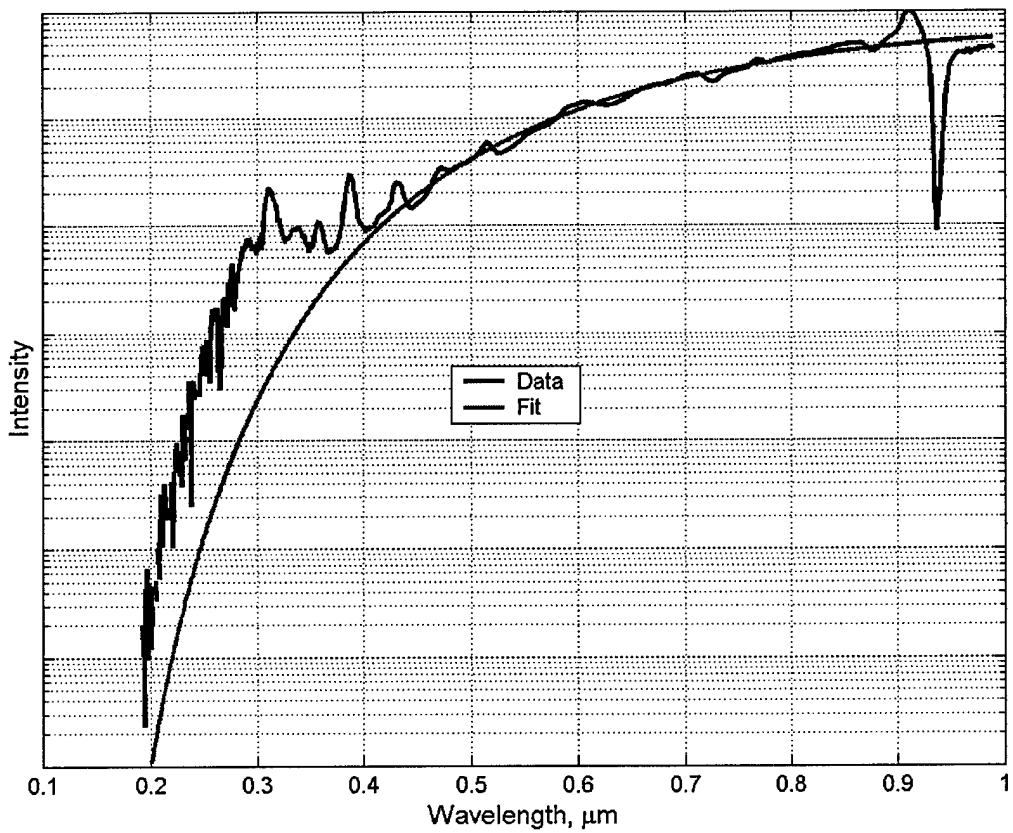

Figure 96: UV/VIS spectra fit with the Planck function.

A fit of the shape of the UV/VIS spectra between 0.4 and 0.9μm, and the Planck function multiplied by the soot emissivity curve[46] is shown in **Figure 96**. The fit yields a blackbody temperature of 2153K.

9.4.2.3 Ultraviolet/Visible (UV/VIS) Spectrometer

An ISA model HR320 0.3 meter Czerny-Turner grating spectrometer with an EG&G PARC 1024 element intensified silicon diode array detector was used to provide relatively high spectral resolution of UV radiation from the exhaust. The 2-inch diameter circular FOV of this spectrometer was located approximately 1-inch from the nozzle exit. No emission features were detected by this spectrometer during the catalyst ignition tests. A typical UV spectrum acquired after combustion was initiated by a spark plug is shown in Figure 97. As can be seen from this plot, UV emission from the exhaust appears to be mostly due to NO(γ) band emission. The presence of NO(γ) bands is expected. Wolfhard describes the generation of NO(γ) bands in numerous[44,45] nitrous oxide/hydrocarbon flames.
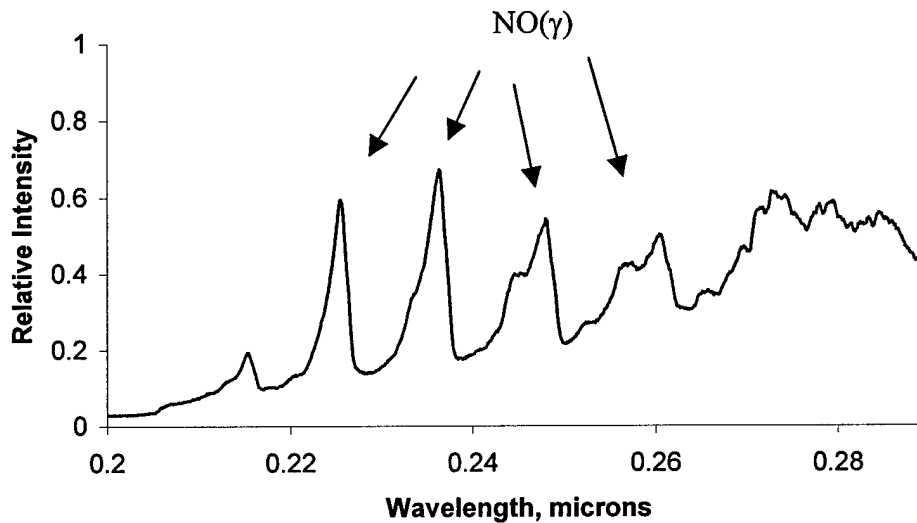
Figure 97: UV emission from the exhaust acquired during spark plug initiated combustion.

Figure 98 shows the UV spectra obtained during testing. The upper image in the figure shows the time dependence of the spectra. The vertical axis is time, which progresses downward, and the horizontal axis is wavelength. The color code runs from blue to deep red and indicates the radiation intensity. The intensity increase with time may be a result of increasing chamber pressure or nozzle heating. The lower figure shows the average spectra from 0.2-4.6sec. The band structure is due to NO(γ) bands. There is an underlying continuum which is probably due to a combination of soot and the CO+O radiative

recombination continuum. These bands have been observed previously in N_2O/hydrocarbon laboratory flames[44,45]. The presence of these bands indicates some small level of unmixedness and lack of complete combustion.
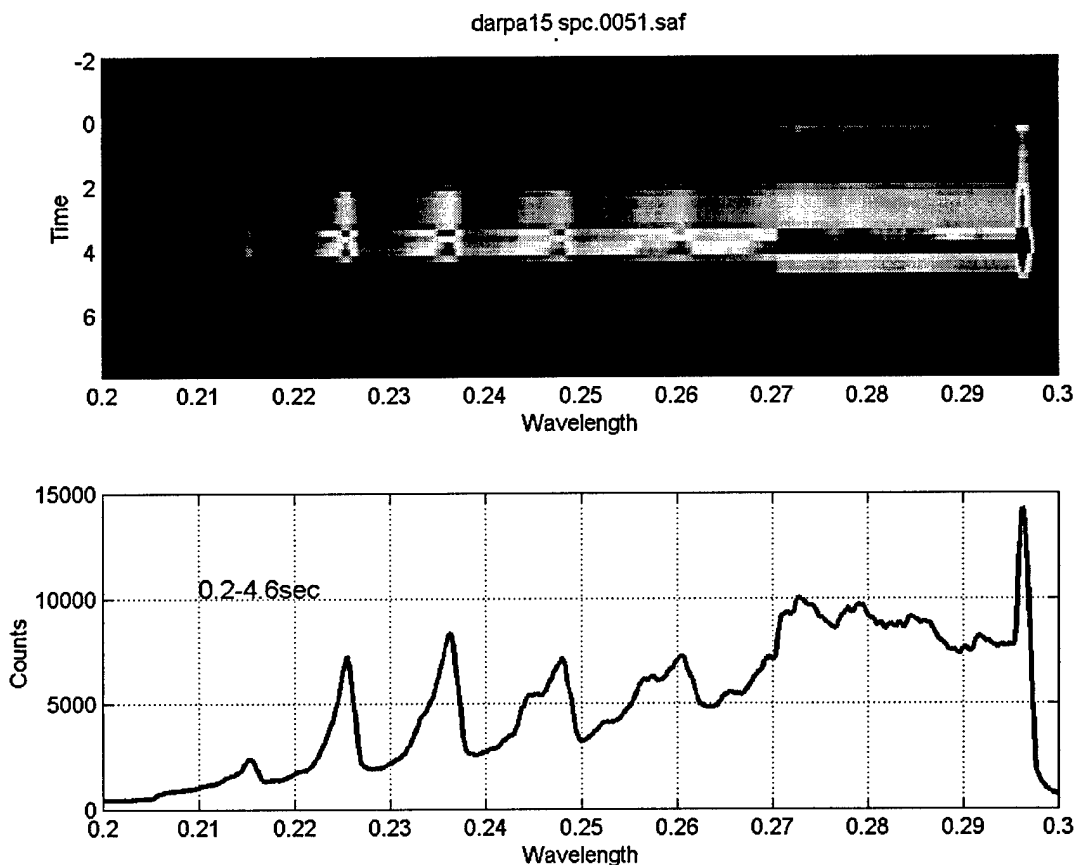
darpa15 spc.0051.saf

Figure 98: UV spectra time history and average spectra.

9.4.3 Exhaust Plume Optical Data Modeling

Exhaust plume modeling of the NOP rocket engine was performed as an aid to identification of unexpected features in the optical exhaust plume data acquired. The computations of the exhaust plume flow were based on the GASP computed nozzle exit plane profiles (for a chamber pressure of 150psia) of flow conditions and composition provided by GASL (see Figure 99 for the nozzle exit pressure profile). The JANNAF standard plume flow modeling code the "Standardized Plume Flowfield Model, v4.2" (SPF) was started at the nozzle exit plane with the GASP profiles, and the external plume flowfield was computed. Flow thermodynamic conditions and composition output from the SPF model were used by the JANNAF standard "Standard Plume Ultraviolet Radiation Code, LA v1.3" (SPURC) to compute the exhaust plume optical radiation.

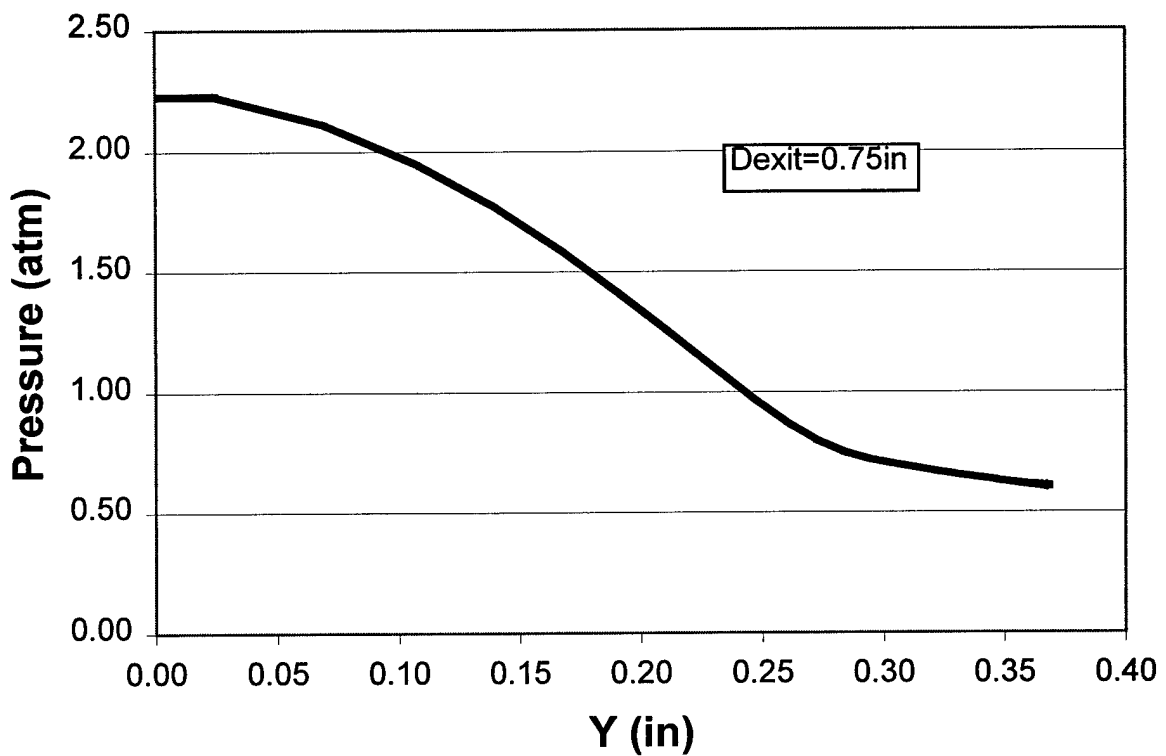**Figure 99: GASP nozzle exit pressure profile (150psia chamber pressure, provided by GASL).**

A computed MWIR radiance image of approximately 1ft. of the plume is shown in Figure 100 (flow is from left to right). The colormap for the figure uses red for high emission, and blue for low emission. The inviscid Mach cell structure typical of an underexpanded jet is seen in the data images (Figure 33) as well as the computed image.
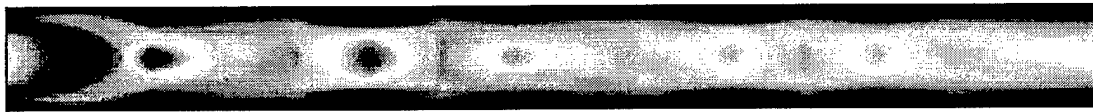
Figure 100: Exhaust plume MWIR prediction.

The computations confirm that the data images are of reasonable shape and structure.

A computed MWIR spectra with the same field of view of the exhaust plume as the MWIR imager is shown in Figure 101.
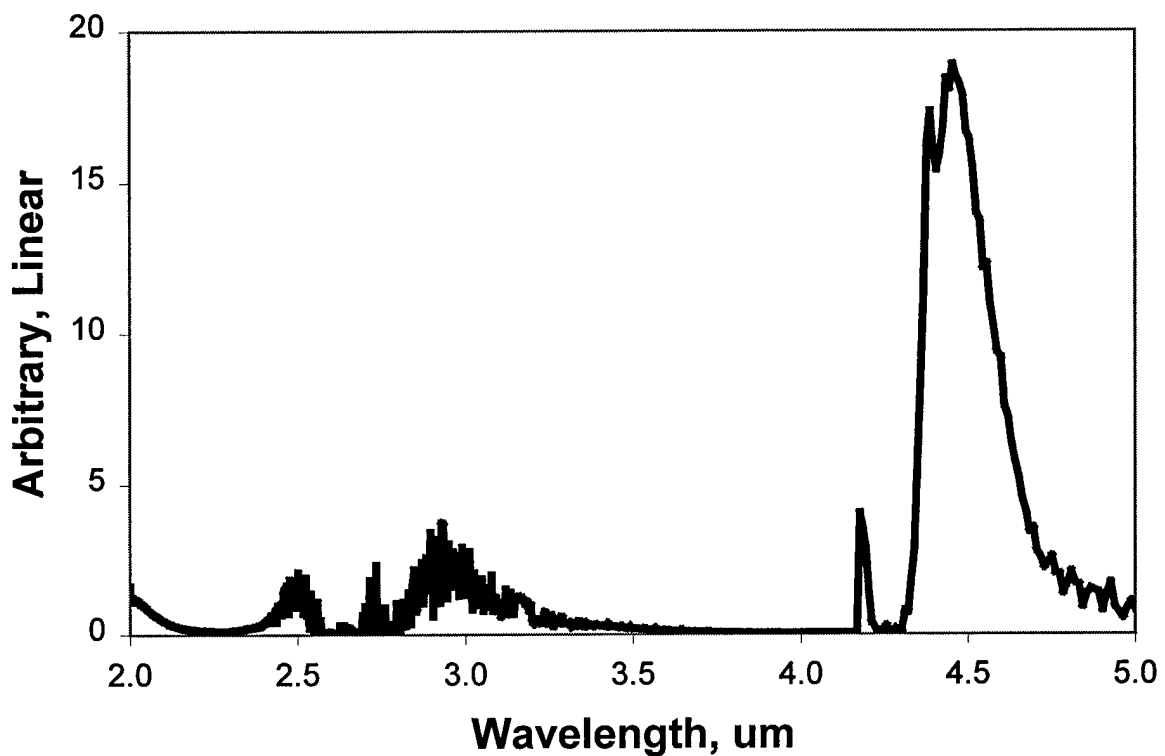
Figure 101: Computed MWIR spectra.

Again, comparing this computed spectrum with the spectral data (Figure 89), the computations indicate that there are no unexpected features in the data. This spectrum was computed without adding soot to the flow.

A detailed modeling effort would require closer attention to several engine operating parameters. The as-tested chamber conditions (pressure and O/F ratio) would need to be used in the nozzle calculations as well as the thrust chamber wall profile. Chamber

pressure data from the spark plug runs on 27 March indicate engine chamber pressures from 120 to 170psia. Also, some of the optical data indicate the presence of soot in the exhaust plume. A methodology of adding unmixidness to the thrust chamber flow would be required, to fully analyze the soot production.

To implement the standard plume code modeling methodology, the CPIA distributed Viscous Interaction Performance Evaluation Routine, v3.0 (VIPER) was used to compute the nozzle flowfield downstream of the nozzle throat for conditions similar to those of the run (Pc=150psia, O/F=7.1). A 15-deg cone was used to approximate the nozzle wall contour. The resultant computed nozzle exit plane conditions were then used with the SPF code to compute the external plume flow conditions, and SPURC code was used to generate plume optical signatures. It was necessary to add approximately 1.5% (by mass) of soot, biased near the nozzle wall, to account for the emission measured in the continuum band (3.85-4.15μm) by the imager. Figure 102 shows a measured nozzle exit plane lateral emission profile and a profile from the SPURC model using 1.5% soot. The profiles are in the particle continuum band (3.85-4.15μm). The computed emission profile is extremely sensitive to the amount and spatial distribution of the soot.
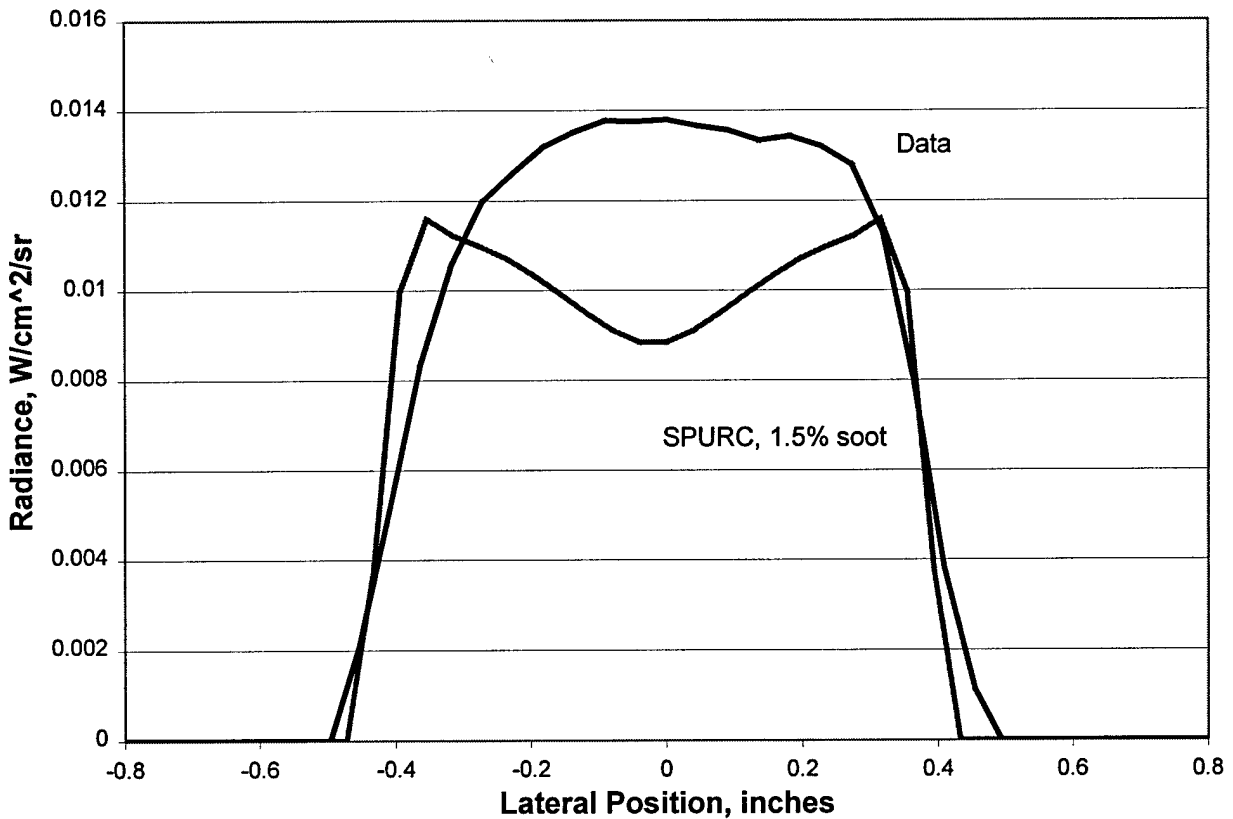

Figure 102: Near exit plane lateral emission profiles, 3.85-4.15μm.

144

The SPF code was operated in two different modes; inviscid (SCIPPY module only, no viscous mixing or afterburning), and viscous (SCIPPY and SPLITP modules, mixing and chemistry at the plume edge).

Figure 103 shows the qualitative appearance of MWIR SPURC calculations from these two modes of SPF operation. The inviscid SPF calculation shows the repeating Mach cells as seen in the data. Also note the absence of afterburning in this calculation. The inviscid calculation would continue these cells until they are dissipated by the internal flow. The viscous mixing calculation, however, indicates that the cell structure of the plume is damped after the first two cells and the bright plume periphery is an indication of afterburning. The features seen in these two calculations bound the plume structure seen in the imagery acquired during the NOP ROCKET tests.
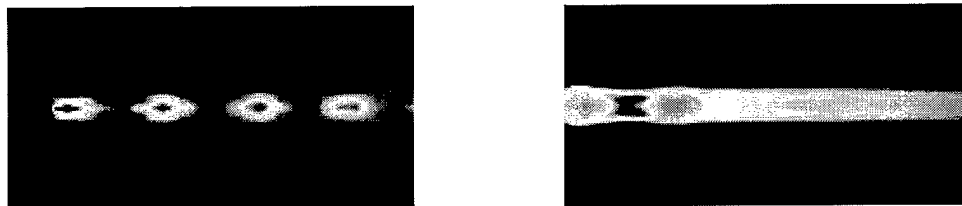
Figure 103: Radiation predictions using inviscid and viscous plume calculations.

10   Alternative Applications

Technologies developed under this BAA 99-22 program have other applications for propulsion systems and other technologies. The use of nitrous oxide as a source for high temperature nitrogen and oxygen lends itself to a variety of propulsion systems. Already mentioned is the use of catalytically-decomposed nitrous oxide as a monopropellant for a rocket engine. Monopropellant rockets are used for space propulsion and employ both hypergolic propellants and cold gases. Catalytically-decomposed nitrous oxide can be used as a hydrazine replacement or can be used to greatly improve mission performance for propulsion systems previously employing cold gas thrusters.

The exothermic nature of the nitrous oxide decomposition process can also find use as a torch igniter for airbreathing engines. In particular, ignition systems for hypersonic airbreathing engines are limited by their ability to ignite fuel under certain flight conditions, in particular for low-speed operation. A nitrous oxide torch igniter could be used to increase combustor entrance temperature while providing hot oxidizer to autoignite the fuel. Nitrous oxide can be made to thermally decompose by exposure to the hot incoming air or by exposure to the hot engine structure.

Decomposed nitrous oxide has also been proposed as a high density source of breathable air. One such idea for a self-contained breathing apparatus (SCBA) is pending for an international patent.[47] In addition to this, catalytic decomposition of nitrous oxide has been incorporated into several industrial air scrubbers, including the CRI Catalyst DeNOx system.[48]

11   Conclusions

A new rocket test stand facility, equipped with palletized propellant feed systems, 1000 lbs$_f$ thrust stand, and data acquisition systems, was built to test a nitrous oxide/propane (NOP) rocket engine. The NOP rocket was tested over a range of mixture ratios (4.89<M.R.<8.68). A unique ignition concept using catalytically decomposed nitrous oxide to autoignite propane, was explored and various catalyst materials were evaluated. Shell-405 and cobalt based ZSM-5 showed promising reactivity, demonstrating sufficient decomposition of N_2O to ignite hydrocarbon fuels. Laboratory experiments with the catalyst reactor have shown that N_2O catalytic decomposition is achievable at 400 °F for pure nitrous oxide flowing over Shell 405, and, with the use of trace amounts of a hydrocarbon (e.g. propane or propylene), this temperature is lowered to approximately 200 °F.

In addition to developing the catalyst ignition system, NOP rocket performance was experimentally determined to match well with theoretical predictions, with proper modeling of heat losses. Radiometric measurements were also used to determine rocket exhaust temperature and plume composition and plume pitot probe measurements provided another method for verifying thrust data. Future work will focus on demonstrating NOP rocket ignition using catalytically decomposed N_2O, and on exploring the use of catalytic decomposed N_2O for monopropellant rockets as well as torch igniters.

A traversing, water-cooled rake with a single, integral spherical nose tip designed with a stagnation point pressure sensing tube was used to obtain pitot pressures during test firings of the nitrous oxide/propane engine at UAH on 15 March 2001. The probe assembly survived the firings with no melting or erosion. Data were obtained on Runs 2, 4, 8, 9, and 10. However, the chamber pressure varied to such an extent on Runs 2, 4, and 8 to preclude further analysis of this data. The chamber pressure was relatively steady during Runs 9 and 10, and the data from these runs were used to determine thrust

for comparison to the thrust stand measurements using the procedure described above. The pitot pressure derived thrust as either between the minimum and maximum thrust stand values over the time of the rake traverse, or slightly above the maximum. The base pressure was shown not to be important in these comparisons. In general, the pitot pressure derived thrust values agreed with the thrust stand data to better than 5%. However, the variations in chamber pressure (and thus thrust) are too great to draw firmer conclusions about the validity of the pitot pressure method.

Optical data was taken of the NOP rocket tests on 27 March 2001 for both catalyst ignition and spark plug ignition. The data include UV thru MWIR spectra, and MWIR and LWIR imagery. The imagery shows flow details such as the Mach cell structure and mixing layer of the exhaust plume, as well as indications of the presence of soot. The spectral data allow the identification of specific emitters including CO_2 and H_2O as well as hydrocarbon fragments in the infrared, Na and K in the visible wavelengths, and NO, CH, C_2, and OH in the UV.

While not a quantitative comparison, computations of the IR plume flowfield and radiation bound the features seen in the data. In order to match the optical signature of the NOP ROCKET engine exhaust plume, further modeling of the thrust chamber and quantity and spatial distribution of soot would be required.

The nonintrusive data show the spectral, spatial, and intensity features expected for a rocket engine of this size utilizing nitrous oxide and propane propellants. There are no features that indicate extremely poor overall mixing. However, the presence of unburned hydrocarbons (e.g. Figure 38) and the presence of soot indicate incomplete combustion and small-scale unmixedness. This is also borne out by the C* and Isp efficiencies indicated by the facility thrust, chamber pressure, and mass flow data shown in Section 8.2.

In conclusion, the use of nitrous oxide and propane as a rocket propellant combination has many potential applications for which it is well suited. This propellant combination is highly reactive when catalyzed and combined, yet benign and nontoxic in storage. Its storage density and specific impulse are suitable for many missions currently employing hypergolic, toxic, or cryogenic propellants. The benign nature of the propellants holds promise for reducing launch costs due to that incurred as a result of the volatile nature of current rocket propellants.

The alternative uses for nitrous oxide as a monopropellant lead to other space applications where nitrous oxide is highly competitive with existing systems. The ability to decompose nitrous oxide with the same flight proven catalyst that has decomposed hydrazine in space for decades paves the way for an easy transition to its use. The undeniable superiority of nitrous oxide as a cold gas propellant over both nitrogen and helium completes the package, making possible a true multi-modal propulsion system that uses the same propellants for all space applications.

It is the belief of the authors that the NOP propellants should be pursued with continued research that targets the most appropriate mission applications. This applied research should be paralleled by a scientific effort to understand and maximize the capabilities of catalytic decomposition of nitrous oxide. The ability to control these reactions will accommodate better reactor design for real systems.

12 Acknowledgements

13 Appendix I

Property	Units	Nitrous Oxide	Propane	Nitrogen Tetroxide (NTO)	Hydrazine	Monomethyl Hydrazine (MMH)	Unsymmetrical Dimethyl Hydrazine (UDMH)	Hydrogen Peroxide 90%	Hydrogen Peroxide 70%
Formula	-	N_2O	C_3H_8	N_2O_4	N_2H_4	$CH_3\text{-}N_2H_3$	$(CH_3)_2\text{-}N_2H_2$	H_2O_2	H_2O_2
CAS Registry No.	-	10024-97-2	74-98-6	10544-72-6	302-01-2	60-34-4	57-14-7	7722-84-1	7722-84-1
NFPA Flammability	-	0	4	0	3	4	3	0	0
NFPA Reactivity	-	0	0	0	3	0	1		3
NFPA Health	-	2	1	3	4	3	4		2
NFPA Other	-	OX		OX					OX
NIOSH REL	ppm	25	1000	1	0.03	0.01	0.01		
ACGIH TLV	ppm	50	Asp.	3	0.01			1	1
OSHA PEL	ppm	ND²	1000	5	1 ppm (skin)	0.2 (skin)	0.5	1	1
IDLH	ppm	Asp.	2,100 Fl³	20	50	20	15	75	75
Inhale. LC₅₀	ppm	1500 (rat)	NA	315 ppm, 15 min (rabbit)	570 ppm, 240 min (rat)	34 ppm, 240 minutes (rat)	252 ppm, 240 min (rat)	1,790 ppm, 240 min (rat)	
Specific Gravity, Liquid	-		NA	1.49		0.87	0.78	1.4	1.3
Vapor Density	Air = 1	1.53 @ 21 °C	1.55	1.58		1.59	2.1	1	1
Melting Point	°C	-90.8	-187.7	-9.3	2	-52	-58	-11	-39
Boiling Point	°C	-88.49	-42	21 (decomposes)	114	87.5	63	141	125
Flash Point	°C	NA²	-104	NA	38 (cc)	21 °C (coc)	-15 (cc)	NA	NA
Autoignition Temperature (Inert)	°C	NA	450	NA	270	382F	249	NA	NA
Autoignition Temperature (Cat.)	°C	NA	-	NA	24 (Fe₂O₃)			NA	NA
Autodecomposition Temperature (inert)	°C	651	-	100 (complete dissociation to NO₂)		190F		All Temperatures⁴	All Temperatures⁴
Autodecomposition Temperature (cat.)	°C	~200 (nominal)	-					All Temperatures⁴	All Temperatures⁴
LEL	%	NS²	2.2	NA	1.8	2.5	2		26 (equil. vapor over 75% soln @ boiling, abt 128 °C)
UEL	%	NS	9.5	NA	100	98	95		100
Vapor Pressure	mm Hg	39,277 @ 21°C	6,395 @ 21 °C	18 @ 21°C 400 @ 80°C	11 @ 20°C	49.6 @ 21 °C	157 @ 25 °C		23 @ 30 °C
Lowest Ionization Energy	eV	12.889	10.94	10.8	8.1	7.7	7.29		10.58

Property	Units	Nitrous Oxide	Propane	Nitrogen Tetroxide (NTO)	Hydrazine	Monomethyl Hydrazine (MMH)	Unsymmetrical Dimethyl Hydrazine (UDMH)	Hydrogen Peroxide 90%	Hydrogen Peroxide 70%
Ionization Energy Range	eV	-	-	10.8 – 11.6	8.1 – 10.68	7.7 – 9.36	7.29 – 8.88	10.54 – 11.70	
Lowest Appearance Energy (gnd state)	eV	NO^+, 15.01	$C_2H_4^+$, 10.5	N/A	$N_2H_3^+$, 10.6	$CH_3N_2^+$, 9.2	$H_2N_2CH_3^+$, 8.4	H_2O^+, 14.09	
Appearance Energy Range	eV	15.0 – 20.1	10.5 – 40.0	N/A	10.6 – 16.2	9.2 – 15.2	8.4 – 14.5	14.09 – 17.0	
Reportable or Threshold Quantity[6]	kg	RQ = ND TPQ = ND	RQ = ND TPQ = ND TQ = 4535	RQ = 4.54 TPQ = 45.4 OSHA TQ = 113	RQ = 0.454 TPQ = 454	RQ = 4.54 TPQ = 226.8	RQ = 4.54 TPQ = 454	RQ = ND TPQ = 454 (sol. > 52%)	
Toxic Effect	-	Asphyxiant; anesthetic; teratogen	Asphyxiant	chemical irritant and burning	chemical burns, possible carcinogen	chemical burns, not considered a carcinogen	Chemical burns on body and in lungs; carcinogen	Chemical burns to skin, body, lungs; carcinogen	
Trace constituents	-	moisture, air, corrosion products	moisture, hydrogen, air, low molecular weight alkanes and alkenes, alcohols	moisture, nitrogen dioxide, nitric oxide, nitric acid, corrosion products	moisture, ammonia, corrosion products	moisture, ammonia, methane, corrosion products	moisture, ammonia, methane, corrosion products	water, corrosion products	
Toxic or Hazardous Decomposition Products	-	oxygen	NA	NO, NO_2	ammonia, nitrogen oxides	CO, nitrogen oxides	NO_x hydrogen, CO, ammonia, amines, hydrazoic acid	oxygen, hydrogen, steam	
Required respiratory protection	-	SCBA under asphyxiant conditions	SCBA above the LEL	SCBA up to 20 ppm, then escape	Ventilate. Approved respirator above TLV.	Full Face Mask at all times	Ventilate. Approved respirator above TLV.		
Firefighting Materials	-	excess water	water spray or foam	excess water or water spray; do not use CO_2 or halogenated materials	Powder, alcohol foam, excess water, CO_2	Dry Powder, alcohol foam, excess water, CO_2	Powder, alcohol foam, excess water, CO_2	excess water	

Property	Units	Nitrous Oxide	Propane	Nitrogen Tetroxide (NTO)	Hydrazine	Monomethyl Hydrazine (MMH)	Unsymmetrical Dimethyl Hydrazine (UDMH)	Hydrogen Peroxide 90%	Hydrogen Peroxide 70%
Materials to Avoid	-	reductants, Al, B, Na, Li, hydrides, reactive metals and their salts including Pt, W, WC, Ag	strong oxidizers	water, bases, most metals, hydrocarbons, fluorine	strong reducing agents; strong oxidizers	Oxidizers incl.: H_2O_2, NTO, fluorine, halogen fluorides, bleach,	Fuming nitric acid; acids. metal oxides, iron, copper, lead, manganese, molybdenum, cotton waste, sawdust. Corrosive to plastics	combustibles, organic substances, reducing agents, metals including copper alloys, powdered metal, reactive iron, silver, nickel, palladium, platinum, chromium, salt of iron, copper, chromium, vanadium, tungsten, molybdenum, platinum	
Materials specified for Use		(Perry's §23) stainless steels, Ti, passivated AL, fluoride, plastics	Aluminum, stainless, Teflon,	(Perry's §23) stainless steels, Ti, passivated AL, fluoride, plastics	stainless steel, Teflon, aluminum, titanium, various plastics	stainless steel, Teflon, aluminum, titanium, epoxy, styrene, phenolic resins	stainless steel, Teflon, aluminum, titanium, epoxy, styrene, phenolic resins	Opaque containers; aluminum, PVC (up to 30%), stainless steel (moderately acceptable to 50%).	
Price[5]		$2.76/kg (cylinder quantities)	$0.41/kg C_3H_8 (current mkt; may be higher for higher purity product)	$6/kg (1990)	$6.95/kg N_2H_4 (as hydrate, current mkt) $17/kg (1990)	$176/kg (1990)	$24/kg (1990)	$1.047/kg H_2O_2 (as 70% H_2O_4, current market) $2.00/kg ($H_2O_2$, 98%, 1990)	
Comments		NFPA Health rating for the liquid is 3 due to refrigeration properties	ethyl mercaptan added at 50 ppm level to commercial propane as odorant/indicator	Liquid NTO is a mixture of NO_2 and N_2O_4; the vapor phase is all NO_2	Material compatibility based on aqueous ammonia	Material compatibility based on aqueous ammonia	Material compatibility based on aqueous ammonia	Photodecomposition at almost all temperatures. Some metals acceptable after passivation of contact surface by oxidation using HNO_3	

Property	Units	Nitrous Oxide	Propane	Nitrogen Tetroxide (NTO)	Hydrazine	Monomethyl Hydrazine (MMH)	Unsymmetrical Dimethyl Hydrazine (UDMH)	Hydrogen Peroxide 90%	Hydrogen Peroxide 70%

NOTES:

[1] Simple asphyxiant. IDLH determined by depression of available oxygen to below 19.5% based on N_2O as sole contaminant.

[2] NA – Not Applicable; NS – Not Specified; ND – Not Defined

[3] Flammable asphyxiant. IDLH determined as 10% of the LEL.

[4] Hydrogen peroxide decomposes at all temperatures into water and oxygen. As temperature increases, the rate increases as a first-order reaction (2.3x greater rate for each 10 °C in temperature. This process is catalytically accelerated by silver, many metal surfaces which have not been passivated (e.g. by treatment with nitric acid to form an oxide layer), and organic contaminants in the peroxide. Under some conditions, this can lead to runaway reactions.

[5] 1990 price data is quoted from material descriptions in the Encyclopedia Astronomical (www.friends-partners.org/~mwade/props). Current quotes are developed from various sources including the Chemical Market Reporter, on-line sources, and vendor price estimates. The hydrazines and NTO are a captive market and prices are subject to controls; however, comments in the Encyclopedia Astronomical indicate that a large fraction of the prices of these commodities is due to the imposition of environmental and safety controls to meet current regulatory requirements. Price information is as available; to the extent possible, sources have been examined for price for large quantity supply (e.g. tanks) but clarification of quantity is not always available. Nitrous oxide data is obtained from http://www.cganet.com/N2O/factsht.htm and is quoted as a price per cylinder, so the cost does not directly compare with bulk costs quoted elsewhere on the line. Due to its use as a fuel, propane costs are seasonable; the quoted propane price is for bulk fuel grade propane for late December 2000 delivery ($0.90/gal).

[6] Reportable Quantity (RQ) – Quantity subject to reporting to regulatory agencies in the event of a leak or release (CERCLA). Threshold Planning Quantity (TPQ) – Quantity subject to preparation of emergency plans and other documents (SARA). Threshold Quantity (TQ) – Same (CAA or OSHA). The TQ for all flammable materials stored for use other than fuel is 10,000 lb (4535 kg)

154

14 References

[1] Frisbee, Robert H., "Advanced Propulsion Concepts," www.sec353.jpl.nasa.gov/apc/

[2] Hydrogen peroxide is unstable in its pure form. It is stabilized by dilution in water up to 85% peroxide. Hydrogen peroxide also decomposes over time due to small quantities of contaminants.

[3] Mark Wade's Encyclopedia Astronautica – www.friends-partners.org

[4] Primex, Inc., now General Dynamics.

[5] Brown, Charles D., "Spacecraft Propulsion," AIAA Inc., Washington DC, 1996.

[6] www.ee.surrey.ac.uk

[7] www.polyflex.co.uk

[8] Whitehead, John C.,"Hydrogen Peroxide Propulsion for Smaller satellites," 1st Hydrogen Peroxide Propulsion Workshop, The University of Surrey, July, 1998.

[9] Surrey Satellite Technology Limited, Nitrous Oxide Resistojet Data Sheet

[10] Zakirov, V., Sweeting, M., Goeman, V., Lawrence, T., "Surrey Research on Nitrous Oxide Catalytic decomposition for Space Applications," 14th AIAA/USU Conference on Small Satellites.

[11] Personal conversation with Dave Gibbon of SSTL, December 19, 2000

[12] Zakirov, V., Lawrence, T., Sellers, J., Sweeting, M., "Nitrous Oxide as a Rocket Propellant For Small Satellites," Proceedings of the 5th International Symposium on Small Satellite Systems and Services, France, June 2000.

[13] Zakirov, V., Sweeting, M., Lawrence, T., Sellers, J., "Nitrous Oxide as a Rocket Propellant," Proceedings of the 51st International Astronautical Congress, Rio de Janeiro, Brazil, October 2000.

[14] Keith, E., "The Peroxide Counter Revolution: Replacing Toxic Propellants in Space", International Space Propulsion Inc., 1st Hydrogen Peroxide Propulsion Workshop, The University of Surrey, July, 1998.

[15] Whitehead, John C., "Hydrogen Peroxide Propulsion for Smaller Satellites", 1st Hydrogen Peroxide Propulsion Workshop, The University of Surrey, July, 1998.

[16] www.bealaerospace.com

[17] While it is common in the literature to relate the increased costs incurred to the mandated levels of protection, there are hidden costs associated with a lack of protection, including increased health and life insurance costs and the very high liabilities (some of which are intangible) associated with a release which causes serious illness or loss of life by the public and/or long term environmental degradation.

[18] Whitehead, J.C., "Hydrogen Peroxide Propulsion for Smaller Satellites," www.cc.surrey.ac.uk/SSC/H2O2CONF/jwhitehead.htm.

[19] Mark Wade's Encyclopedia Astronautica – www.friends-partners.org

[20] Ozawa, R.I., "Survey of Basic Data on Flame Stabilization and Propagation for High Speed Combustion Systems, Technical Report AFAPL-TR-70-81, January 1971, The Marquardt Company.

[21] Billig, F. S., "Design and Development of Single-Stage-To-Orbit Vehicles," APL Technical Review, Volume 2, Number 1, 1990.

[22] Rose, John J., "Continuous Spark Ignition for Rapid Relight After Flameout of Gas Turbine Engines", Technical Note #WADC-TN-59-64, Wright Air Development Center, Wright-Patterson AFB, OH, 1997.

[23] http://www.rvs.uni-bielefeld.de/publications/Incidents/DOCS/ComAndRep/ChinaAir/AAR8603.html

[24] Communication with Mr. Jack Ito, Technical Principal Engineer, Engineering Analysis, GenCorp-Aerojet. October 27, 2000.

[25] Communication with Mr. Curtis Johnson, Sierra Engineering. October 19, 2000.

[26] Sutton, G.P., Rocket Propulsion Elements, Sixth Edition, Co. 1992, John Wiley & Sons, Inc., pp.288.

[27] Hill, P.G., and Peterson, C.R., "Mechanics and Thermodynamics of Propulsion," Addison-Wesley, Nov., 1970.

[28] Ahlberg, J.H., Hamilton, S., and Nilson, E.N., "Truncated Perfect Nozzles in Optimum Nozzle Design," J. Amer. Rocket Soc., Vol 31, No. 5, May 1961, pps. 614-620.

[29] GASP-"Users Manual", Co. 1996, Aerosoft, Inc.

[30] ASME MFC-3M-1989, "Measurement of Fluid Flow in Pipes Using Orifice, Nozzle, and Venturi", Copyright 1990 by the American Society of Mechanical Engineers.

[31] Matheson Gas Products, 1971

[32] Vannice.M.A., A. Dandekar. " Decomposition and reduction of N_2O over copper catalysts", Applied Catalysis: Environmental, Volume 22, 1999, 179-200.

[33] Heck, R.M., and Farrauto, R.J., "Catalytic Air Pollution Control-Commercial Technology", Co. 1995, Van Nostrand Reinhold, pp.17.

[34] Gordon, S., McBride, B., "Computer Program for Calculation of Complex Chemical Equilibrium Compositions, Rocket Performance, Incident and Reflected Shocks, and Chapman-Jouguet Detonations," NASA, Washington DC, March 1976.

[35] Bartz, D.R., "A Simple Equation for Rapid Estimation of Rocket Nozzle Convective Heat Transfer Coefficients," ARS Journal, January, 1957.

[36] Brower, W. B., Jr., *A Primer in Fluid Mechanics*, CRC Press, New York, 1999, pp. 164-166.

[37] Bore, C. L., "Some Contributions to Propulsions Theory – The Stream Force Theorem and Applications to Propulsion," Aeronautical Journal, April 1993, pp. 138-144.

[38] Sforzino, R. H., "Derivation of the Thrust Equation from Conservation of Energy," Journal of Aircraft, Vol. 7, No. 5, December 1, 1970, pp. 538-540.

[39] MIDAP Study Group, "Guide to In-Flight Thrust Measurement of Turbojets and Fan Engines", AGARDograph No. 237, January, 1979, pp. 94-95.

[40] Kawasaki, A. H., Coats, D. E., and Berker, D. R., "A Two-Phase, Two-Dimensional, Reacting Parabolized Navier-Stokes Flow Solver for the Prediction of Solid Rocket Motor Flowfields", AIAA 92-3600, 28th AIAA, SAE, ASME, and ASEE Joint Propulsion Conference and Exhibit, Nashville, TN, July 6-8, 1992.

[41] McGregor, W. K., Hiers, R. S., and Brown, D. G., "Non-Intrusive Performance Measurement Techniques for Static Testing of Liquid Rocket Engines – The SA-2 (Volga) as an Example", AEDC Informal Report, 13 February 2000, Revised 13 April 2000.

[42] Hiers, R. S., and Pruitt. D. W., "Determination of Thrust from Pitot Pressure Measurements," AIAA 2001-3314, 37th AIAA/ASME/SAE/ASEE Joint Propulsion Conference and Exhibit, 8-11 July 2001, Salt Lake City, Utah.

[43] Tatum, J.B. and Jaworski, W.A., "A Solution of Abel's Equation", *Journal of Quantitative Spectroscopy and Radiative Transfer*, Vol. 38, No. 4, 1987, pp. 319-322.

[44] Wolfhard, H. G., and Parker, W. G., "Spectra and Combustion Mechanism of Flames Supported by the Oxides of Nitrogen," *5th Symposium on Combustion*, Reinhold Publishing Co., 1955, p. 718.

[45] Gaydon, A. G., and Wolfhard, H. G., "Spectroscopic Studies of Low-Pressure Flames," *3rd Symposium on Combustion*, Williams and Wilkins Company, 1949, p. 504.

[46] Lee, S.C. and Tien, C.L., "Optical Constants of Soot in Hydrocarbon Flames", *Eighteenth Symposium (International) on Combustion*, The Combustion Institute, pp. 1159-1166, 1981.

[47] Zubrin, R.M., et.al. "Nitrous Oxide Based Oxygen Supply System," Pioneer Inventions, Inc., A61M 15/00, A62B 7/00, October, 1999.

[48] Clark, D.M., "Cost-Effective Combined N2O Destruction and NOx Removal Using the Shell DeNOx System," Presented at Asia Nitrogen '98 Conference, Kuala Lumpur, February, 1998.